Mass spectral molecular networking of living microbial colonies

Jeramie Watrous[a,b,c], Patrick Roach[d,1], Theodore Alexandrov[c,e], Brandi S. Heath[d], Jane Y. Yang[a,b,c], Roland D. Kersten[a,b,f], Menno van der Voort[g], Kit Pogliano[h], Harald Gross[i], Jos M. Raaijmakers[g], Bradley S. Moore[c,f], Julia Laskin[d,2], Nuno Bandeira[c,j,k,2], and Pieter C. Dorrestein[a,b,c,f,2]

Departments of [a]Pharmacology and [b]Chemistry and Biochemistry, University of California at San Diego, La Jolla, CA 92093; [c]Skaggs School of Pharmacy and Pharmaceutical Sciences, University of California at San Diego, La Jolla, CA 92093; [d]Chemical and Materials Sciences Division, Pacific Northwest National Laboratory, Richland, WA 99352; [e]Center for Industrial Mathematics, University of Bremen, D-28334 Bremen, Germany; [f]Center for Marine Biotechnology and Biomedicine, Scripps Institution of Oceanography, University of California at San Diego, La Jolla, CA 92093; [g]Laboratory of Phytopathology, Wageningen University, PB6708, Wageningen, The Netherlands; [h]Division of Biological Sciences, University of California at San Diego, La Jolla, CA 92093; [i]Institute for Pharmaceutical Biology, University of Bonn, 53115 Bonn, Germany; [j]Department of Computer Science and Engineering, University of California at San Diego, La Jolla, CA 92093; and [k]National Center for Research Resources, University of California at San Diego, Center for Computational Mass Spectrometry, La Jolla, CA 92093

Edited by Jerrold Meinwald, Cornell University, Ithaca, NY, and approved April 18, 2012 (received for review March 2, 2012)

Integrating the governing chemistry with the genomics and phenotypes of microbial colonies has been a "holy grail" in microbiology. This work describes a highly sensitive, broadly applicable, and cost-effective approach that allows metabolic profiling of live microbial colonies directly from a Petri dish without any sample preparation. Nanospray desorption electrospray ionization mass spectrometry (MS), combined with alignment of MS data and molecular networking, enabled monitoring of metabolite production from live microbial colonies from diverse bacterial genera, including *Bacillus subtilis, Streptomyces coelicolor, Mycobacterium smegmatis*, and *Pseudomonas aeruginosa*. This work demonstrates that, by using these tools to visualize small molecular changes within bacterial interactions, insights can be gained into bacterial developmental processes as a result of the improved organization of MS/MS data. To validate this experimental platform, metabolic profiling was performed on *Pseudomonas* sp. SH-C52, which protects sugar beet plants from infections by specific soil-borne fungi [R. Mendes et al. (2011) *Science* 332:1097–1100]. The antifungal effect of strain SH-C52 was attributed to thanamycin, a predicted lipopeptide encoded by a nonribosomal peptide synthetase gene cluster. Our technology, in combination with our recently developed peptidogenomics strategy, enabled the detection and partial characterization of thanamycin and showed that it is a monochlorinated lipopeptide that belongs to the syringomycin family of antifungal agents. In conclusion, the platform presented here provides a significant advancement in our ability to understand the spatiotemporal dynamics of metabolite production in live microbial colonies and communities.

ambient mass spectrometry | microbial ecology | natural products

Microbes use secreted factors to interact, communicate with, and manipulate their local environment and neighboring cell populations in a process known as metabolic exchange (1–5). By using a wide breadth of molecules ranging from signaling compounds to defensive metabolites, metabolic exchange dictates not only basic microbial behavior, such as biofilm formation, sporulation, and motility, but also social interactions, such as syntrophy and quorum sensing, which enables microbes to establish communities (1–5). Despite these secreted factors, also known as the parvome, having a major impact on the phenotypic development of microbial populations, there is a lack of tools that enable scientists to probe the chemistry of microbial colonies in a direct manner. Currently, the chemistry of microbes is usually studied by monitoring individual molecular species and requires a significant time and monetary investment. Our laboratories are interested in the development of tools that make this process more efficient as well as making it easier for nonchemists to study the chemistry of microbes and nonmicrobe cell populations. Ideally, these tools should be easy to implement, compatible with existing infrastructure, and easily incorporated into future protocols. Most of all, they should provide information that current techniques cannot provide and/or improve the ease by which this information is obtained and analyzed. It is also important that chemical changes can be monitored temporally and spatially, as the timing of production and the distribution of metabolic exchange factors within microbial populations can provide valuable insight into the function of these molecules.

Here we present an integration of two methodologies: nanospray desorption electrospray ionization (nanoDESI) MS for direct chemical monitoring of living microbial populations in conjunction with the generation of molecular networks. The latter method enables one to visualize observed molecules as familial groupings in which commonalities within the MS fragmentation data are assessed via vector correlations and displayed as an MS/MS network. Together, these methods provide a powerful workflow for direct chemical analysis of secreted microbial exchange factors in live colonies. To demonstrate this ability, we used nanoDESI to temporally and spatially characterize single and interacting live microbial colonies and then used molecular networking to probe their molecular landscapes providing powerful and unique insight into the extracellular chemistry of pathogenic microbes such as *Serratia marcescens*, *Pseudomonas aeruginosa* PA01, and *Mycobacterium smegmatis* MC2, as well as beneficial microbes such as *Pseudomonas* sp. strain SH-C52, which protects plants from fungal infections (6). Mass spectral molecular networking of strain SH-C52 in conjunction with our peptidogenomic strategy (7) enabled the detection and partial characterization of thanamycin, a chlorinated nonribosomal peptide synthetase derived peptide with antifungal activity.

Results and Discussion

In the past decade, it has become possible to ionize molecules from native surfaces with MS at ambient pressures through the development of novel ionization sources (8–18). Each ionization

Author contributions: J.W., T.A., K.P., B.S.M., J.L., N.B., and P.C.D. designed research; J.W., P.R., T.A., B.S.H., J.Y.Y., R.D.K., J.L., N.B., and P.C.D. performed research; J.W., M.v.d.V., H.G., J.M.R., J.L., N.B., and P.C.D. contributed new reagents/analytic tools; J.W., P.R., T.A., B.S.H., J.Y.Y., R.D.K., M.v.d.V., K.P., H.G., J.M.R., B.S.M., J.L., N.B., and P.C.D. analyzed data; and J.W., N.B., and P.C.D. wrote the paper.

The authors declare no conflict of interest.

This article is a PNAS Direct Submission.

See Commentary on page 10128.

[1]Present address: Roach and Associates, Seymour, WI 54165.

[2]To whom correspondence may be addressed. Email: For the computational aspects of the molecular networks, N.B. (bandeira@ucsd.edu); the development of nanoDESI, J.L. (julia.laskin@pnnl.gov); and MS profiling of microbial colonies and interpretation and generation of molecular networks, P.C.D. (pdorrestein@ucsd.edu).

See Author Summary on page 10150 (volume 109, number 26).

This article contains supporting information online at www.pnas.org/lookup/suppl/doi:10.1073/pnas.1203689109/-/DCSupplemental.

technique, because of its unique ionization mechanisms, has specific applications and uses in diagnostics, forensics, histopathology, and high-throughput screening. Although many of these ionization sources provide "gentle" desorption of surface ions, none of the most widely used ambient ionization methods are delicate enough to not significantly disturb microbial colonies grown on the relatively soft surface of agar medium in a Petri dish. MS analysis of such samples typically results in the destruction of the agar and of the microbial colony (19).

Analysis of solid agar as opposed to liquid culture-based growth conditions is essential, as some microbial behavior including many developmental processes and production of certain secreted factors, such as cannibalistic factors in *Bacillus subtilis*, have only been observed when the microbes were grown on solid media (20). Furthermore, soft-agar culturing is very common in microbiology laboratories. As the ionization source usually dictates the types of samples that can be characterized with MS, we surveyed available ambient pressure ionization sources and discovered that the recently invented nanoDESI source was able to ionize dyes, peptides, and proteins from glass slides and Teflon surfaces without needing a destructive vector, such as a carrier gas (21). Importantly, the nanoDESI ionization source is of fairly simple and straightforward design that can be built at low cost on most common mass spectrometers such as ion traps, Orbitraps, Q-TOFs, and others.

NanoDESI uses solvent delivered via a syringe pump or HPLC through a primary line of fused silica capillary (Fig. 1*A*) in which the terminal end is positioned slightly above the sample surface. A second self-aspirating nanospray capillary is then positioned to form a liquid bridge between the terminal end of the primary fused silica capillary and the anterior end of the nanospray capillary. The analyte is desorbed from the sample surface at the liquid bridge and transferred into the nanospray capillary by capillary action and by vacuum from the heated mass spectrometer inlet. Solvent flow through the nanospray capillary and subsequent electrospray into the mass spectrometer is maintained by the effective vacuum from the mass spectrometer inlet as well as the application of high voltage to the solvent allowing for a constantly flowing yet constant volume microliter sized droplet at the liquid bridge. The size of the droplet formed at the junction between the two capillaries is controlled by adjusting the flow rate into and out of the liquid bridge with the latter being accomplished by adjusting the position of the terminal end of the nanospray capillary relative to the mass spectrometer inlet. When the desired droplet size is achieved at the liquid bridge, surface sampling is achieved by simply making contact with the droplet at the liquid bridge with the sample surface allowing molecules to desorb into the solvent stream followed by immediate analysis by MS. This simple instrument design allows for good interlaboratory reproducibility, as this work was performed on an LTQ-Orbitrap and an LTQ-FT-ICR located in two different laboratories using two independently built custom nanoDESI ionization sources constructed from two different starting platforms and yet yielded very similar results.

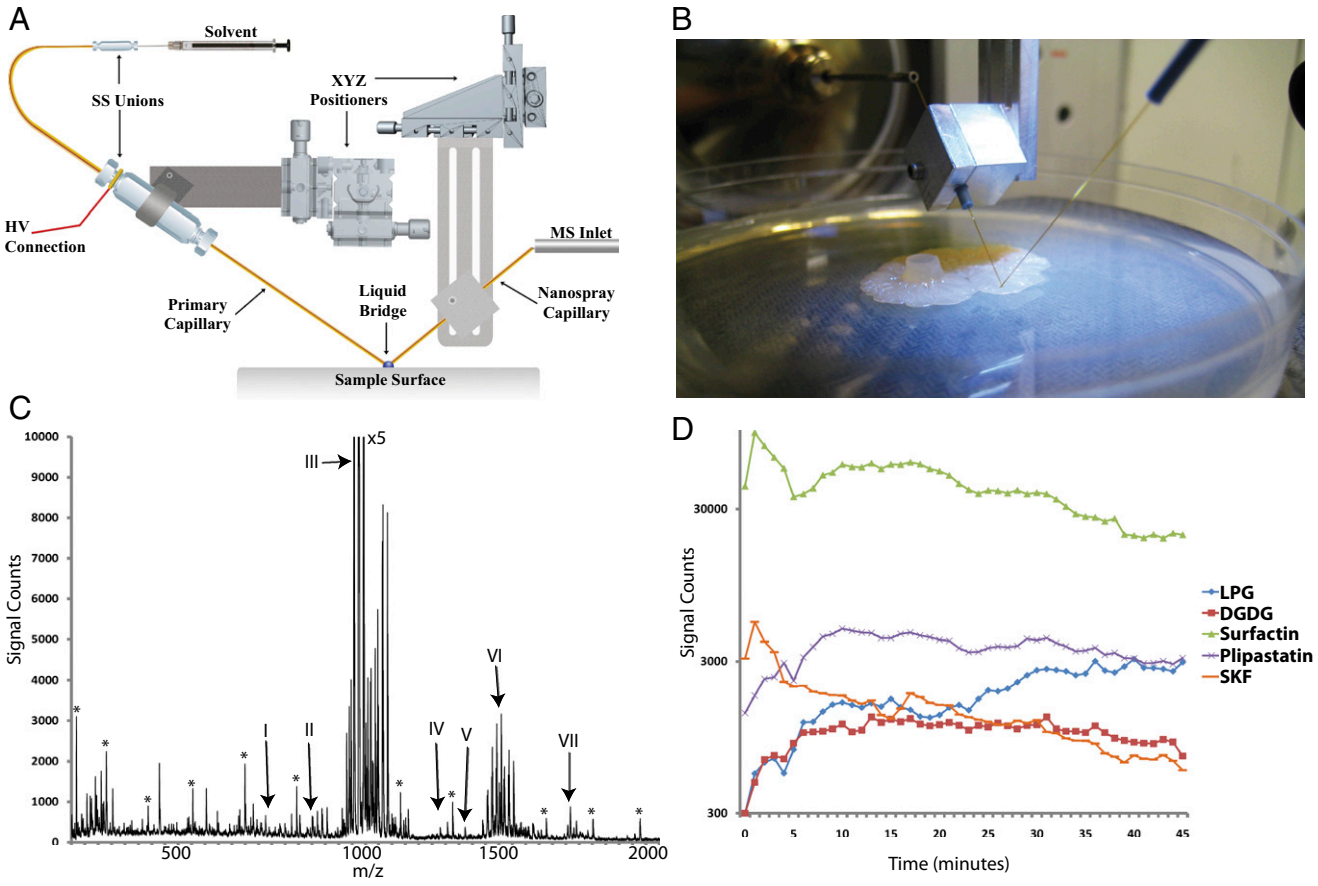

Fig. 1. An overview of nanoDESI analysis of microbial colonies from a Petri dish. (*A*) A schematic overview of nanoDESI. HV, high voltage; SS, stainless steel. (*B*) A photograph of the nanoDESI setup with a microbial colony grown on an agar surface in a Petri dish. (*C*) A mass spectrum obtained from a *B. subtilis* 3610 colony with nanoDESI. Asterisks mark agar sugar signals, "I" is diglycosyl diglyceride, "II" is lysyl-phosphatidylglycerol, "III" is surfactin, "IV" is sublancin (3^+), "V" is sporulation killing factor (2^+), "VI" is plipastatin, and "VII" is subtilosin (2^+). (*D*) Time-dependent analysis at a single location within a 3-d-old *B. subtilis* 3610 colony to indicate the changes in signal intensity of specific molecules over time. DGDG, diglycosyl diglyceride; LPG, lysyl-phosphatidylglycerol; SKF, sporulation killing factor. Solvent used was methanol:acetonitrile:toluene (50:35:15). Movie S1 shows how nanoDESI works in real time.

Initial nanoDESI experiments were carried out on individual biofilm forming colonies of *B. subtilis* 3610, which produces a wide range of well characterized compounds, and therefore provides an ideal test system (20, 22). NanoDESI analysis was shown to be very sensitive in its ability to detect metabolic exchange factors compared with our previous studies of the same system using MALDI thin-layer agar analysis as well as desorption electrospray ionization imprinting (19, 20, 23). As the analysis requires absolutely no sample preparation, the Petri dish containing the sample can simply be placed under the liquid bridge and raised into position until the nanoDESI liquid probe makes contact with the living colony, allowing for instant chemical characterization of the sample surface. Movie S1 provides a live demonstration of this technique where a Petri dish containing colonies of *B. subtilis* 3610 (Movie S1, *Left*) can be seen moving into position while the time-synced computer screen capture of the mass spectra (Movie S1, *Right*) shows the signal response in real time (Fig. 1*B* and Movie S1). As with any surface liquid extraction method, the types of the molecules observed in the spectrum depend on the solvent used. Specifically, compounds soluble in a particular solvent are preferentially desorbed and ionized by nanospray. This flexibility allows for careful tuning of the detection of certain compounds, which can greatly aid in data collection and analysis. The use of a nanospray capillary to direct the postdesorption solvent stream toward the mass spectrometer inlet also results in great signal intensity, as little to no solvent is lost and this allows for fast and easy cleaning of the ionization source because this is the only piece of the source that gets dirty.

Although this technique has proved very versatile within our laboratories across many sample types, no method is without its limitations. First, MS has inherent limitations whereby certain molecules ionize preferentially to other molecules present in the sample. Second, as nanoDESI is a surface sampling method, the chemical composition of the surface will influence ionization efficiency. For instance, although many agar media perform well using nanoDESI, such as Luria–Bertani (LB), International Streptomyces Project Media 2 (ISP2), bovine heart infusion (BHI), potato dextrose agar (PDA), M9 minimal media, Kings medium B (KB), Bennett's medium, and Spider media that we have tested, certain media containing extreme amounts of salt, such as M1 or A1 salt water marine media, and high amounts of glycerol, such as minimal salts glycerol glutamate (MSgg) media, are more challenging because they may cause ion suppression, resulting in decreased analyte signal. This becomes less of an issue as the microbial colony becomes larger and thicker, as the liquid droplet will have minimal contact with the media directly. Also, analysis of viscous samples can lead to clogging of the secondary capillary; however, this can usually be compensated for by changing the polarity of the solvent or by increasing the droplet size. Finally, very conductive sample surfaces, such as conductive indium-tin-oxidemicroscope slides, usually resulted in poor ionization and can be partially corrected for by changing the sample surface or by repeatedly "touching" the sample surface with the droplet as analyte signal is regained when it has been lifted from the conductive surface and will persist for a short time.

As no enrichment steps are performed before analysis, data collected via nanoDESI often result in numerous different classes of compounds represented within a single data set (Fig. 1*C*). In addition, signal for most analytes will persist from a single sampling location for extended periods of time (Fig. 1*D*), allowing for automated collection of tandem MS data. Characterization, annotation, and/or identification of the observed signals thus present a significant challenge. In metabolomics, identification of a molecule is usually carried out by targeted tandem mass fragmentation. The resulting fragmentation pattern can then be compared with metabolomics databases such as METLIN, MassBank, LIPID MAPS, or similar types of databases (24–26). However, as most molecules involved in metabolic exchange are unique to one or a few organisms, there is currently no database that has a searchable mass fragmentation library accessible to the public of sufficient size to cover the unique molecules produced by most known microbes. Therefore, one has to usually resort to manual interpretation of fragmentation data, which unfortunately is currently the state of the art in the natural products field, with the basic experimental paradigm for discovery remaining essentially unchanged since the discovery of penicillin in the late 1920s. Manual analysis of a single MS/MS spectrum typically takes between 10 min to several hours depending on its nature and complexity and is therefore incredibly time-consuming and becomes impractical when the data consists of thousands to millions of MS/MS spectra. Furthermore, even with more evolved "omics"-based analysis methods, obtaining a global visualization of collected data for quality assessment and analysis is a key bottleneck within the workflow (27, 28). In the context of natural products, such tools for data organization and navigation, let alone compound identification, are simply nonexistent. Hence, alternative ways to look at fragmentation data need to be developed.

The visualization of networks by using freeware such as Cytoscape (www.cytoscape.org) is often used for the global display of large data sets such as protein interactions, biochemical pathways, population networks, and even airplane travel (29–32). In biology, such networks enable the direct observation of similarities as well as differences between two or more conditions in which similar entities within the network are clustered together while disparate or unique entities are grouped separately. As MS fragmentation of each individual molecule results in a unique MS/MS fingerprint, we decided to develop network-based workflows to organize large data sets of tandem mass spectra based on the similarity between fragmentation patterns of different, but related, precursor ions. By using a variation of spectral networks designed for proteomic applications, the data are initially simplified by forming consensus spectra whereby identical spectra exhibiting identical precursor ion mass-to-charge ratios (m/z) and fragmentation patterns are merged (33). The simplified MS/MS data are then used for generation of the molecular networks analysis (Fig. 2*A*). Vector similarities are calculated for every possible pair of spectra with a minimum of six matching fragment ions (i.e., peaks) with similarity determined by using a modified cosine calculation that takes into account the relative intensities of the fragment ions as well as the precursor m/z difference between the paired spectra. This extends the concept of spectral alignment as applied in proteomics, with the key exception that certain peptide-specific parameters, such as the use of peak likelihood scores, are generalized to apply this approach to all classes of molecules including lipids, polysaccharides, peptides, metabolites, and proteins. This is important because it is not known ahead of time what class of molecules will be ionized during analysis. When this has been completed, the significantly matched spectrum pairs are reported as a molecular network by using MATLAB scripts whereby each spectrum is allowed to connect to its top K scoring matches (we typically allow a maximum of 10 connections per node). Edges between spectra are retained only if in the top K for both paired spectra and the vector similarity score, represented as a cosine value, of the match is greater than the user-defined threshold. Cosine threshold values are usually set between 0.5 to 0.7 whereby a cosine value of 1.0 indicates identical spectra. Furthermore, the created MS/MS network is processed in MATLAB by removing control spectra representing agar, solvent, or control colonies and assigning colors and m/z-values to nodes. These data are then imported into the free visualization program Cytoscape to visualize the MS/MS networks (29). Cytoscape produces a visual representation of the molecular network where each node (i.e., circle) represents a single consensus MS/MS spectrum for a given parent mass, with the thickness of an edge between connecting nodes being indicative of the similarity score for that spectral pair, with higher scoring matches resulting in thicker connecting edges and, when possible, in closer distances. Depending on Cytoscape's nondeterministic network rendering algorithms, the distance between nodes also depends on the direction and number of connections.

The benefit of such an approach is that, as spectra are organized based on fragmentation similarity, identification of analogues and related compounds becomes much easier. A subset of

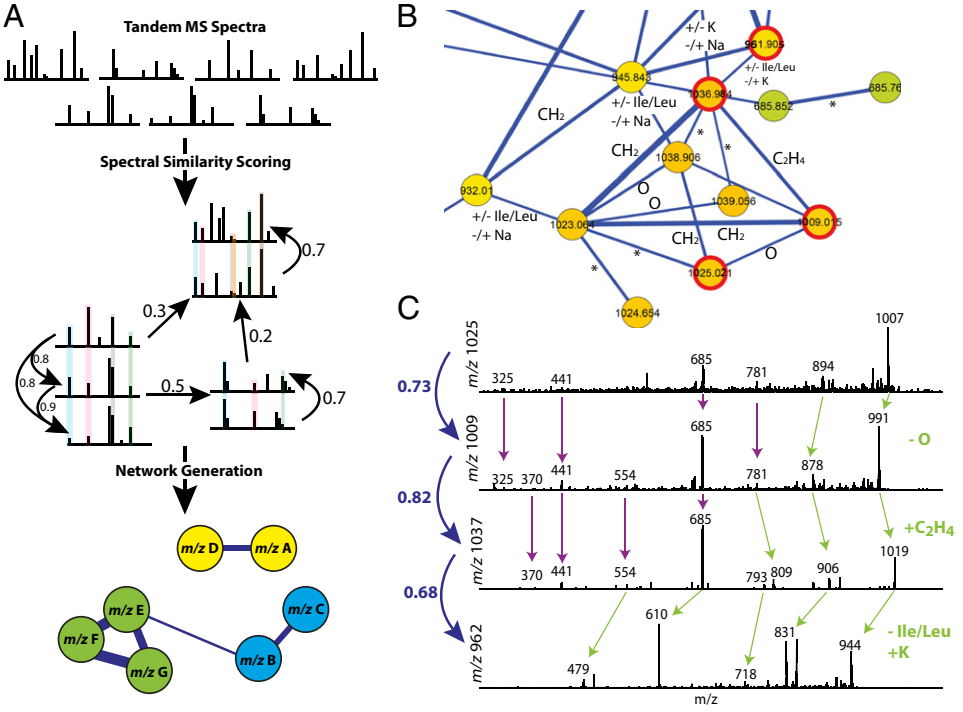

Fig. 2. The generation of molecular networks via spectral alignment. (*A*) A schematic representation of how the molecular networks are generated. The values are representative of cosine scores from 0 to 1, where 1 indicates identical spectra and 0 means no similarity whatsoever. In our data, we found that a cosine cutoff of 0.5 resulted in molecular networks that could be interpreted. The thickness of the edges (blue lines connecting nodes) indicates the level of similarity. (*B*) A Cytoscape visualization of the surfactin single adduct cluster from *B. subtilis* 3610. The full MS/MS network is shown in Fig. 3*A*. Nodes with red border are represented in *C*. (*C*) An example of four spectra from the molecular network shown in *B* that show a strong cosine score.

a molecular network generated for *B. subtilis* 3610 from approximately 25,000 fragmentation spectra is shown in Fig. 2*B*. It shows that analogues of the cyclic lipopeptide surfactin are localized in one region within the MS/MS network. One can see analogues of surfactin separated by 14 or 28 Da largely as a result of differences in lipid side chains and exchange of amino acids (e.g., Gly and Ala) consistent with fragmentation data (Fig. 2*C*). This is a common observation with lipopeptides made via the nonribosomal peptide synthetase paradigm (34). Furthermore, the cluster shows numerous differences of 16 Da between nodes, which is usually attributed to loss or gain of oxygen as well as between Na and K adduct forms of the molecule, and differences by loss of 113 Da consistent with the amino acids Leu and Ile. Although the mass differences caused by oxidation and varying lipid chain length were expected, the loss of Leu/Ile was not. Comparison of the neighboring surfactin MS/MS spectra with the −113 Da MS/MS spectra (*SI Appendix*, Fig. S1) indicated that the parent compound exhibiting the loss of Leu/Ile was still a cyclic lipopeptide. The data are consistent with the biosynthetic pathway "skipping" one of the N-terminal leucine residues during the biosynthesis (Fig. 3*A* and *SI Appendix*, Fig. S2). It should be noted that the location of the nodes within the planar representation of the MS/MS network is not related to the nature of the molecule, as the spatial orientation of the MS/MS network is randomly generated when the network is rendered by Cytoscape. To further aid in identification, MS/MS of known molecules can be included within the MS/MS network and tracked for comparison and for propagation of annotations from known to unknown metabolites. In addition, data visualization using molecular networks allows one to discover molecules that are still unclassified but may be biologically relevant especially when comparing samples from two states, such as different time points or mutants.

To generate a more complete MS/MS network for *B. subtilis*, we combined data sets collected by using a variety of solvents. Specifically, we acquired nanoDESI data by using two solvents: (*i*) a mixture of acetonitrile and 0.05% formic acid in water (ratio of 65:35) for extraction of polar compounds and (*ii*) a methanol: acetonitrile:toluene (50:35:15) mixture for extraction of nonpolar compounds. These experiments enabled the detection of a wide range of molecules within a single mass spectral MS/MS data set including lipids, peptides, small metabolites, and polysaccharides (*SI Appendix*, Fig. S3). Molecular networking of these data revealed metabolic exchange factors such as the lipopeptides surfactin and plipastatin, the ribosomally encoded peptides SKF and subtilosin, fatty acids and lipids such as diglycosyl glycerides and lysyl-phosphatidylglycerols, and various polysaccharides from the agar medium (Fig. 3*A*). For each identified compound, the fragmentation pattern is consistent with the MS/MS reported in the literature (when available), with additional confidence through detection of multiple variations for almost all compounds including H^+, Na^+, and K^+ adducts as well as comparison with purified standards (*SI Appendix*, Fig. S4) (20, 35–37). By using molecular networking, another unique surfactin analogue was found: two nodes with masses of *m/z* 685 (because of variances in spectral quality) were tightly clustered with known surfactins (*m/z* 990–1,100). Further inspection of the spectrum revealed that the mass at *m/z* 685 is a linear analogue of surfactin with the sequence (I/L)(I/L)VD(I/L)(I/L) (Fig. 3*A* and *SI Appendix*, Fig. S5). As the molecular weight of this compound is significantly lower than for any reported surfactin, it would have been much more difficult to recognize the relationship between the MS/MS spectrum of this compound and other surfactins without molecular network visualization.

To highlight the broad applicability of nanoDESI-based molecular networking in microbiology, molecular networks were also constructed for the soil bacteria *Streptomyces coelicolor*, *S. marcescens* ES129 (a common soil organism as well as an opportunistic pathogen that is also associated with eczema), *M. smegmatis* MC2 (a model organism for *Mycobacterium tuberculosis*), and *P. aeruginosa* PAO1 (an opportunistic pathogen of the lung that is also associated with other infections; Fig. 3*B*). A variety of structurally and functionally diverse molecules were identified by using these MS/MS networks, which included quorum-sensing molecules like quinolones and peptides as well as glycolipids, antibiotics, pigments, and oligosaccharides (*SI Appendix*, Fig. S4). Furthermore, it is intriguing to note that a large number of tightly clustered nodes were not annotated, thus highlighting the capability of molecular networks to reveal molecular diversity and potentially novel unidentified compounds.

By using a liquid sampling protocol such as nanoDESI, in conjunction with MS-based molecular networking, the molecular profiles from intact microbial colonies of ~50 different microbes

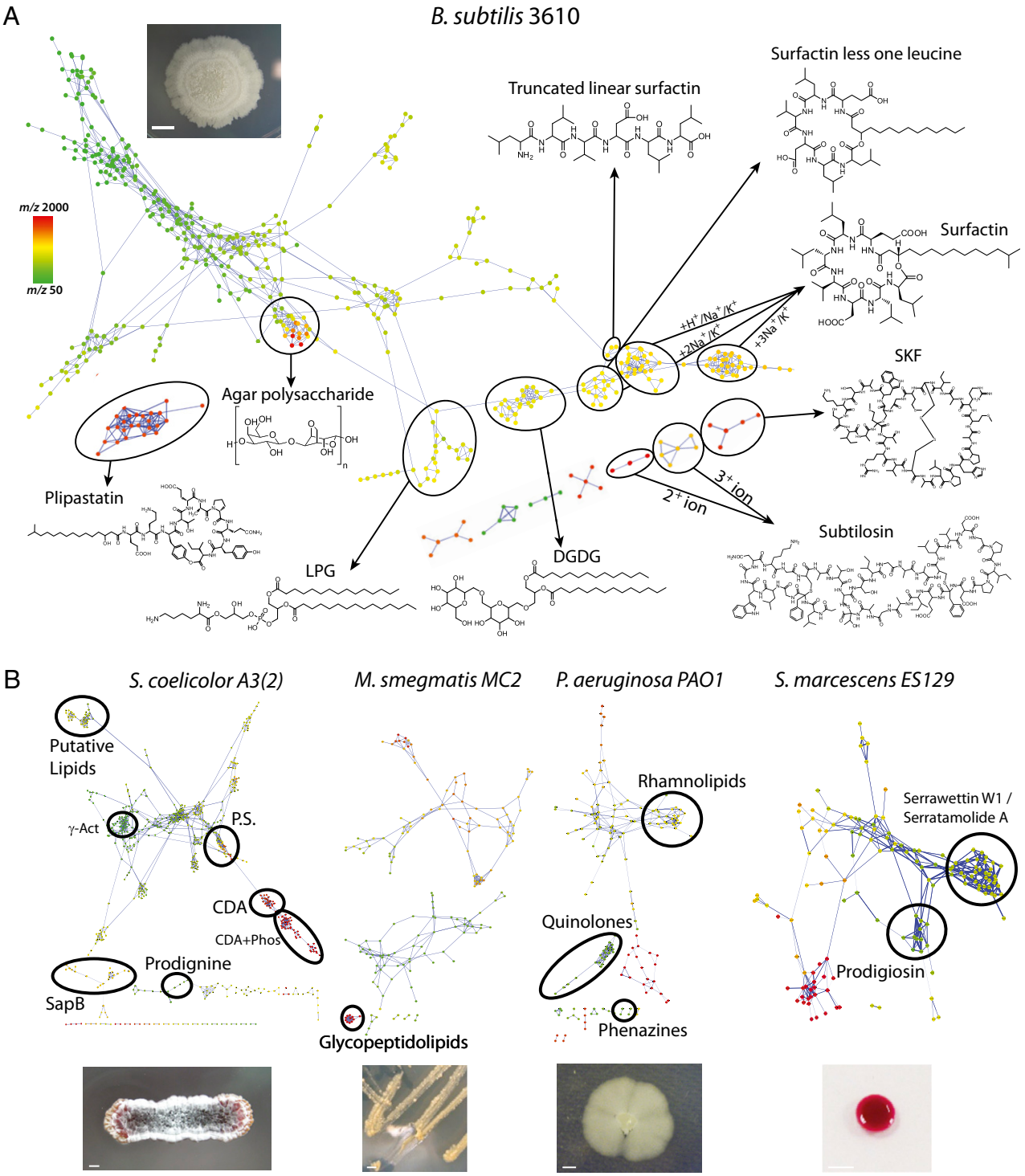

Fig. 3. Molecular networks of nanoDESI fragmentation data obtained from single microbial colonies. (*A*) The annotated molecular network from *B. subtilis* 3610. (*B*) The annotated molecular network of *S. coelicolor* A3(2), *M. smegmatis MC2*, *P. aeruginosa PAO1*, and *S. marcescens* ES129. *Insets*: Images of samples were probed with nanoDESI. The structures of each of the annotated clusters are shown in *SI Appendix*, Figs. S1, S4, and S5. The color scale shows the mass range of the parent ions: green nodes represent the smallest masses; red nodes represent the largest masses fragmented. (Scale bar: 1 mm.)

have already been collected, with the rate-limiting step being the time needed to culture the organisms themselves. Most MS laboratories are not set up for culturing, and therefore tools such as this provide unique opportunities for collaborations with microbiologists and other life scientists. Also, by not selecting for a single class of compounds, these data sets give microbiologists the unique opportunity to gain insight into the general molecular content of their living systems at a given point in time. The small footprint of the probe, ranging from 10 μm to 500 μm depending on capillary size, also allows for discrete profiling across the sample surface to observe differences in metabolic output within a single colony or within a complex microbial population while at the same time providing minimal destructive impact on the sample being analyzed.

Molecular Networking Over Time. Although current tools for temporally monitoring chemical changes of microbial colonies from solid surfaces are time-consuming, nanoDESI analysis combined with data visualization using molecular networking improves the efficiency of such experiments as data are acquired in real time (Movie S1). To monitor live colonies, single colonies of *B. subtilis* 3610 were subjected to repeated nanoDESI measurements over the course of 60 h (Fig. 4*A*), whereby, at each time point, single colonies, grown on ISP2 nutrient agar, were removed from the incubator, photographed, analyzed by nanoDESI for 10 to 20 s, and then placed back into the incubator until the following measurement. Upon visual inspection after each measurement, there appeared to be no significant physical damage and no contamination to the bacterial colony. However, decreased growth of the biomass was observed in the small area (<300 μm^2) sampled during the analysis (Fig. 4*B*, arrow). This resulted in only local effects and did not appear to impact the overall growth of the entire colony compared with control colonies that were not analyzed by nanoDESI (Fig. 4*B*). This local damage to the colony can likely be minimized by using different solvents or smaller capillaries, which can bring the size of the nanoDESI droplet down to less than 10 μm in diameter.

An additional time-course experiment was performed by using separate colonies of *B. subtilis* 3610 whereby, at each time point, approximately 4,000 MS/MS spectra were collected from the colony surface, enabling the creation of molecular networks in a time dependent manner (Fig. 4*C*). The resulting MS/MS network showed a clear increase in metabolic output within *B. subtilis* across the 60-h time period, with increased production of structural variants of the cyclic peptides surfactin, plipastatin, and subtilosin steadily increasing over time. Surfactin can be seen immediately produced after inoculation followed by plipastatin at 12 h and finally subtilosin at 24 h. This latter result mirrors what we have seen by using MALDI-based imaging MS, in which there is a metabolic switch observed between 16 and 22 h resulting in the production of plipastatin and subtilosin. In addition to what we have annotated using MALDI-based imaging MS, we observed the production of the glycopeptide sublancin (38), whose signal only appeared between 12 and 36 h. There was also a major shift in lipid production at the 36-h mark indicating possible

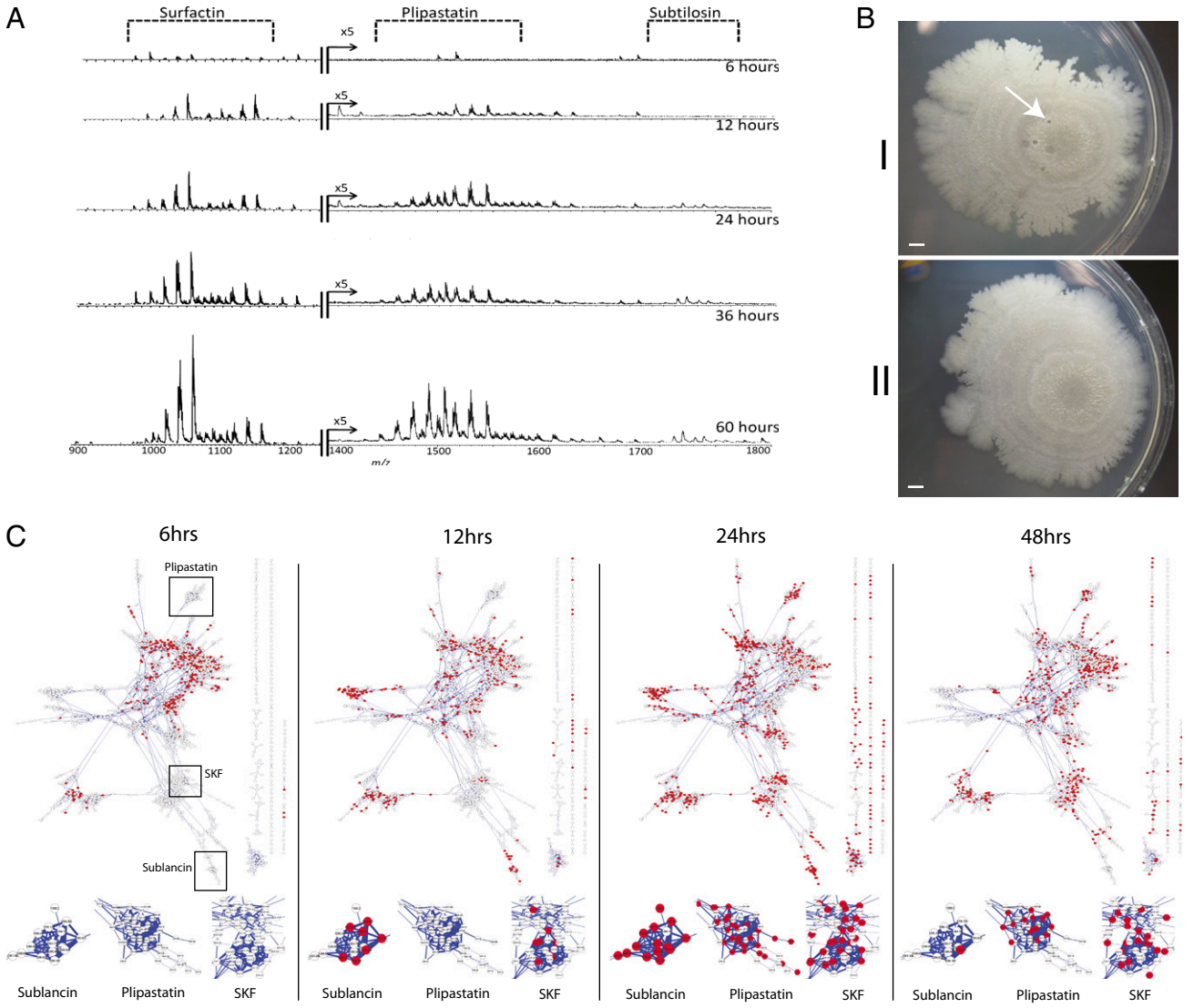

Fig. 4. NanoDESI and molecular networking in a time-dependent manner. (*A*) NanoDESI analysis over time of a single microbial colony of *B. subtilis* 3610. (*B*) An optical photograph of a 72-h colony that was probed eight times and the effect nanoDESI has on the colony phenotype. "I" is the sample (arrow points to one of sampling locations) and "II" is the control that was not subjected to nanoDESI analysis. (*C*) The molecular network and annotation of specific clusters from tandem MS/MS data taken from *B. subtilis* 3610 over time. (Scale bar: 1 mm.)

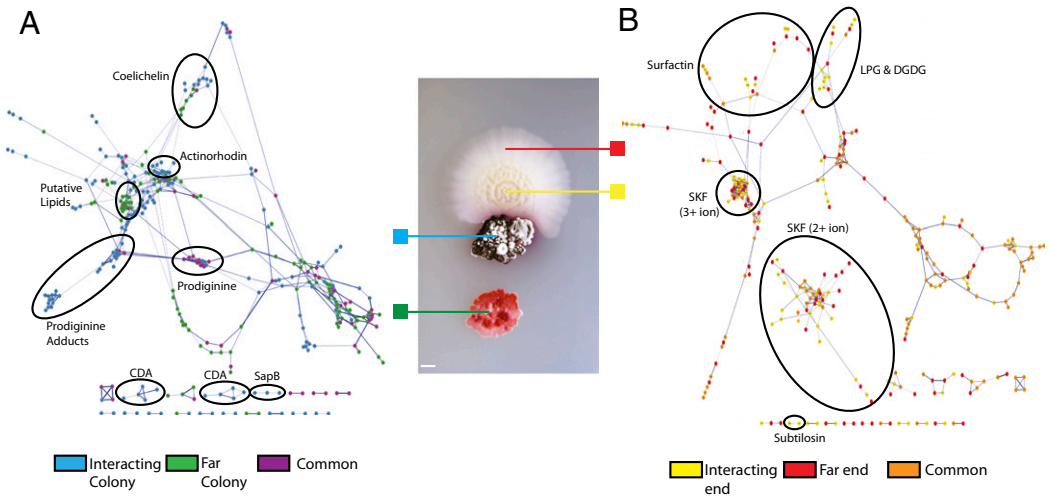

Fig. 5. The molecular network of *S. coelicolor* A3(2) interacting with *B. subtilis* PY79. (*A*) The comparison of the molecular data from the *S. coelicolor* colony adjacent to *B. subtilis* vs. the *S. coelicolor* colony further away. (*B*) The comparison of the molecular data from the interacting and noninteracting sides of the *B. subtilis* PY79 colony. It should be noted that, although PY79 has a frame shift in *sfp*, the phosphopantetheinyl transferase required for surfactin and plipastatin biosynthesis, surfactin is still produced in small amounts (41). This has been observed before by MALDI imaging, as well as imprint desorption electrospray ionization, and can be attributed to promiscuity of another phosphopantetheinyl transferase or a ribosome slippage providing a low amount of in-frame translation of the frame-shifted *sfp* gene (19, 23).

temporal, nutritional or quorum-sensing–based regulation of sublancin production. This observation of transient sublancin production is consistent with the RNA transcript analysis of the biosynthetic enzymes involved in the production of sublancin, which steeply declined after 27 h of culturing (*SI Appendix*, Fig. S6) (39). Lastly, a closer look at the surfactin and plipastatin node clusters show changes in production for specific compound variants over time. Plipastatin is initially produced in its A and B forms, with a gradual shift to only production of plipastatin B (*SI Appendix*, Fig. S7), whereas surfactin produces its longer lipid length variants across the whole time course but produces shorter lipid chain length variants only between 24 and 48 h (*SI Appendix*, Fig. S8). This again shows how the combination of nanoDESI analysis on live microbial colonies and molecular networking is giving unprecedented access to molecular information of microbial systems.

Molecular Networking of Microbial Interactions. Microbial populations in nature almost always exist in assemblages interacting with their neighbors. When *B. subtilis* PY79 (a laboratory domesticated strain of *B. subtilis* 3610 in which most of the polyketide synthase and nonribosomal peptide synthetase metabolic machinery is nonfunctional) interacts with *S. coelicolor* A3(2), *B. subtilis* PY79 elicits pigment production and aerial hyphae formation in *S. coelicolor*, whereas *S. coelicolor* increases production of the cannibalistic factors SKF and SDP in PY79 in the region of interaction (23, 40). Here we show that such interactions can be easily examined by using nanoDESI in combination with molecular networking (Fig. 5).

Samples were prepared by inoculating two individual colonies of *S. coelicolor* 5 mm apart and allowing growth for 18 h at 30 °C, at which time a single 0.5-μL inoculum of *B. subtilis* PY79 was placed 1 mm from one of the *S. coelicolor* colonies. After 36 h, the Petri plate was removed from the incubator and immediately analyzed by nanoDESI whereby tandem mass spectra were automatically collected from each of four sampling locations: the *S. coelicolor* colony farthest from the *B. subtilis* PY79 colony, the *S. coelicolor* colony closest to the *B. subtilis* PY79 colony, the side of the *B. subtilis* PY79 colony closest to *S. coelicolor*, and the side of the *B. subtilis* colony furthest from *S. coelicolor*. Two MS/MS networks were created (one from both *S. coelicolor* colonies combined and one for both *B. subtilis* sampling locations combined as shown in Figure 5*A* and 5*B*, respectively) where background nodes from solvent and agar were removed. The resulting MS/MS network confirms previous reports with findings that actinorhodin and SapB are present at the *S. coelicolor* colony nearest *B. subtilis* whereas the signals for SKF from *B. subtilis* appear more prominently on the interacting side of the *B. subtilis* colony. In addition, the analyses showed that calcium-dependent antibiotic in *S. coelicolor* is also present at the colony interaction interface, as well as many other signals that are currently unknown. Also, although the red pigment prodiginine is present in the near and far *S. coelicolor* colonies, increased production of the compound in the near colony resulted in the formation of prodiginine oligomers and adducts, which range from 400 Da to 1,800 Da as determined by the MS/MS fragmentation data (*SI Appendix*, Fig. S9). The data indicate that multispecies comparative molecular networking is a powerful strategy to characterize molecular differences in live, interacting microbial colonies.

Detection and Partial Characterization of Thanamycin by Comparative Molecular Networks. A recent metagenomic analysis of the rhizosphere microbiome showed that specific members of *Pseudomonadaceae* were identified as key players in the natural protection of sugar beet plants against specific fungal root pathogens (6). Bioassays followed by genetic analyses revealed that the antifungal activity of *Pseudomonas* sp. strain SH-C52 was mediated by a putative 9-aa lipopeptide designated thanamycin (7). Despite significant time and efforts, the investigators were not able to detect this novel compound by traditional biochemical assays. To demonstrate the capacity of the tools described here, live colony analysis by nanoDESI MS coupled with molecular networking were used to detect thanamycin by comparing the WT strain SH-C52 vs. two mutants; one disrupted in the nonribosomal peptide synthetase gene *thaB* and the other in the halogenase gene *thaC2* (Fig. 6*A*). As there were a large number of signals that were fragmented (Fig. 6*B*), the clusters within the MS/MS networks were compared and only the signals unique to specific samples are displayed (Fig. 6*A*). The signals that were only found in the WT strain were subjected to peptidogenomics, an approach that matches peptidic natural products to their genetic signatures, including molecules that are made via the nonribosomal peptide synthetase paradigm (7).

Peptidogenomic analysis revealed that the clusters containing *m/z* 646 $[M+2H]^{2+}$ and *m/z* 1,291 $[M+H]^{+}$ were monochlorinated

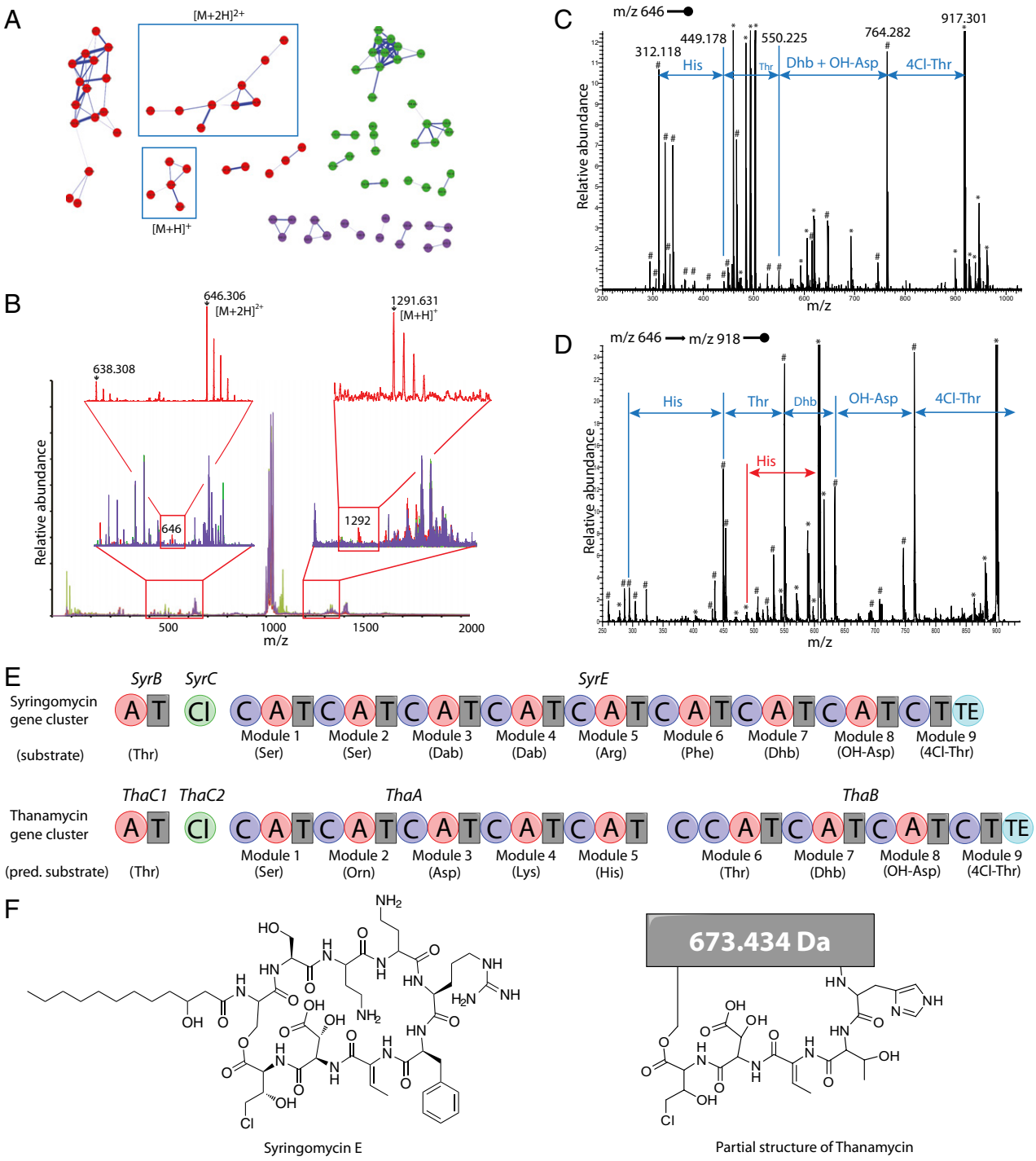

Fig. 6. Partial characterization of thanamycin from live colony analysis: molecular networking and peptidogenomics of *Pseudomonas* sp. strain SH-C52. (*A*) Comparative molecular network of WT strain SH-C52 and two mutants, disrupted in *thaB* or *thaC2*. Red indicates only found in WT, green indicates only found in the *thaC2* mutant, and purple indicates only found in the *thaB* mutant. (*B*) Overlay of the MS spectra of all three strains with the same colors as in *A*. (*C*) MS/MS spectrum of the 2^+ thanamycin ion and annotated sequence tag for thanamycin. Signals with asterisks are the chlorination isotopic signature, and signals with a number sign do not display this feature. (*D*) MS/MS/MS confirmation of the thanamycin signal and its sequence tag. (*E*) Comparison of the syringomycin gene cluster to the thanamycin gene cluster and the corresponding "best" predictions of the adenylation domain specificity according to the Stachelhaus rules (45, 46). The domains described are as follows: T, thiolation domain; A, adenylation domain; Cl, halogenase; TE, thioesterase domain. (*F*) Comparison of the structure of syringomycin and the partial sequence obtained for thanamycin that is consistent with the observed tandem MS data.

(7). In particular, the monochlorination is evident by the 24% contribution of intensity in the +2 Da isotope of ^{37}Cl that is consistent with monochlorinated molecules (Fig. 6*B*, *Inset*), which was also observed in the isotopic patterns in the fragmentation data (*SI Appendix*, Fig.S10). The chlorination is consistent with the non–heme-dependent halogenase found in the thanamycin cluster, which itself exhibits high sequence similarity to the syringomycin biosynthetic pathway from the plant pathogen *P. syringae* pv. Syringae (42, 43), suggesting that thanamycin belongs to the syringomycin family of antifungal agents. Annotation of the MS/

MS and MS/MS/MS data for thanamycin showed that it contained a chlorinated threonine followed by a hydroxyaspartate and a dehydrobutyrate (Fig. 6 *C* and *D*), which is also consistent with the structure of syringomycin (Fig. 6 *E* and *F*) (42–44). Further annotation of the mass spectra extended this sequence tag to include a threonine and histidine, which is consistent with the predictions for the adenylation domain specificities of the gene cluster (45, 46). Full structural and bioactivity characterization of thanamycin is ongoing.

Comparison of the molecular networks of the WT SH-C52 strain and its mutants followed by peptidogenomic analysis allowed us to confirm that we had detected the thanamycin molecule that, despite application of several different cultivation and extraction procedures, eluded detection by traditional approaches. A possible reason why thanamycin was initially missed by conventional approaches was because thanamycin is produced transiently and in low quantities compared with the rest of the molecules observed in the sample. The discovery of thanamycin was made possible by using nanoDESI techniques, and this exemplifies that our methodology allows for the detection of the proverbial needle in the haystack.

Conclusion

By adapting nanoDESI MS for profiling live microbial colonies grown on Petri dishes, we have demonstrated that it is possible to perform highly sensitive metabolic profiling directly off living microbial communities without the need for chemical tags, labels, or any sample preparation whatsoever. This ability to capture a wide variety of molecular classes within a single mass spectrum directly from a live specimen will prove extremely useful in visualizing the "big picture" of these signal transduction networks and will allow researchers to see a more complete chemotype, resulting in more accurate correlations to their observed phenotype. We have also shown that analysis of the MS/MS data by using molecular networking enables detection and visualization of related compounds via spectral relationships within and between data sets as chemical families are grouped together. In addition, MS/MS networks enable dereplication (47) (i.e., finding "known unknowns") and allow for prioritization of the analysis of individual MS/MS signals by finding variation/diversity of molecules across multiple conditions/species even before its identity is determined, as we have shown for detection and partial characterization of thanamycin. Tools such as nanoDESI and molecular networking by spectral alignment are an important addition to our effort to create a "Rosetta stone" for microbial interactions through observing and classifying metabolic exchange (3). In a more general context, the methods described here constitute a powerful set of tools in systems (micro)biology for investigating the spatiotemporal dynamics of diverse metabolic exchange processes.

Methods

Preparation of Bacterial Samples. Colonies of *S. coelicolor* A3(2) were prepared by inoculating 1 μL of harvested spores onto ISP2 nutrient agar (7.5 g agar, 5 g malt extract, 2 g yeast extract, and 2 g dextrose in 500 mL milli-Q water) and incubating at 30 °C until the desired time point. Colonies of *B. subtilis* 3610/PY79, *S. marcescens* ES129, *P. aeruginosa* PAO1, and *Pseudomonas* sp. strain SH-C52 were prepared by inoculating 1 μL of cell stock into 4 mL of LB broth and incubating at 30 °C until an OD_{600} of 0.4 was reached. From this starter culture, 0.2 to 1.0 μL was inoculated onto ISP2 nutrient agar and allowed to grow at 30 °C until the desired time point. Colonies of *M. smegmatis* MC2 were prepared by inoculating 1 μL of cell stock into 4 mL of LB broth and incubating at 30 °C until an OD_{600} of 0.4 was reached. From this starter culture, 1.0 μL was inoculated onto LB nutrient agar and allowed to grow at 30 °C until the desired time point. For the data shown, *S. coelicolor*, *S. marcescens*, *P. aeruginosa*, *M. smegmatis*, and *P. SH-C52* were analyzed by nanoDESI at 72, 48, 36, 48, and 42 h after inoculation, respectively.

Cocultures of *B. subtilis* PY79 and *S. coelicolor* A3(2) were prepared by inoculating two 1-μL colonies of *S. coelicolor* onto ISP2 nutrient agar ~5 mm apart and allowing to grow for 18 h at 30 °C, to fortify the colony, after which 0.2 μL of *B. subtilis* PY79 was inoculated 1 mm from the terminal end of one of the *S. coelicolor* colonies and allowed to grow for an additional 36 h at 30 °C.

NanoDESI Instrument Setup. Data collection was performed by using two different nanoDESI ionization sources of similar design in two different laboratories. The first was located in the Laskin laboratory at Pacific Northwest National Laboratory and was coupled to a Thermo LTQ-Orbitrap mass spectrometer equipped with collision-induced dissociation capabilities. The second nanoDESI source was located in the Dorrestein laboratory at the University of California, San Diego, and was coupled to a Thermo LTQ-FT-ICR MS also capable of collision-induced dissociation. The overall design of both instruments, as illustrated in Fig. 1*A*, is very simple in that solvent is loaded into a 250- or 500-μL syringe, which is placed in a syringe pump. Solvent is initially pushed through 300 μm o.d. × 100 μm i.d. fused silica capillary tubing to a stainless steel union in which voltage is applied and the tubing is stepped down to 150 μm o.d. × 50 μm i.d., which continues to the liquid bridge, where it meets the self-aspirating nanospray capillary. The position of both the primary and the nanospray capillaries are controlled by two separate xyz manual positioners and monitored by mounted video cameras. All analyses were performed in positive ion mode in the mass range of *m/z* from 100 to 2,000. Both the primary and the nanospray capillaries were 150 μm o.d. × 50 μm i.d., with solvent being delivered and removed from the liquid bridge at approximate 45° angles. The spray voltage was kept between 2.0 and 3.0 kV depending on the solvent, with the solvents largely being acetonitrile/0.05% formic acid in water (1:1) or acetonitrile:toluene: methanol (35:15:50) running at a flow rate of 0.8 to 2.5 μL/min. The droplet size using this configuration was ~200 μm in diameter.

NanoDESI Profiling and Time-Course Experiments. Profiling and time-course experiments were performed by using a simple protocol because absolutely no sample preparation is needed for analysis. For each measurement, samples were removed from the incubator, photographed, and placed directly onto the nanoDESI sample stage for analysis. By using a series of mounted cameras for guidance, the sample was manually raised until the liquid bridge came into contact with the sample surface (Movie S1). Signal from the sample surface was produced almost immediately, and, depending on the nature of the sample and analyte, remained consistent enough at a single location to usually allow for 20-min acquisitions of data dependent tandem mass spectra. For time-course experiments, the solvent droplet was only in contact with the colony for 20 s for each measurement, after which the sample was placed back in the incubator until the following time point. For experiments in which voltage was not used, the flow rate of the nanoDESI was stopped before bringing the sample to the probe, the droplet was allowed to sit on the colony surface for 20 s, the sample was removed, and the flow rate and voltage were turned back on for data collection. Control samples were treated exactly the same as samples that were analyzed by using the nanoDESI whereby they were removed from the incubator at each time point, photographed, left outside the incubator while the samples were analyzed, and then placed back into the incubator without being analyzed by nanoDESI themselves.

Construction of Molecular MS/MS Networks. Tandem mass spectra were clustered with MS-Cluster (33) to group repeatedly acquired spectra from the same molecules into cluster-consensus spectra with a higher signal-to-noise ratio. As the obtained spectra contained fragmentation signatures for not only peptides, but also polysaccharides, lipids, small-molecular metabolites, and even small proteins, the following nondefault settings were used to avoid bias toward peptide scoring: clustering model LTQ_TRYP, minimum spectrum quality 0 (to avoid peptide-specific spectrum quality metrics), disabled assign-charges and correct-pm commands. Cluster-consensus spectra were processed by applying square root transforms to fragment peak intensities (to increase/decrease the influence of low/high intensity peaks, respectively), scaled to Euclidian norm 1 and used for the construction of molecular MS/MS networks in two steps: (*i*) pairwise spectral alignment to find pairs of spectra from related molecules and (*ii*) selection of significant pairwise alignments to define the MS/MS network. For each pair of spectra S and S′, spectral alignment was computed by defining modification mass as follows:

$$M = PM(S') - PM(S) \quad [1]$$

With the difference between their precursor masses and by finding matching fragment peaks between S and S′ as follows: (*i*) peaks p∈S and p′∈S′ are eligible matches if $|mz(p) - mz(p')| \leq t$ or if $|mz(p) + M - mz(p')| \leq t$, for a predetermined fragment *m/z* tolerance t; (*ii*) match scores between matching peaks are defined as the product of their normalized peak intensities; (*iii*) peak matches define a bipartite matching problem of selecting the highest scoring subset of matching peaks whereby each peak is matched

to at most one peak in the other spectrum (a classical computer science problem with well known algorithms for finding optimal solutions). As a result of the spectrum intensity scaling and peak match scores, the optimal solution of each bipartite matching problem corresponds to the highest possible cosine between the intensities of matched peaks (48). Pairs of cluster-consensus spectra were considered for spectral alignment if their molecular masses differed by less than 45% and as much as 400 Da. Each spectrum retained only as many as 10 highest-cosine alignments and pair wise alignments with cosine $\geq$0.7 and $\geq$6 matched peaks were used to define the MS/MS networks (49) whereby each node is a cluster-consensus spectrum and each edge corresponds to a significant pair wise alignment. All algorithms assumed precursor mass tolerance of 1.0 Da and fragment mass tolerance of 0.3 Da.

ACKNOWLEDGMENTS. The authors thank Peter Tonge (Stony Brook University) for providing the *Mycobacterium smegamatis* strain. Work in this area in the P.C.D. laboratory for the development of real-time MS was supported by National Institutes of Health (NIH) Grant GM094802; work on interspecies interaction was supported by NIH Grant AI095125 and Johnson & Johnson; work in this area in the N.B. laboratory was supported by NIH Grant 1-P41-RR024851; and work in this area in the K.P. laboratory is supported by NIH grant AI095125. This work was also supported in part by NIH Grant GM085770 (to B.S.M.); the German Research Foundation, Deutsche Forschungsgemeinschaft (DFG), Grant DFG-FOR854 GR2673/2-1 (to H.G.); the Chemical Imaging Program at Pacific Northwest National Laboratory (PNNL) (P.R. and J.L.); the US Department of Energy (DOE) Science Undergraduate Laboratory Internship (SULI) program at PNNL (B.S.H.); Dutch Science Organization Ecology Regarding Gene-Modified Organisms Grant838.06.101 (to M.v.d.V. and J.M.R.); and Netherlands Genomics Initiative (NGI) ECOLINC and PreSeed (M.v.d.V. and J.M.R.). A part of the research described in this paper was performed at the W. R. Wiley Environmental Molecular Sciences Laboratory, a national scientific user facility sponsored by the DOE's Office of Biological and Environmental Research and located at PNNL, which is operated by Battelle for the DOE.

1. Davies J (2011) How to discover new antibiotics: harvesting the parvome. *Curr Opin Chem Biol* 15:5–10.
2. Romero D, Traxler MF, López D, Kolter R (2011) Antibiotics as signal molecules. *Chem Rev* 111:5492–5505.
3. Phelan VV, Liu WT, Pogliano K, Dorrestein PC (2012) Microbial metabolic exchange—the chemotype-to-phenotype link. *Nat Chem Biol* 8:26–35.
4. Davies J, Ryan KS (2011) Introducing the parvome: Bioactive compounds in the microbial world. *ACS Chem Biol* 7:252–259.
5. Ratcliff WC, Denison RF (2011) Microbiology. Alternative actions for antibiotics. *Science* 332:547–548.
6. Mendes R, et al. (2011) Deciphering the rhizosphere microbiome for disease-suppressive bacteria. *Science* 332:1097–1100.
7. Kersten RD, et al. (2011) A mass spectrometry-guided genome mining approach for natural product peptidogenomics. *Nat Chem Biol* 7:794–802.
8. Harris GA, Nyadong L, Fernandez FM (2008) Recent developments in ambient ionization techniques for analytical mass spectrometry. *Analyst (Lond)* 133: 1297–1301.
9. Takáts Z, Wiseman JM, Gologan B, Cooks RG (2004) Mass spectrometry sampling under ambient conditions with desorption electrospray ionization. *Science* 306:471–473.
10. Cody RB, Laramée JA, Durst HD (2005) Versatile new ion source for the analysis of materials in open air under ambient conditions. *Anal Chem* 77:2297–2302.
11. Harper JD, et al. (2008) Low-temperature plasma probe for ambient desorption ionization. *Anal Chem* 80:9097–9104.
12. Peng IX, Shiea J, Ogorzalek Loo RR, Loo JA (2007) Electrospray-assisted laser desorption/ionization and tandem mass spectrometry of peptides and proteins. *Rapid Commun Mass Spectrom* 21:2541–2546.
13. Zhu L, Gamez G, Chen H, Chingin K, Zenobi R (2009) Rapid detection of melamine in untreated milk and wheat gluten by ultrasound-assisted extractive electrospray ionization mass spectrometry (EESI-MS). *Chem Commun (Camb)* 5):559–561.
14. Rosana M, et al. (2011) Ambient mass spectrometry: Bringing MS into the "real world". *Anal Bioanal Chem* 398:265–294.
15. Zhanga I, et al. (2011) Rapid direct lipid profiling of bacteria using desorption electrospray ionization mass spectrometry. *Int J Mass Spectrom* 301:37–44.
16. Song Y, Talaty N, Tao WA, Pan Z, Cooks RG (2007) Rapid ambient mass spectrometric profiling of intact, untreated bacteria using desorption electrospray ionization. *Chem Commun (Camb)* 1):61–63.
17. Shiea J, et al. (2005) Electrospray-assisted laser desorption/ionization mass spectrometry for direct ambient analysis of solids. *Rapid Commun Mass Spectrom* 19: 3701–3704.
18. Nyadong L, et al. (2009) Reactive desorption electrospray ionization mass spectrometry (DESI-MS) of natural products of a marine alga. *Anal Bioanal Chem* 394: 245–254.
19. Watrous JD, Hendricks N, Meehan MJ, Dorrestein PC (2010) Capturing bacterial metabolic exchange using thin film desorption electrospray ionization-imaging mass spectrometry. *Anal Chem* 82:1598–1600.
20. Liu WT, et al. (2010) Imaging mass spectrometry of intraspecies metabolic exchange revealed the cannibalistic factors of Bacillus subtilis. *Proc Natl Acad Sci USA* 107: 16286–16290.
21. Roach PJ, Laskin J, Laskin A (2010) Nanospray desorption electrospray ionization: An ambient method for liquid-extraction surface sampling in mass spectrometry. *Analyst (Lond)* 135:2233–2236.
22. Stein T (2005) Bacillus subtilis antibiotics: Structures, syntheses and specific functions. *Mol Microbiol* 56:845–857.
23. Yang YL, Xu Y, Straight P, Dorrestein PC (2009) Translating metabolic exchange with imaging mass spectrometry. *Nat Chem Biol* 5:885–887.
24. Smith CA, et al. (2005) METLIN: A metabolite mass spectral database. *Ther Drug Monit* 27:747–751.
25. Horai H, et al. (2010) MassBank: A public repository for sharing mass spectral data for life sciences. *J Mass Spectrom* 45:703–714.
26. Dennis EA, et al. (2005) The LIPID MAPS approach to lipidomics. *Functional Lipidomics*, eds Feng L, Prestwich GD (CRC/Taylor and Francis, Boca Raton, FL), pp 1–15.
27. Bowen BP, Northen TR (2010) Dealing with the unknown: metabolomics and metabolite atlases. *J Am Soc Mass Spectrom* 21:1471–1476.
28. Gupta N, Bandeira N, Keich U, Pevzner PA (2011) Target-decoy approach and false discovery rate: when things may go wrong. *J Am Soc Mass Spectrom* 22:1111–1120.
29. Smoot ME, Ono K, Ruscheinski J, Wang PL, Ideker T (2011) Cytoscape 2.8: New features for data integration and network visualization. *Bioinformatics* 27:431–432.
30. Cline MS, et al. (2007) Integration of biological networks and gene expression data using Cytoscape. *Nat Protoc* 2:2366–2382.
31. Shannon P, et al. (2003) Cytoscape: A software environment for integrated models of biomolecular interaction networks. *Genome Res* 13:2498–2504.
32. Dockstader K, et al. (2011) Temporal analysis of mRNA and miRNA expression in transgenic mice overexpressing Arg- and Gly389 polymorphic variants of the β1-adrenergic receptor. *Physiol Genomics* 43:1294–1306.
33. Frank AM, et al. (2008) Clustering millions of tandem mass spectra. *J Proteome Res* 7: 113–122.
34. Fischbach MA, Walsh CT (2006) Assembly-line enzymology for polyketide and nonribosomal Peptide antibiotics: Logic, machinery, and mechanisms. *Chem Rev* 106:3468–3496.
35. Kawulka KE, et al. (2004) Structure of subtilosin A, a cyclic antimicrobial peptide from Bacillus subtilis with unusual sulfur to alpha-carbon cross-links: Formation and reduction of alpha-thio-alpha-amino acid derivatives. *Biochemistry* 43:3385–3395.
36. Gidden J, Denson J, Liyanage R, Ivey DM, Lay JO (2009) Lipid compositions *in Escherichia coli* and *Bacillus subtilis* during growth as determined by MALDI-TOF and TOF/TOF mass spectrometry. *Int J Mass Spectrom* 283:178–184.
37. Clejan S, Krulwich TA, Mondrus KR, Seto-Young D (1986) Membrane lipid composition of obligately and facultatively alkalophilic strains of *Bacillus spp*. *J Bacteriol* 168:334–340.
38. Oman TJ, Boettcher JM, Wang H, Okalibe XN, van der Donk WA (2011) Sublancin is not a lantibiotic but an S-linked glycopeptide. *Nat Chem Biol* 7:78–80.
39. Blom E-J, Ridder AN, Lulko AT, Roerdink JB, Kuipers OP (2011) Time-resolved transcriptomics and bioinformatic analyses reveal intrinsic stress responses during batch culture of *Bacillus subtilis*. *PLoS ONE* 6:e27160.
40. Butcher RA, et al. (2007) The identification of bacillaene, the product of the PksX megacomplex in Bacillus subtilis. *Proc Natl Acad Sci USA* 104:1506–1509.
41. Earl AM, Losick R, Kolter R (2008) Ecology and genomics of *Bacillus subtilis*. *Trends Microbiol* 16:269–275.
42. Vaillancourt FH, Yin J, Walsh CT (2005) SyrB2 in syringomycin E biosynthesis is a nonheme Fe^{II} α-ketoglutarate- and O_2-dependent halogenase. *Proc Natl Acad Sci USA* 102:10111–10116.
43. Singh GM, Vaillancourt FH, Yin J, Walsh CT (2007) Characterization of SyrC, an aminoacyltransferase shuttling threonyl and chlorothreonyl residues in the syringomycin biosynthetic assembly line. *Chem Biol* 14:31–40.
44. Raaijmakers JM, de Bruijn I, de Kock MJD (2006) Cyclic lipopeptide production by plant-associated *Pseudomonas spp*.: Diversity, activity, biosynthesis, and regulation. *Mol Plant Microbe Interact* 19:699–710.
45. Rausch C, Weber T, Kohlbacher O, Wohlleben W, Huson DH (2005) Specificity prediction of adenylation domains in nonribosomal peptide synthetases (NRPS) using transductive support vector machines (TSVMs). *Nucleic Acids Res* 33:5799–5808.
46. Medema MH, et al. (2011) antiSMASH: Rapid identification, annotation and analysis of secondary metabolite biosynthesis gene clusters in bacterial and fungal genome sequences. *Nucleic Acids Res* 39(Web server issue):W339-46.
47. Corley DG, Durley RC (1994) Strategies for database dereplication of natural products. *J Nat Prod* 57:1484–1490.
48. Stein SE, Scott DR (1994) Optimization and testing of mass spectral library search algorithms for compound iden*tification*. *J Am Soc Mass Spectrom* 5:859–866.
49. Bandeira N, Tsur D, Frank A, Pevzner PA (2007) Protein identification by spectral networks analysis. *Proc Natl Acad Sci USA* 104:6140–6145.

Mass spectral molecular networking of living microbial colonies: Supplementary Information

Jeramie Watrous[ab], Patrick J. Roach[c]*, Theodore Alexandrov[bh], Brandi S. Heath[c], Jane Y. Yang[ab], Roland Kersten,[ad] Menno vander Voort[i], Kit Pogliano[j], Harald Gross[k], Jos M. Raaijmakers[i], Bradley S. Moore[ad], Julia Laskin[cl], Nuno Bandeira[bfgl] and Pieter C. Dorrestein[abdl]

[a.] Department of Pharmacology and Department of Chemistry and Biochemistry, University of California, San Diego, La Jolla, California, USA.

[b.] Skaggs School of Pharmacy and Pharmaceutical Sciences, University of California, San Diego, La Jolla, California, USA.

[c.] Chemical and Materials Sciences Division, Pacific Northwest National Laboratory, P.O. Box 999, MSIN K8-88, Richland, WA 99352.

[d.] Center for Marine Biotechnology and Biomedicine, Scripps Institution of Oceanography.

[f.] Department of Computer science and Engineering, University of California, San Diego, La Jolla, California, USA.

[g.] NCRR/UCSD Center for Computational Mass Spectrometry.

[h.] Center for Industrial Mathematics, University of Bremen, Bibliothekstr. 1, Bremen, Germany.

[i.] Laboratory of Phytopathology, Wageningen University, Droevendaalsesteeg 1, Wageningen PB6708, Netherlands.

[j.] Division of biological sciences, University of California, San Diego, La Jolla, California, USA.

[k.] Institute for Pharmaceutical Biology, University of Bonn, 53115 Bonn, Germany

[l.] To whom correspondence should be addressed. For the computational aspects of the molecular networks, Nuno Bandeira [bandeira@ucsd.edu], the development of nanoDESI, Julia Laskin [Julia.Laskin@pnnl.gov], mass spectrometric profiling of microbial colonies and interpretation and generation of molecular networks, Pieter C. Dorrestein [pdorrestein@ucsd.edu].

*. Present address, Roach & Associates, 856 North Main Street, Seymour, WI 54165

Table of Contents

Figure S1: Annotation of surfactin less leucine.....3-5

Figure S2: Proposed biosynthetic skipping mechanism.....6

Figure S3: Example of nanoDESI solvent bias.....7

Figure S4: Annotations for observed molecules.....8-30

Figure S5: Annotation of linear surfactin peptide.....31-32

Figure S6: Sublancin RNA transcript data.....33

Figure S7: Plipastatin time course data.....34

Figure S8: Surfactin time course data.....35

Figure S9: Prodiginine analogs.....36-37

Figure S10: Example MS isotopic peak ratios.....38

Video 1 legend:.....39

References.....40

Figure S1: Annotated MS/MS spectra for surfactin missing one leucine residue

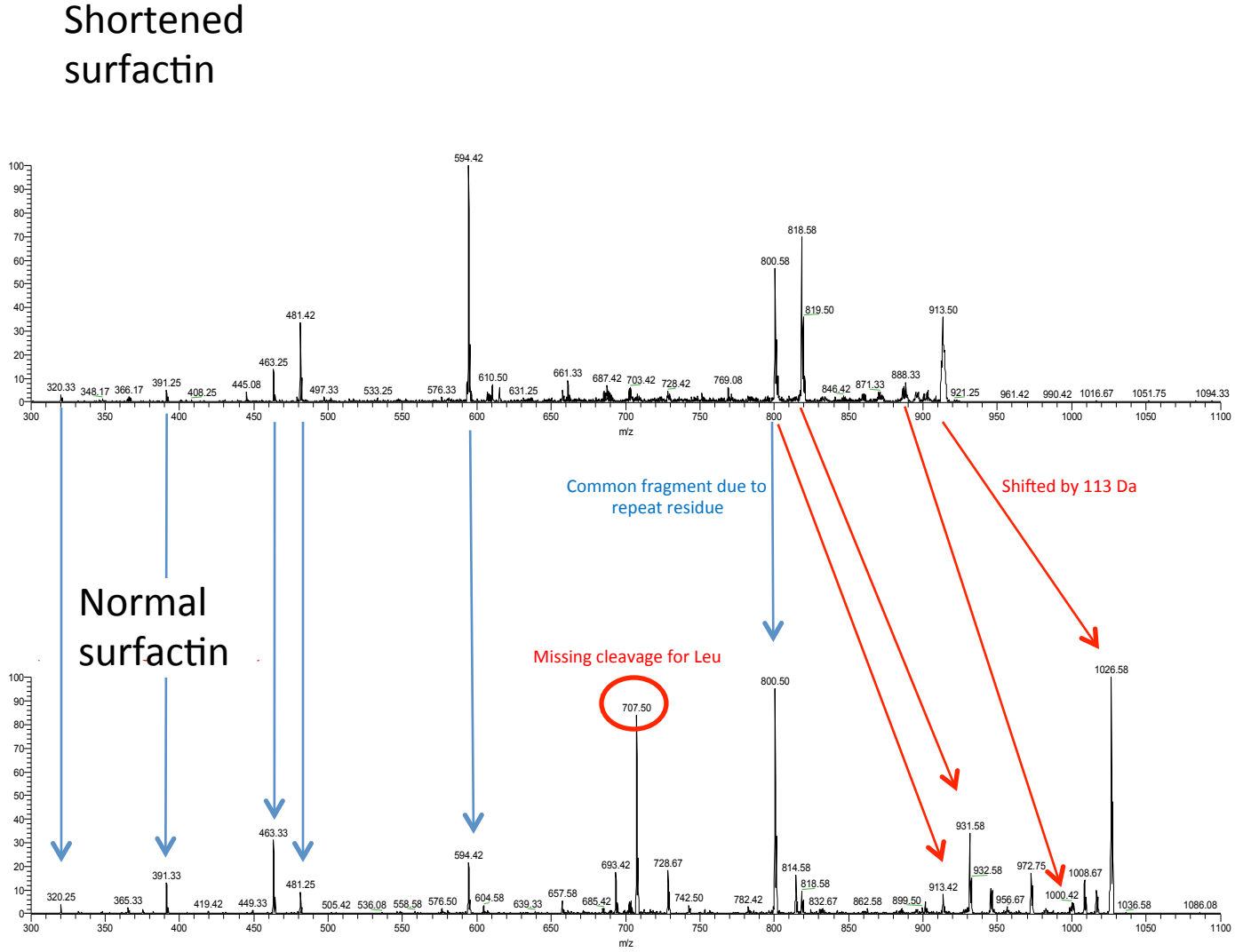

Description: Comparison of the MS^2 CID fragmentation pattern for the surfactin species missing the single leucine residue (top) with the CID fragmentation pattern for the known surfactin compound containing the leucine (bottom) shows identical daughter ions for all fragments on the C-terminal side of the missing leucine (blue arrows) while all daughter ions on the N-terminal side of the missing residue are shifted by the mass of leucine (113 Da...red arrows). Also, the daughter ion for the cleavage between the repeat leucines is missing in the shortened surfactin spectra (red circle).

Figure S1: Annotated MS/MS spectra for surfactin missing one leucine residue

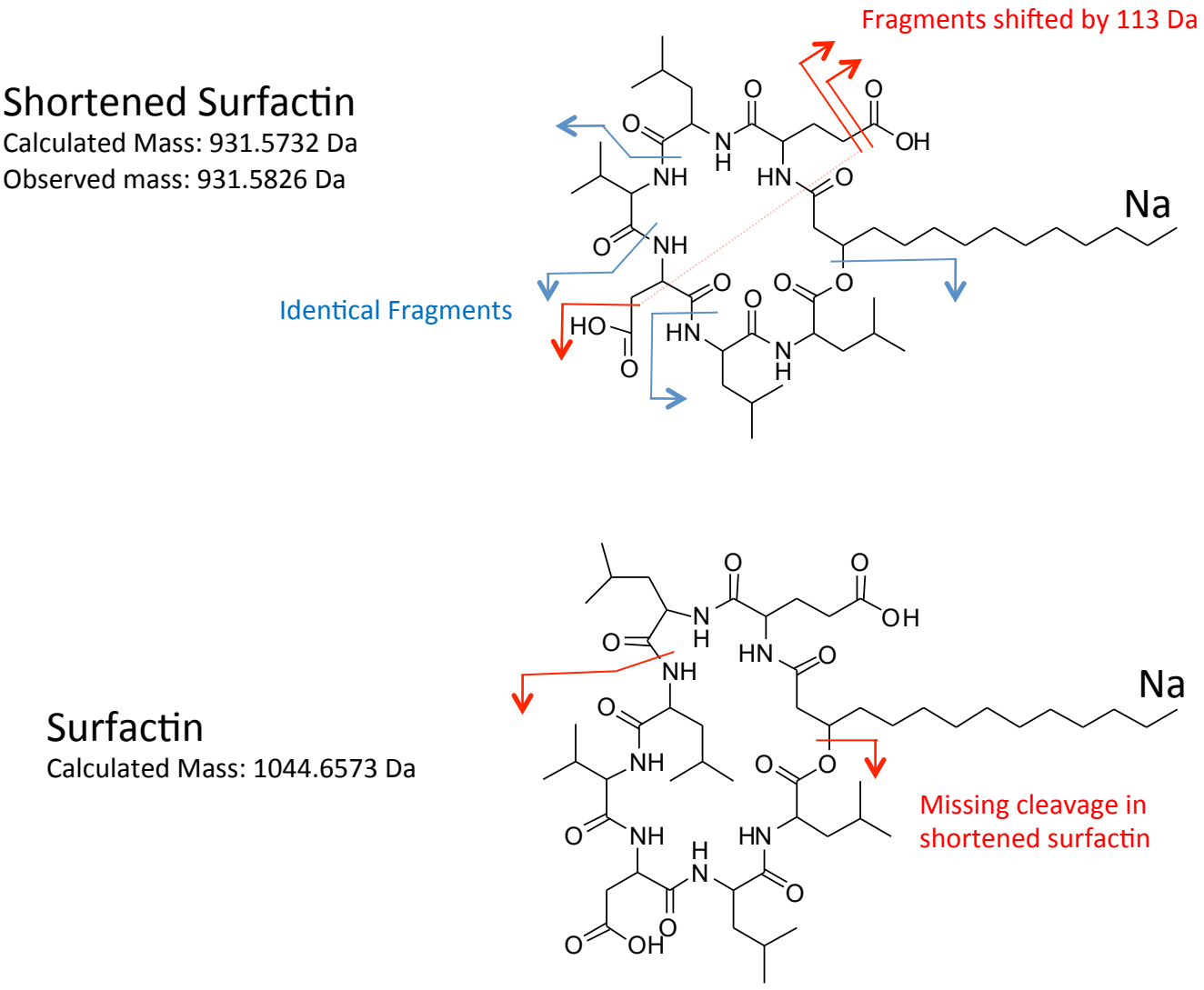

Description: Comparison of the structure for the surfactin species missing the single leucine residue (top) with the structure of the known surfactin compound containing the leucine (bottom) shows identical daughter ions for all fragments on the C-terminal side of the missing leucine (blue arrows) while all daughter ions on the N-terminal side of the missing residue are shifted by the mass of leucine (113 Da...red arrows).

Figure S1: Annotated MS/MS spectra for surfactin missing one leucine residue

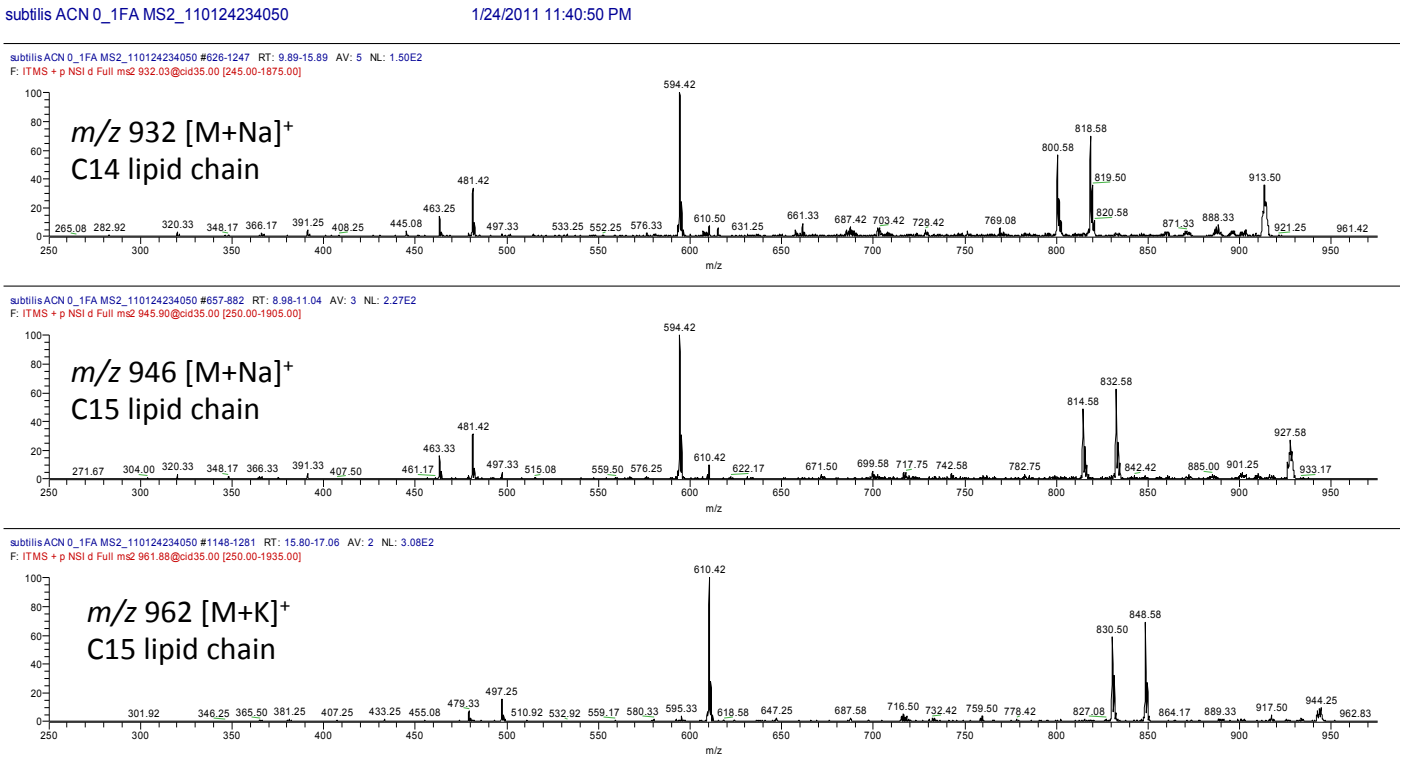

Description: Multiple species of the shortened surfactin compound were observed including C14, C15 and C16 lipid chain lengths with Na and K adducts for each. The above spectra show an example subset of the observed data.

Figure S2: Proposed biosynthetic mechanism for skipping of a leucine residue during surfactin production

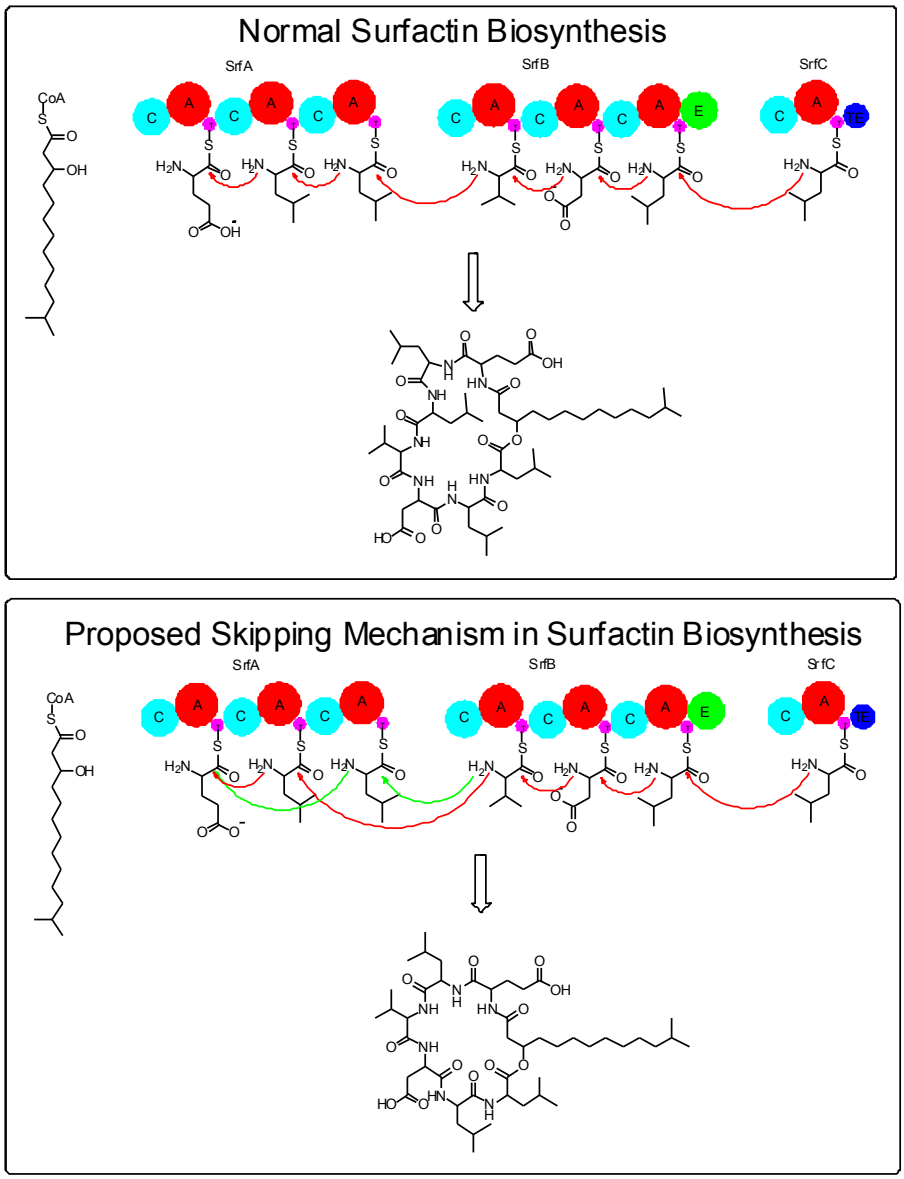

Description: The top mechanism shows the typical surfactin biosynthesis while the bottom figure is a proposed mechanism to possibly explain how the biosynthetic machinery can skip one of the repeat leucine residues during production. Here we hypothesize that it may be possible for SrfB to receive the growing lipopeptide from SrfA after either leucine has been added in module 1 or 2 or that the product from module 1 can skip module 2 and go straight to module 3 (green arrows).

Figure S3: nanoDESI MS1 spectra from *Bacillus subtilis* 3610 using polar and non-polar solvent

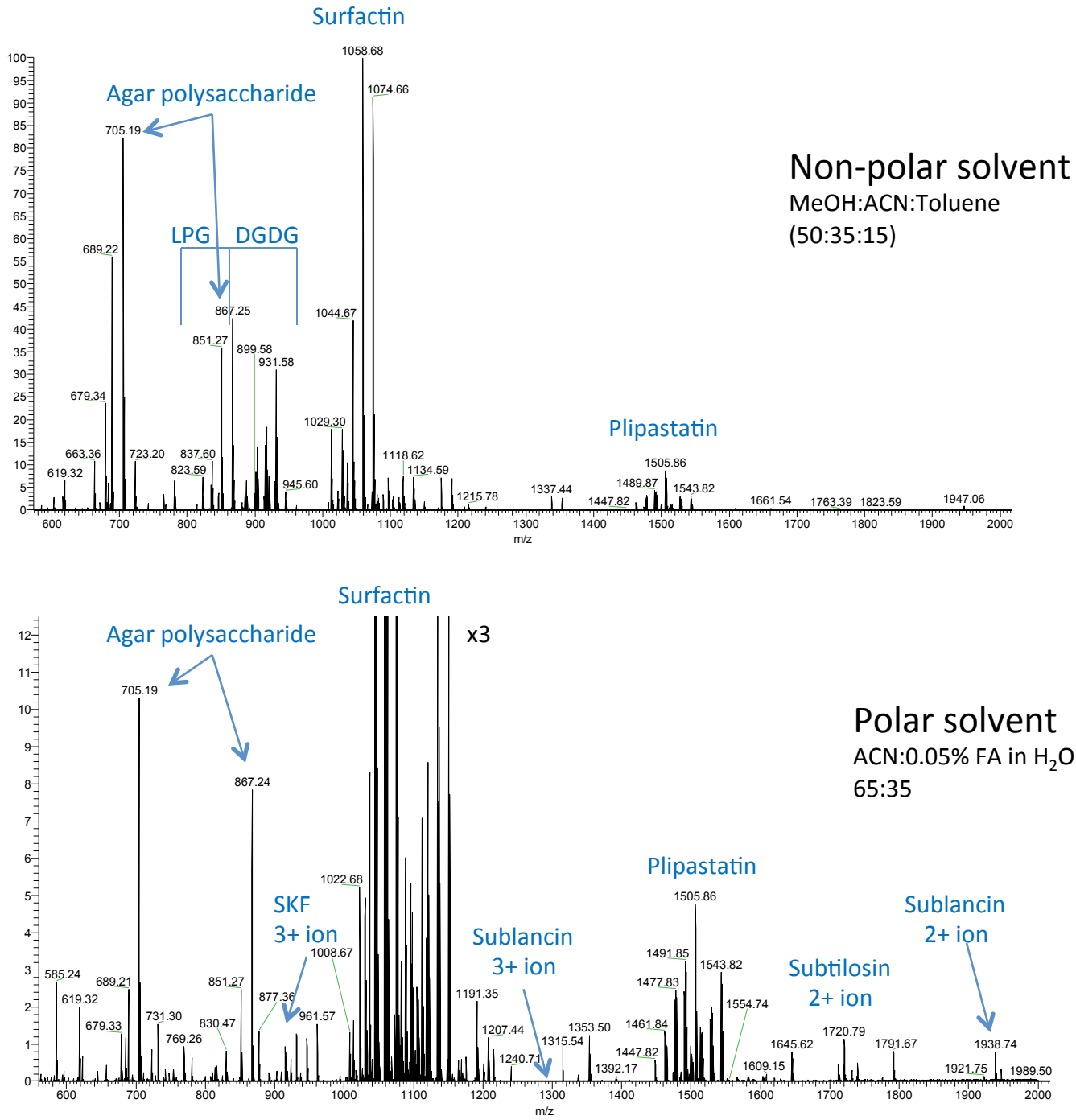

Description: Example MS1 Orbitrap positive mode spectra for *B. subtilis* 3610 using a non-polar (top) and polar (bottom) solvent. While many compounds are soluble in both solvents, certain compounds are unique to each condition such as the lipid families LPG and DGDG in the non-polar solvent and the macrocyclic peptides sublancin, SKF and subtilosin in the polar solvent.

Figure S4: Annotation of MS/MS spectra for reported compounds

Bacillus subtilis 3610: **Lysyl-phosphatodylglycerol (LPG)**

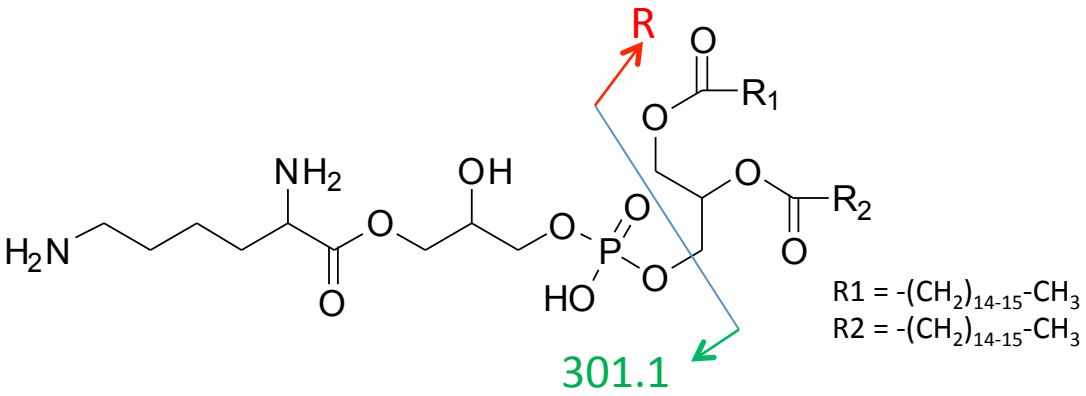

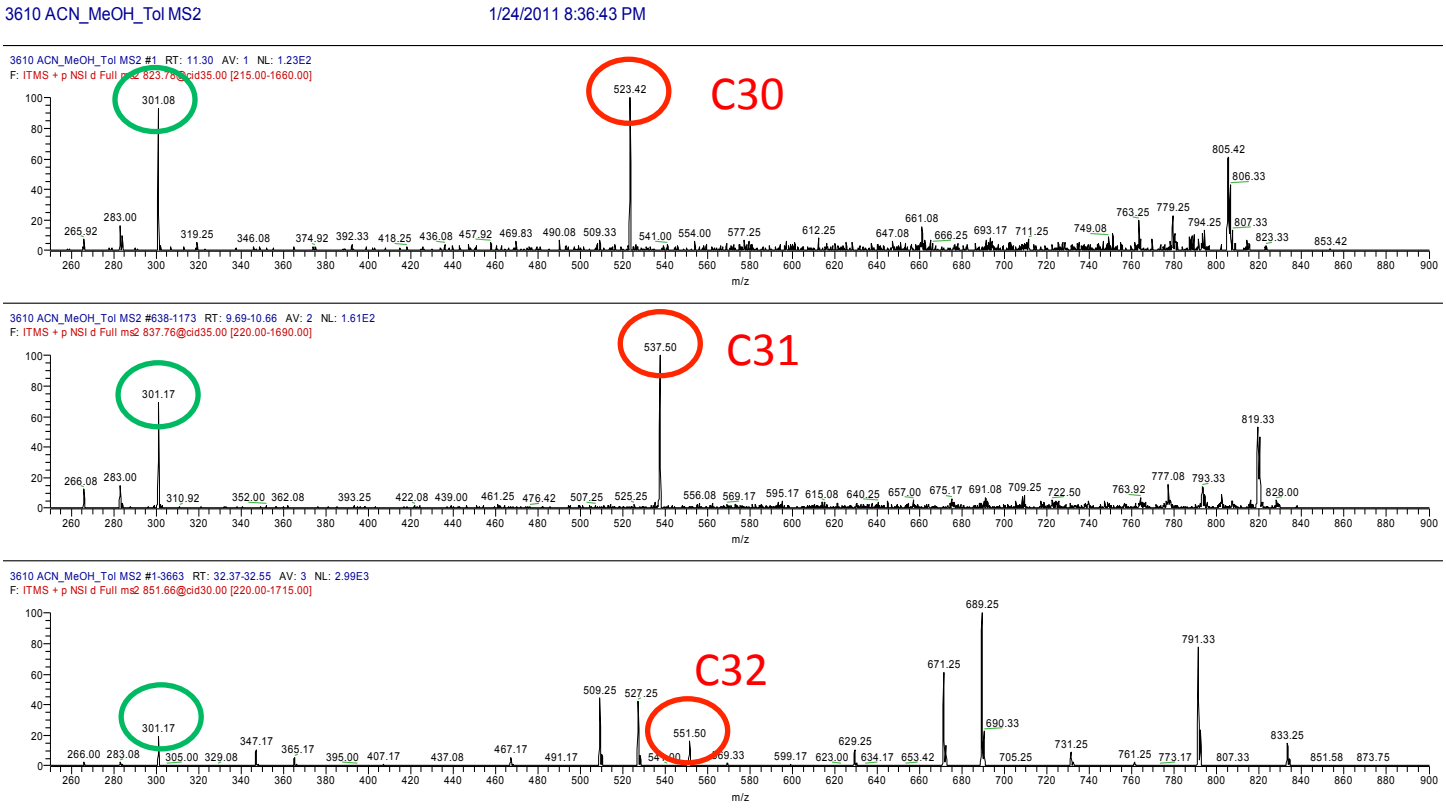

Description: Example subset of MS2 CID spectra for the LPG family of compounds. All LPG compounds exhibited a common loss of the head group at m/z 301 along with a second major fragment containing the lipid chains. The bottom spectra contains extra peaks due to one of the agar polysaccharide peaks being within the mass isolation window. The spectra are consistent with published MS2 data.[2]

Figure S4: Annotation of MS/MS spectra for reported compounds

Bacillus subtilis 3610: **Diglycosyl diglycerides (DGDG)**

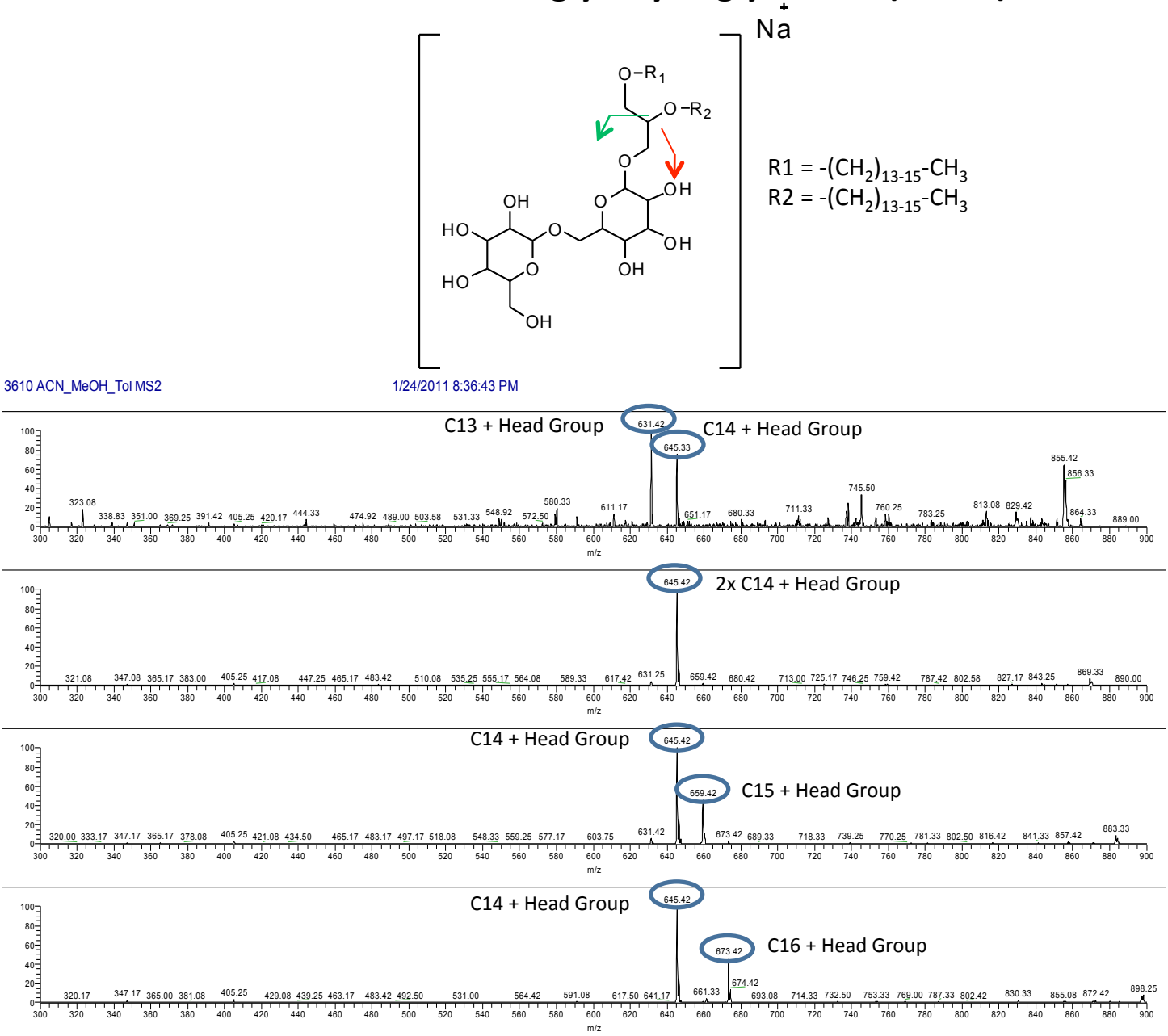

Description: Example subset of MS2 CID spectra for the DGDG family of compounds. Unlike the LPG compounds, the head group is retained in the mass fragments where each of the 2 fragments show the head group plus one of the two lipid chains. The spectra are consistent with published MS2 data.[2]

Figure S4: Annotation of MS/MS spectra for reported compounds

Bacillus subtilis 3610: **Subtilosin**

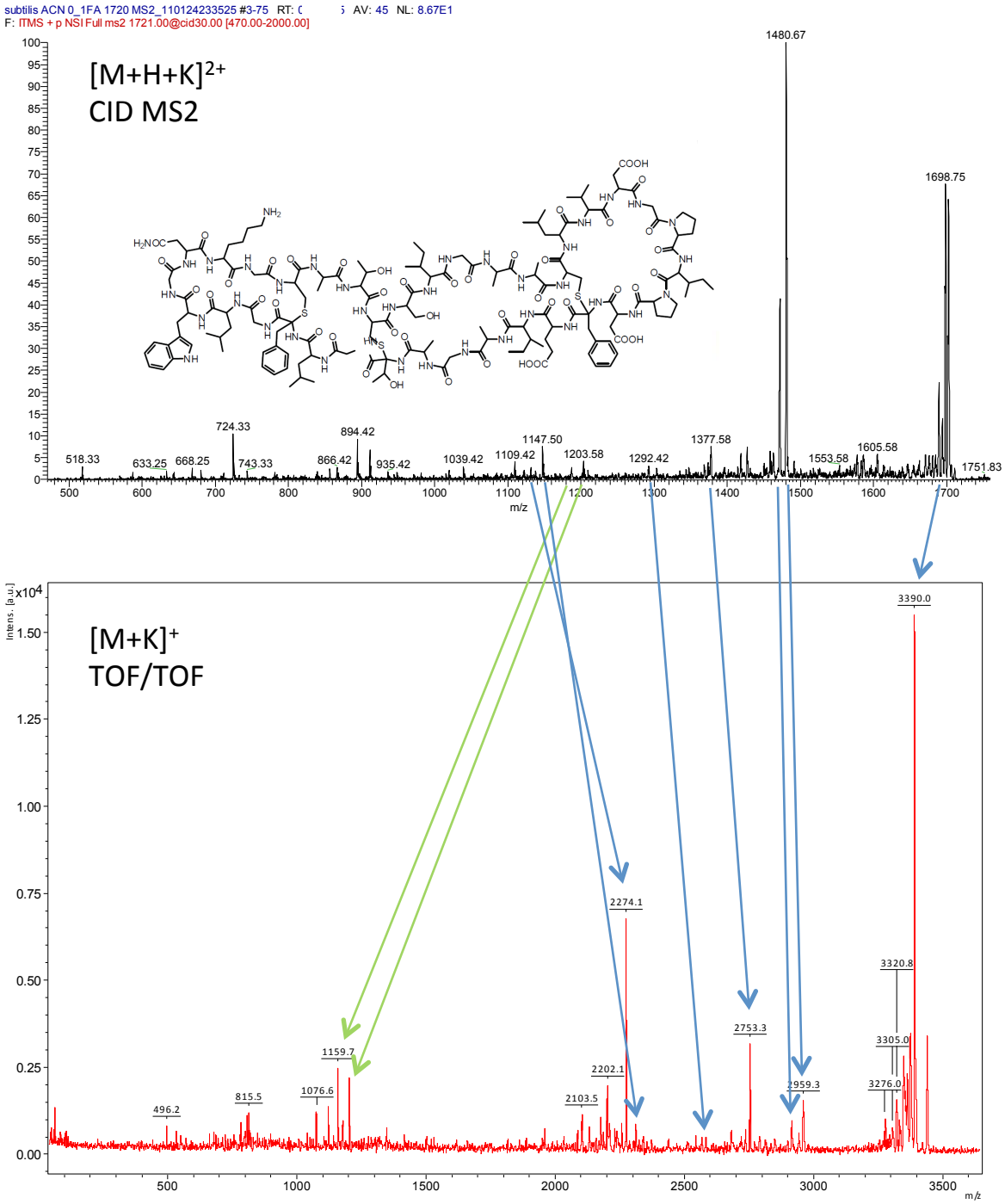

Description: Confirmation of subtilosin from nanoDESI experiments (top) by comparing with TOF/TOF MALDI fragmentation pattern for purified subtilosin (bottom). Blue arrows indicate a 2+ ion in the nanoDESI CID spectra corresponding to a 1+ ion in the TOF/TOF while green arrows indicate both are 1+.

Figure S4: Annotation of MS/MS spectra for reported compounds

Bacillus subtilis 3610: **Subtilosin**

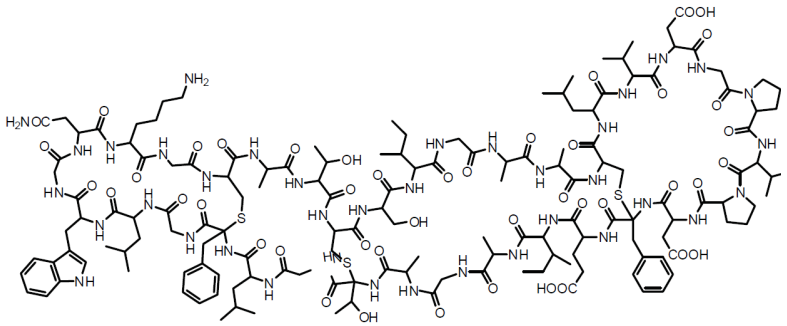

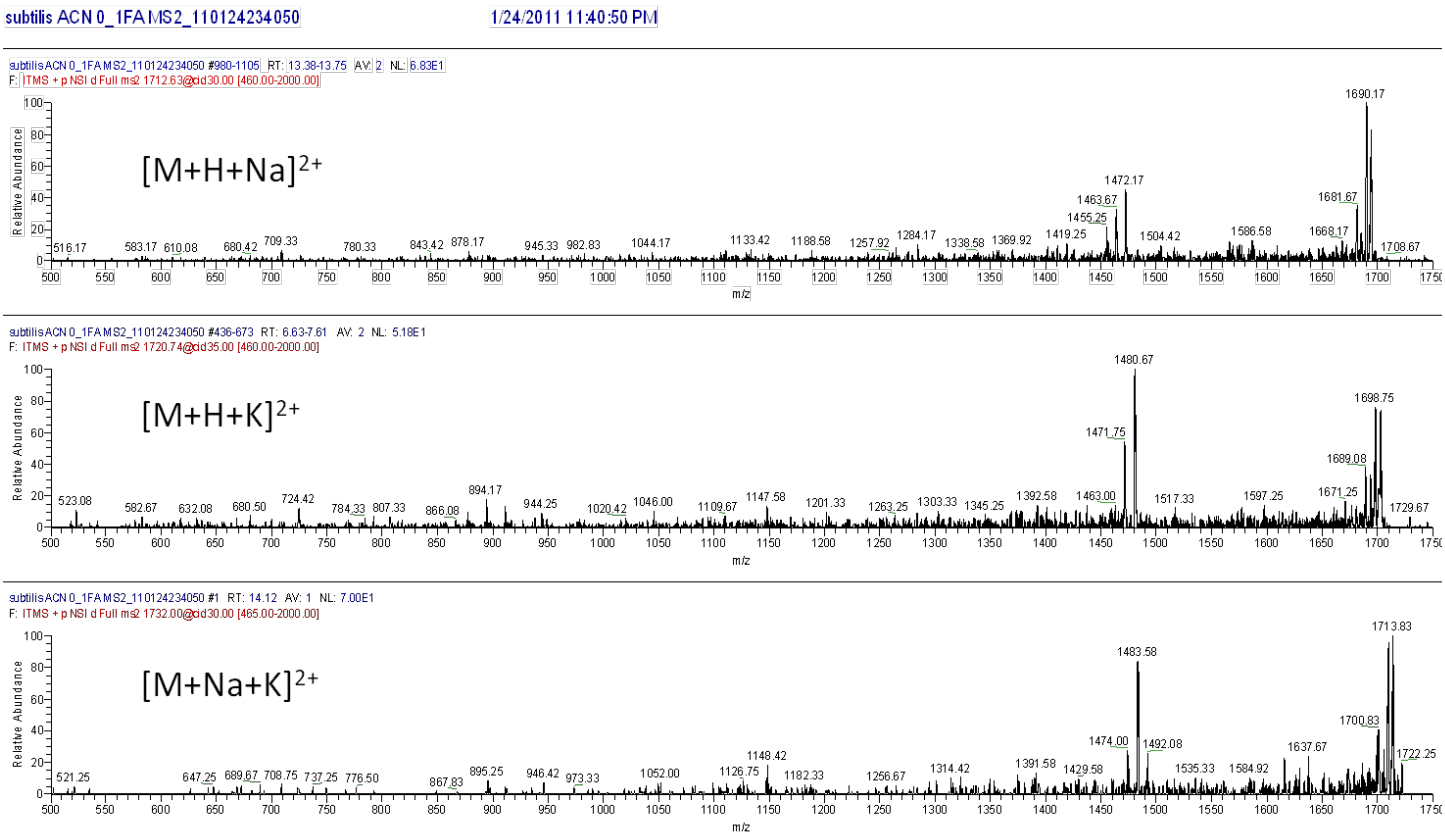

Description: Example subset of MS2 CID spectra for the subtilosin peak cluster. Poor fragmentation is characteristic of cyclic peptides containing disulfide bonds.

Figure S4: Annotation of MS/MS spectra for reported compounds

Bacillus subtilis 3610: **Plipastatin**

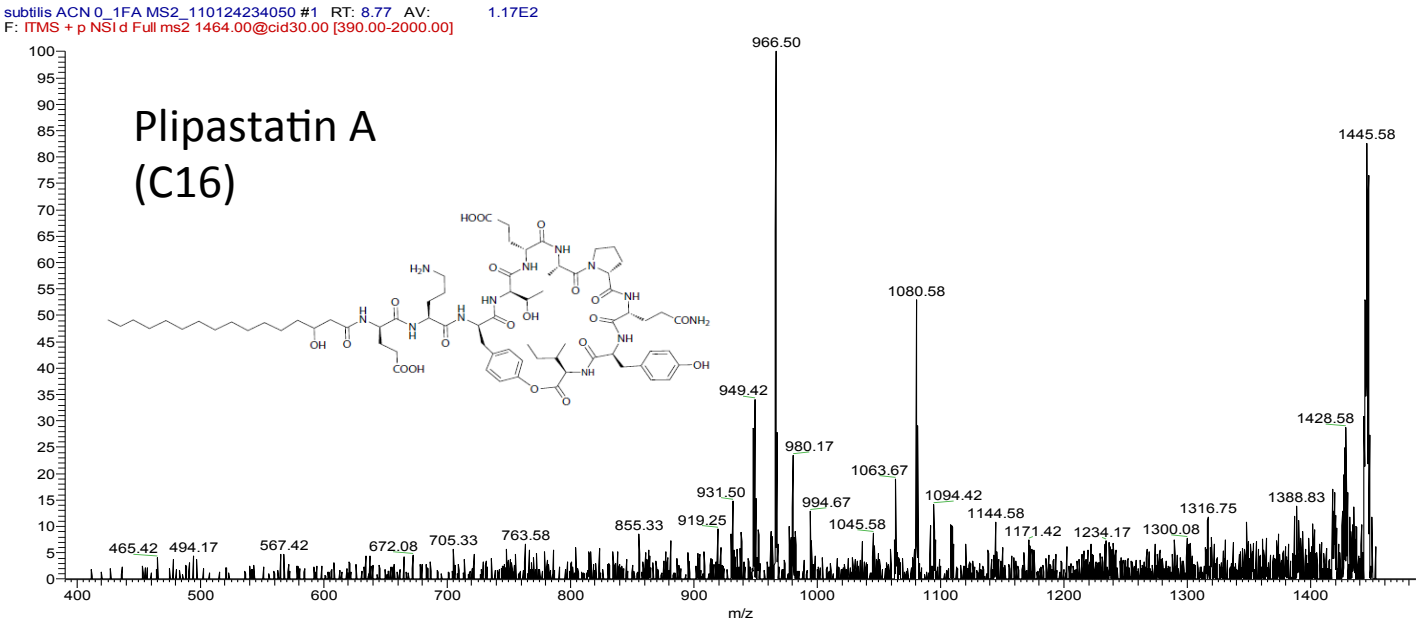

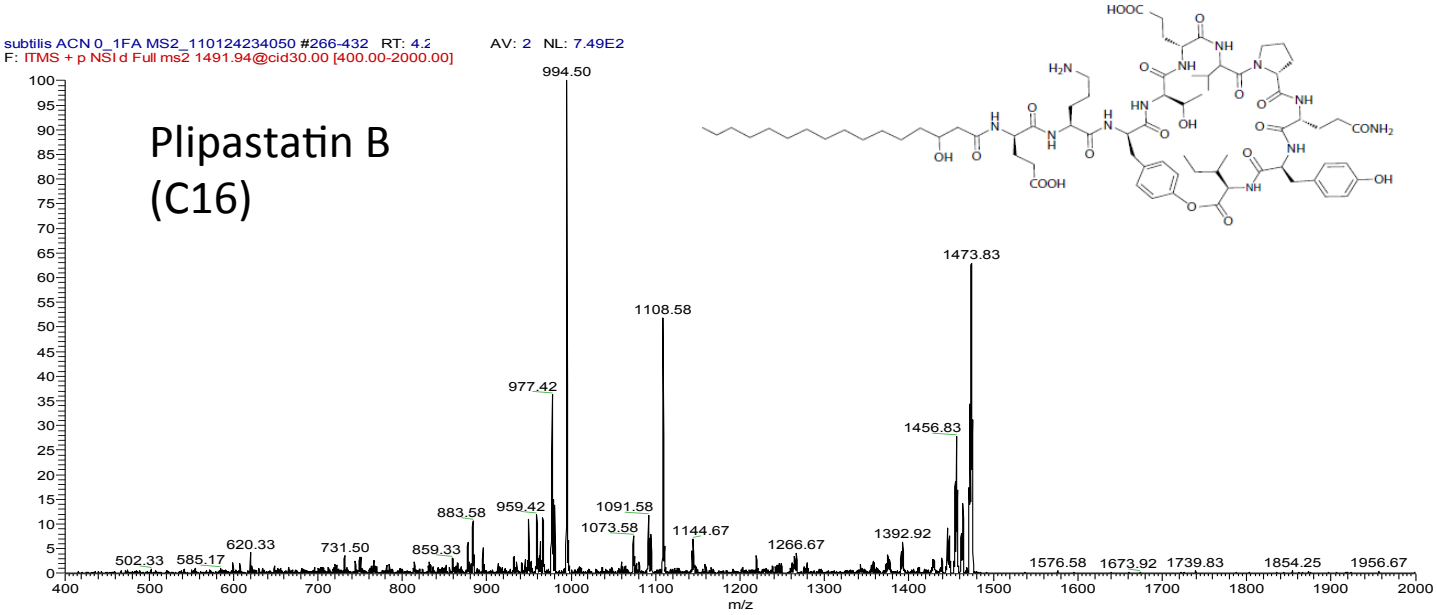

Description: Example subset of MS2 CID spectra for the plipastatin family of compounds. The spectra are consistent with published MS2 spectra.[3]

Figure S4: Annotation of MS/MS spectra for reported compounds

Bacillus subtilis 3610: **Plipastatin**

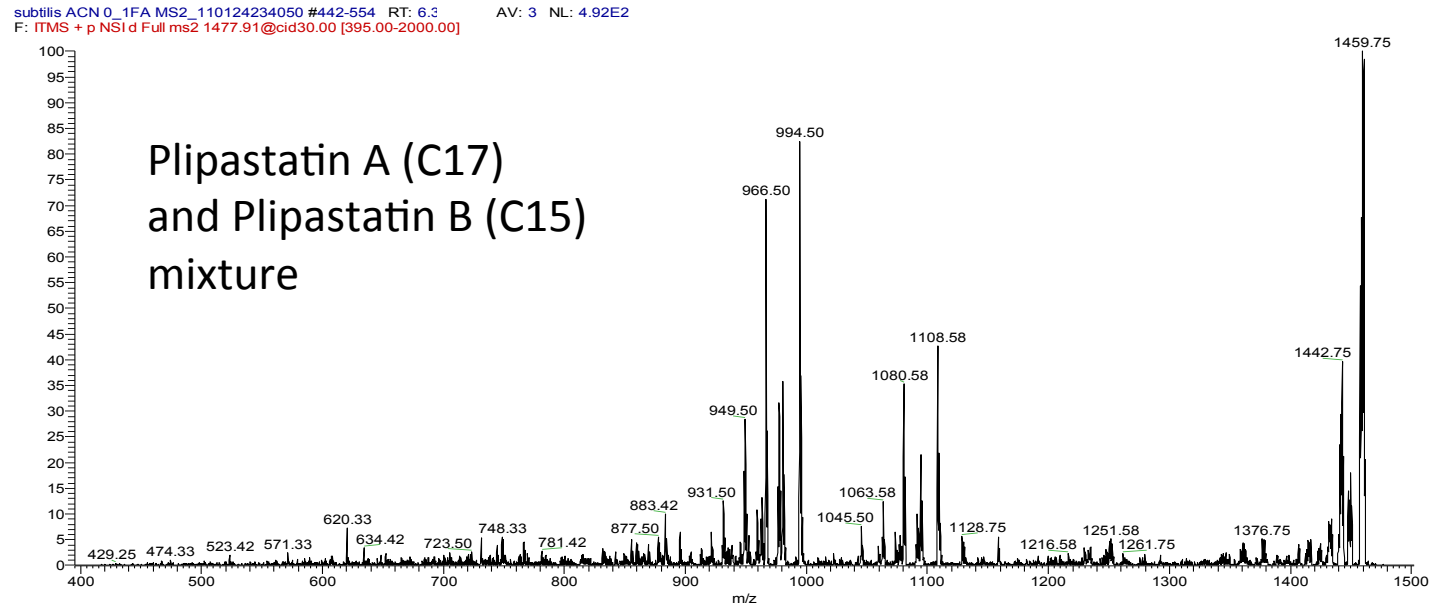

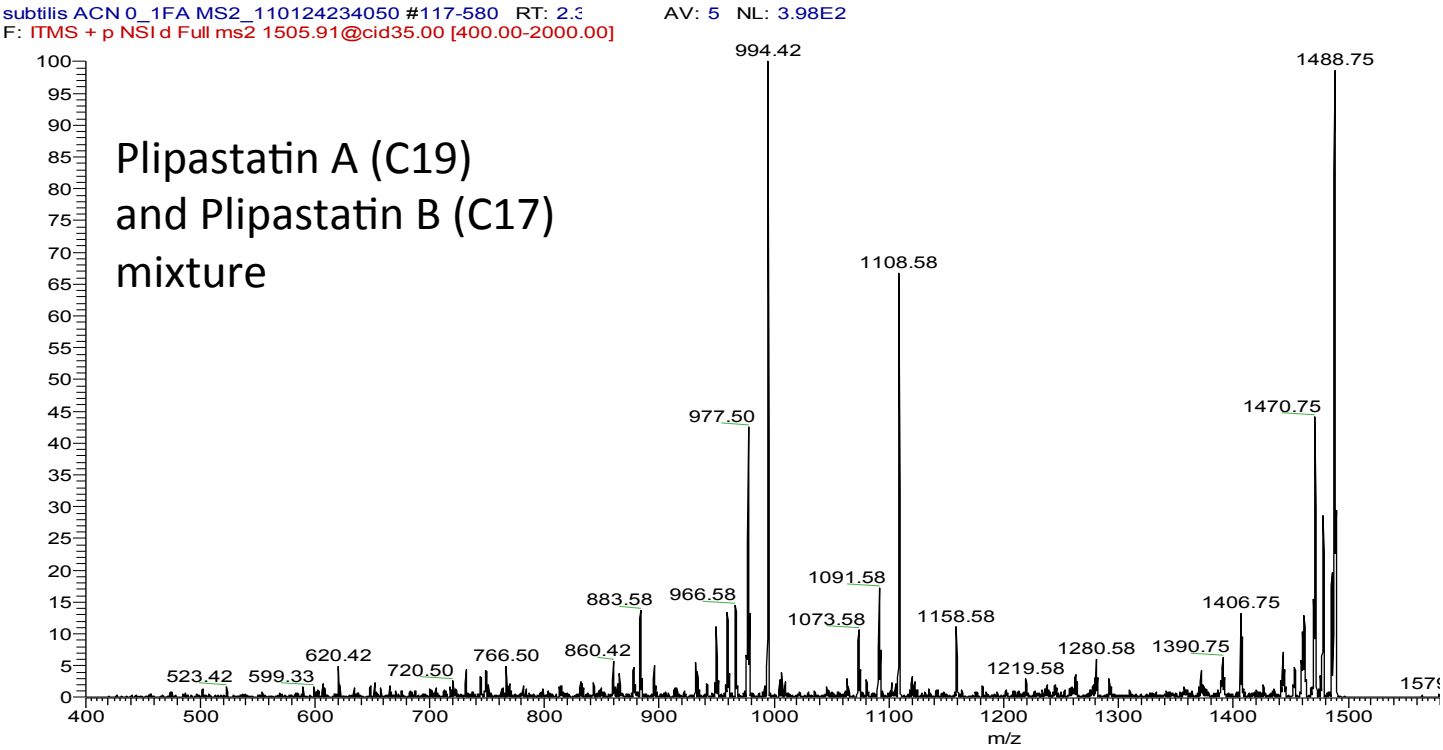

Description: Example subset of MS2 CID spectra for the plipastatin family of compounds. The spectra are consistent with published MS2 spectra.[3]

Figure S4: Annotation of MS/MS spectra for reported compounds

Bacillus subtilis 3610: **Surfactin**

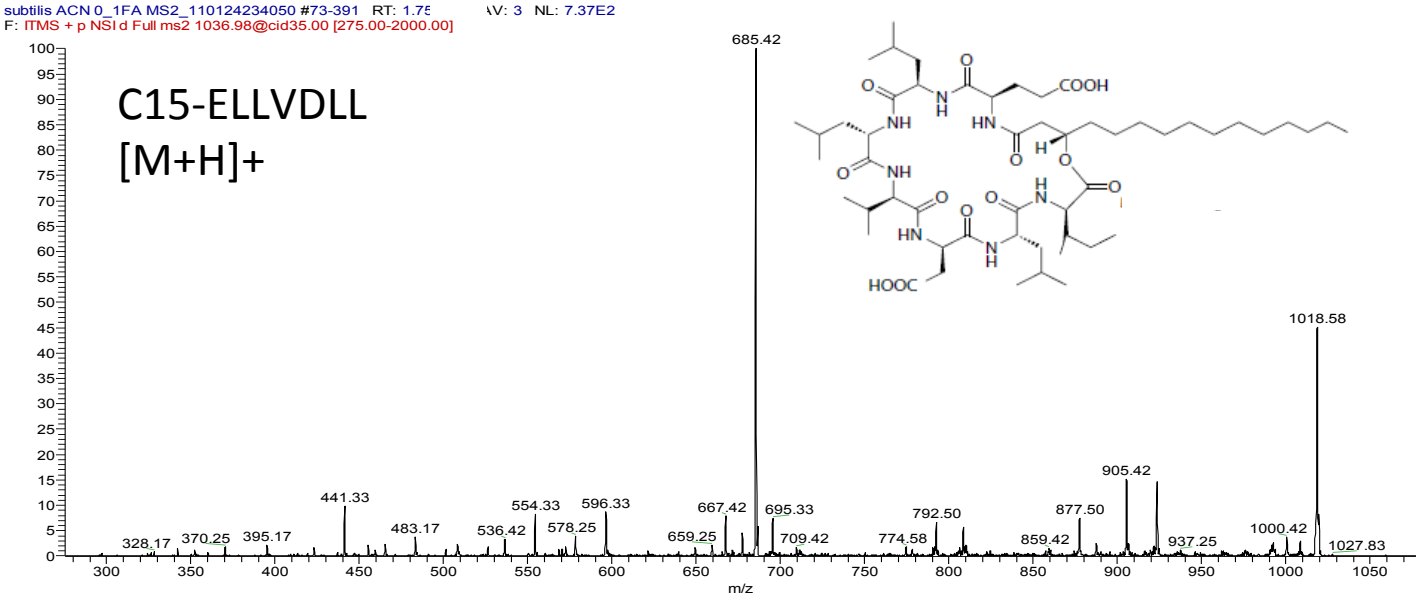

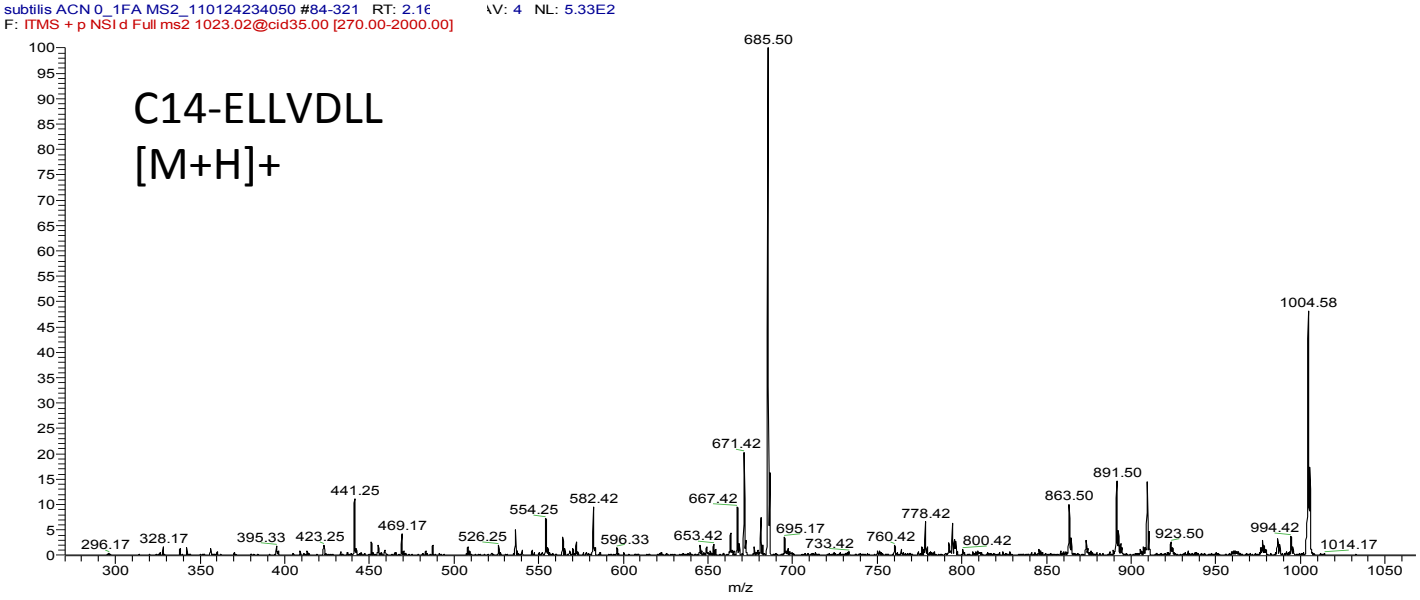

Description: Example subset of MS2 CID spectra for the surfactin family of compounds. The spectra are consistent with published MS2 spectra.[1]

Figure S4: Annotation of MS/MS spectra for reported compounds

Bacillus subtilis 3610: **Sublancin**

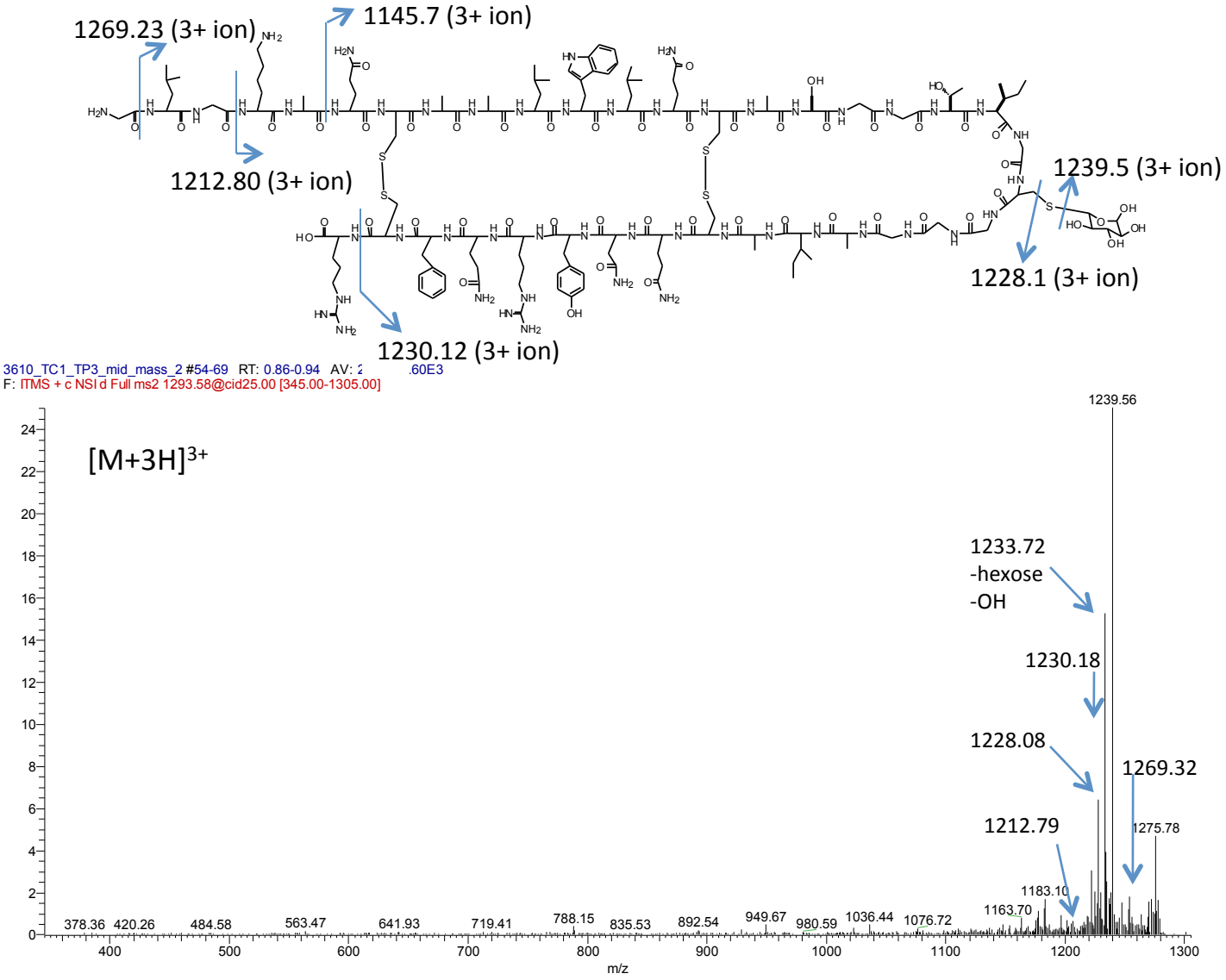

Description: CID MS2 spectrum for sublancin $[M+3H]^{3+}$ ion. The only major fragment observed is the loss of the sugar (m/z 1239.56), which is consistent with the published MS2 spectra for the native glycopeptide.[4]

Figure S4: Annotation of MS/MS spectra for reported compounds

Bacillus subtilis PY79: **SKF**

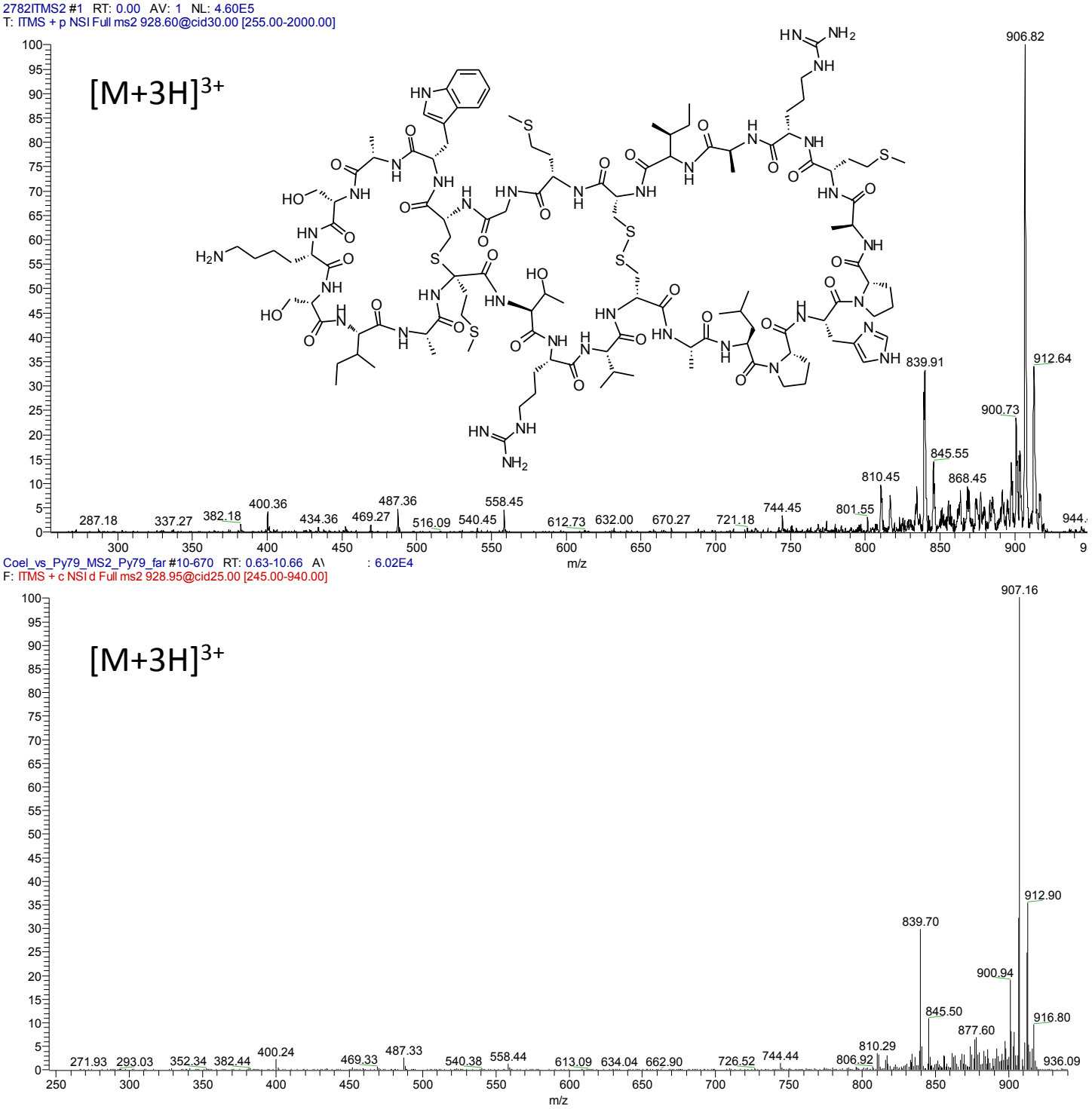

Description: CID MS2 of the $[M+3H]^{3+}$ ion of SKF (bottom). Spectra is consistent with purified SKF (Top).[5]

Figure S4: Annotation of MS/MS spectra for reported compounds

Streptomyces coelicolor A3(2): **SapB**

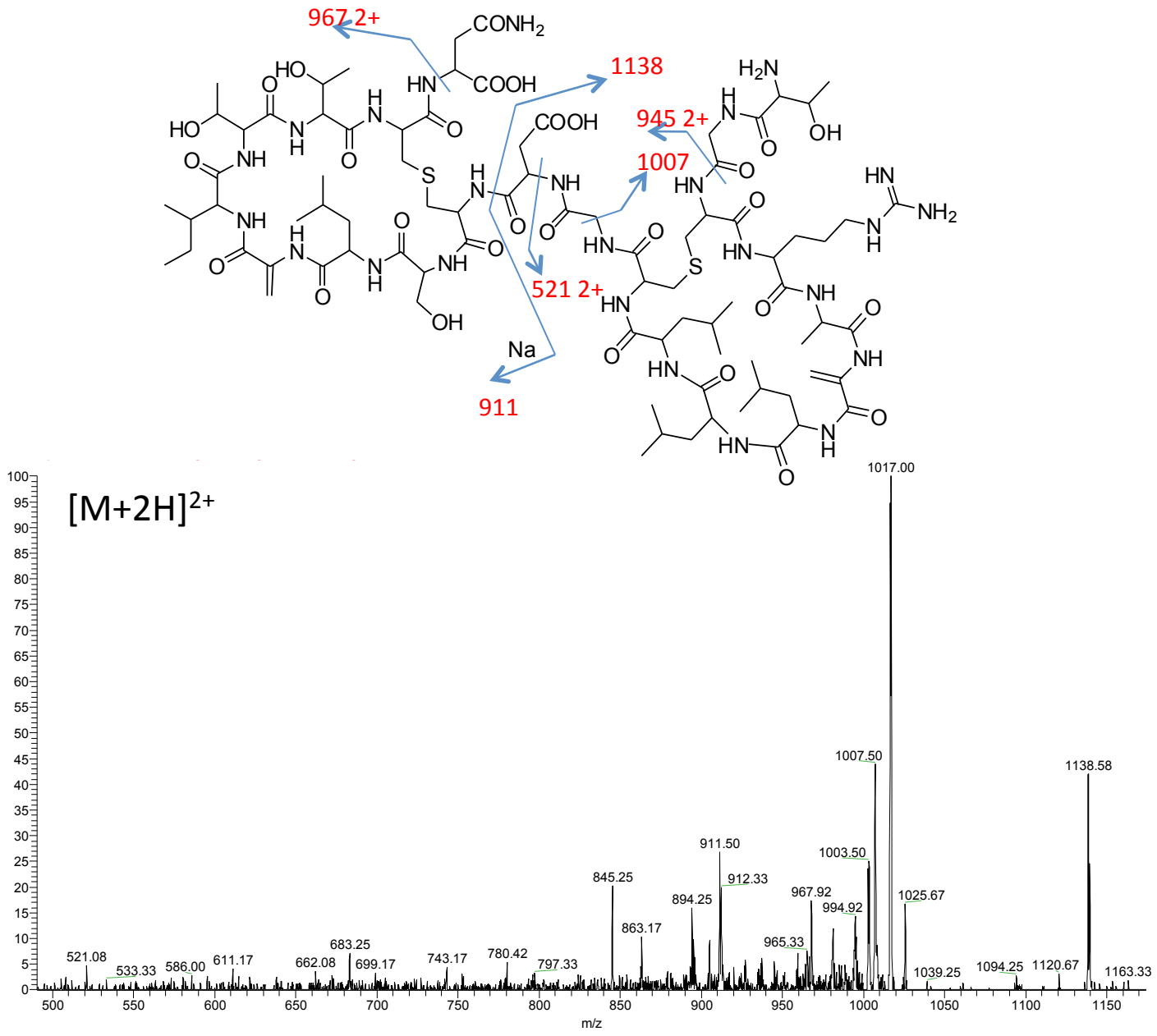

Description: CID MS2 for the $[M+2H]^{2+}$ ion of SapB. The spectrum is consistent with published MS2 data.[6]

Figure S4: Annotation of MS/MS spectra for reported compounds

Streptomyces coelicolor A3(2): **Prodiginine**

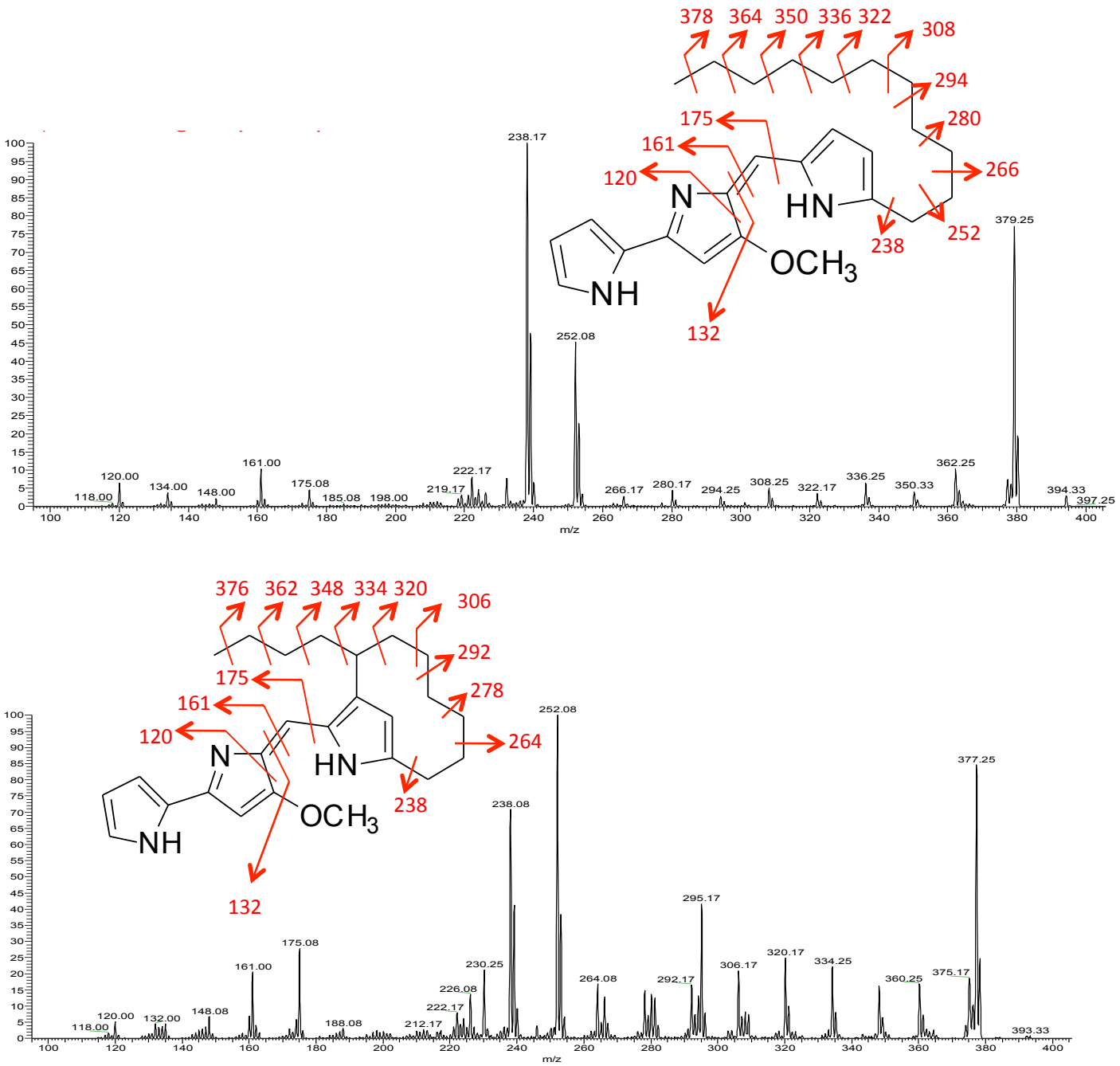

Description: CID MS2 for the $[M+H]^+$ ions of cyclized and linear prodiginine (red pigments in *S. coelicolor*). The spectra are consistent with published MS2 data.[7]

Figure S4: Annotation of MS/MS spectra for reported compounds

Streptomyces coelicolor A3(2): **γ-Actinorhodin**

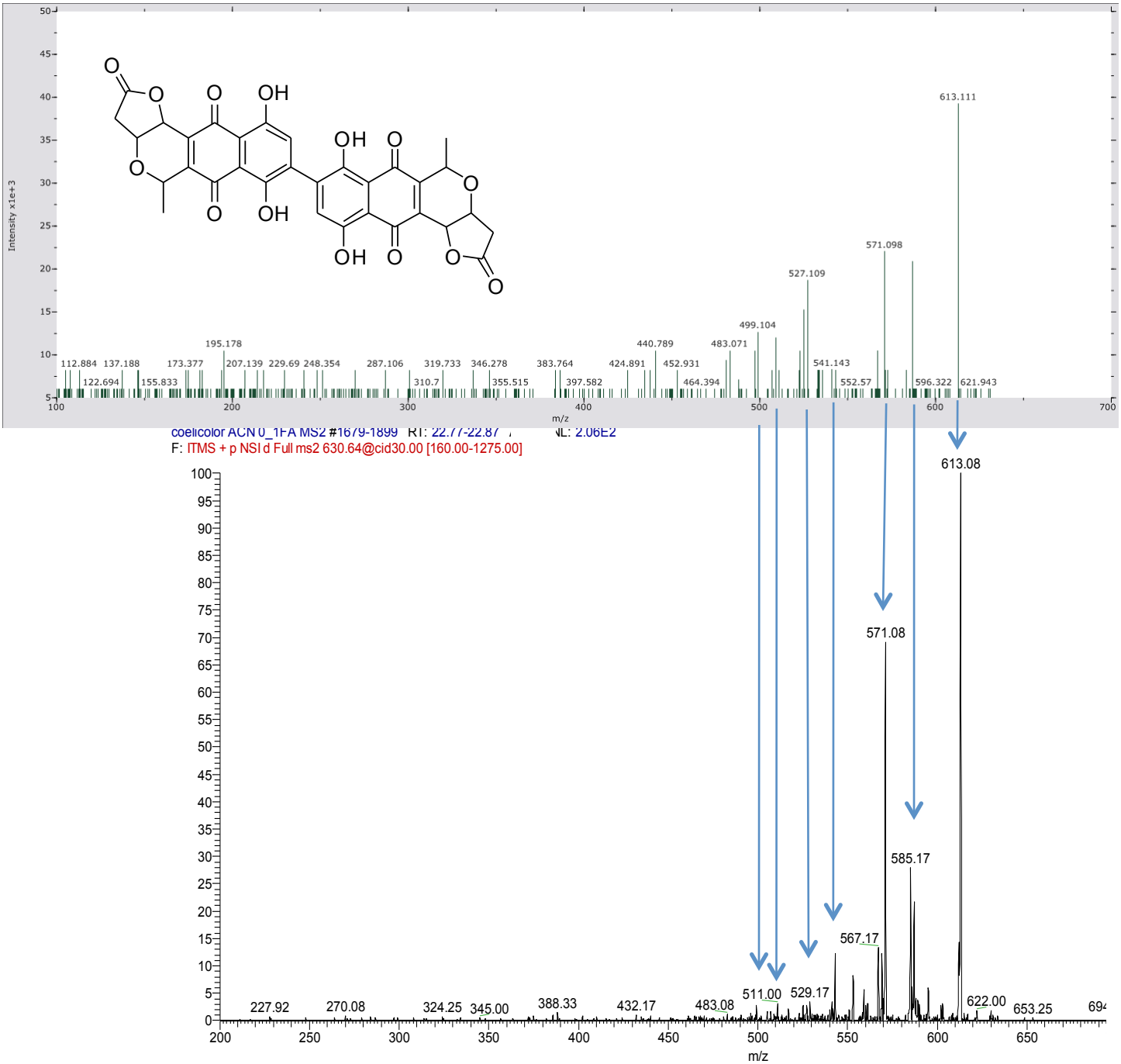

Description: CID MS2 for the $[M+H]^+$ ion of γ-actinorhodin (the blue/purple pigment in *S. coelicolor*). The identity was confirmed by comparing the fragmentation pattern from the observed mass in the nanoDESI data set (bottom) with that of a standard of γ-actinorhodin (top). Blue arrows show identical peaks. We would like to thank Professor Richard van Breemen at University of Illinois at Chicago for donating the γ-actinorhodin reference spectrum.

Figure S4: Annotation of MS/MS spectra for reported compounds

Streptomyces coelicolor A3(2): **CDA**

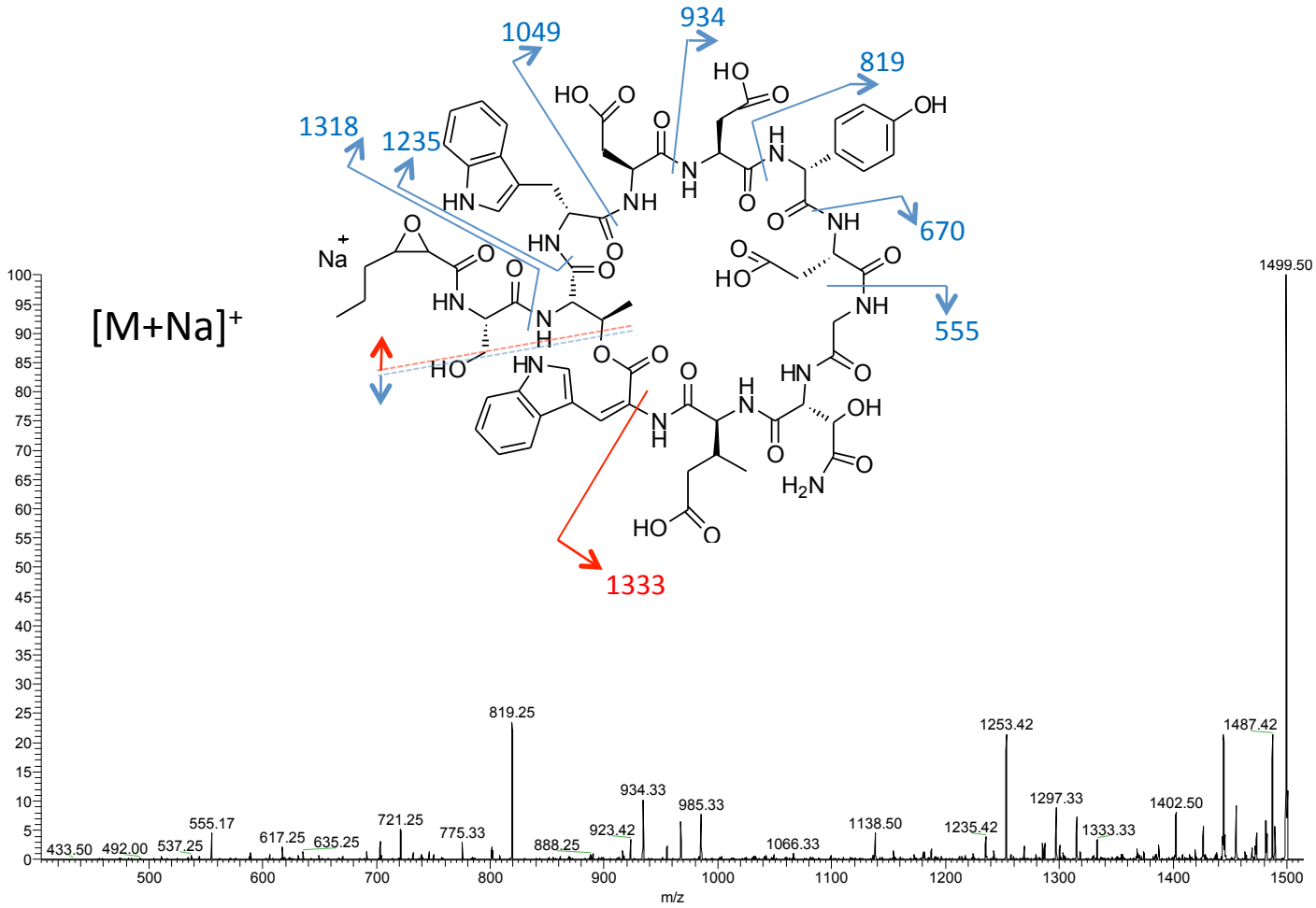

Description: Example MS2 CID spectra for the CDA family of compounds. The spectra are consistent with manual annotation as well as published MS2 spectra.[8]

Figure S4: Annotation of MS/MS spectra for reported compounds

Streptomyces coelicolor A3(2): **Coelichelin**

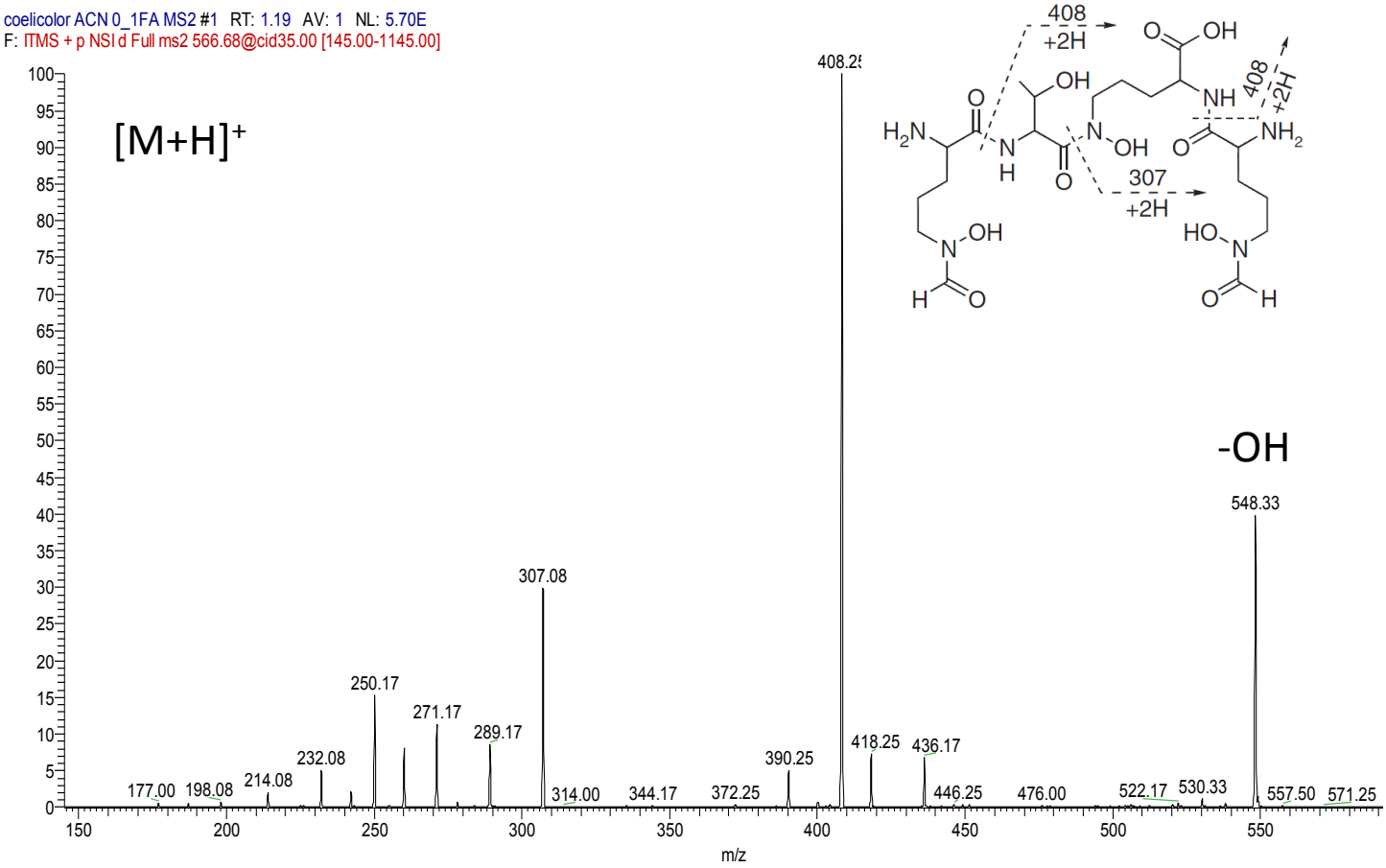

Description: CID MS2 spectra for the [M+H]+ ion of coelichelin. The spectra is consistent with published MS2 spectra.[9]

Figure S4: Annotation of MS/MS spectra for reported compounds

Example of **agar polysaccharide**

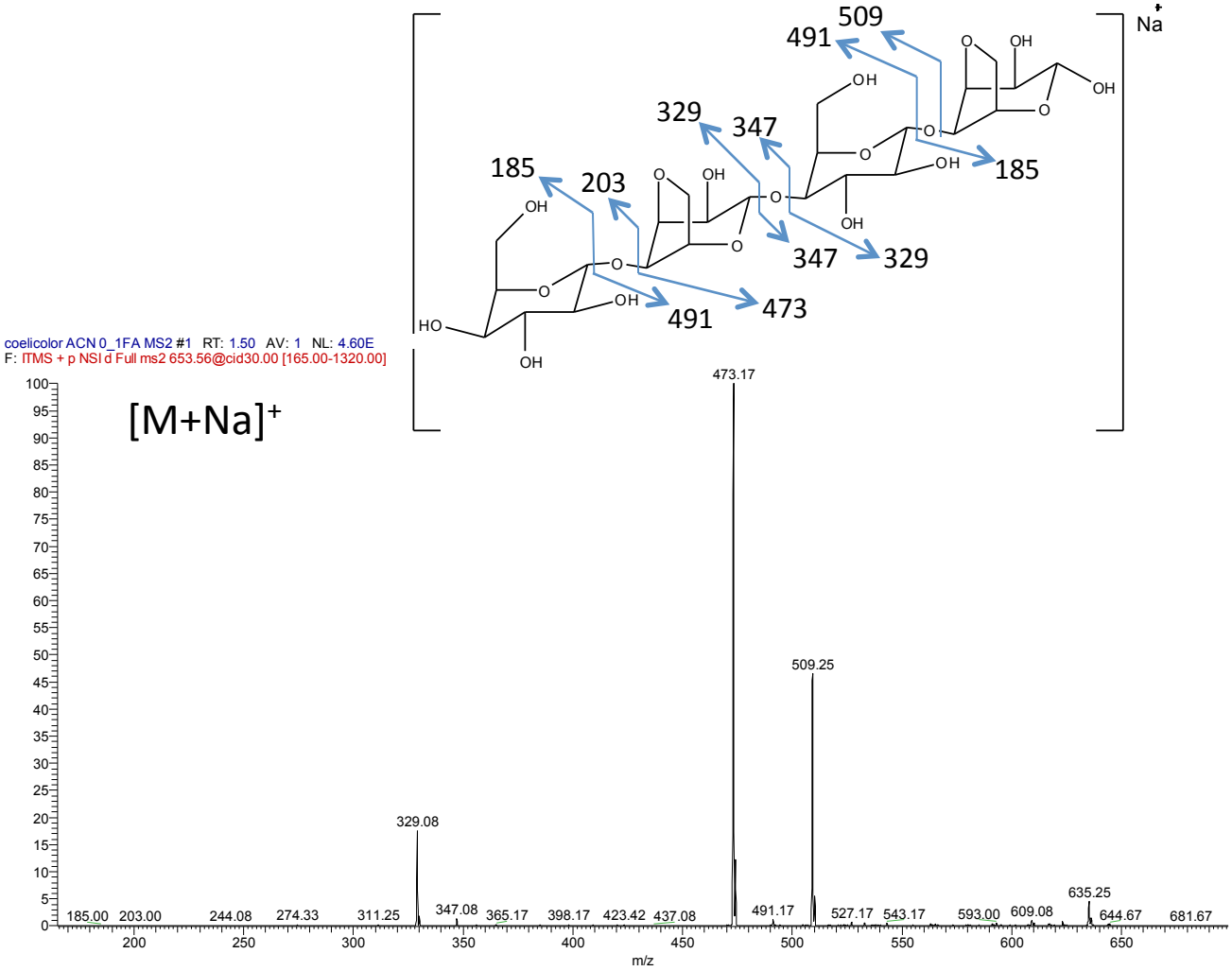

Description: Example subset of MS2 CID spectra for the polysaccharide found in the ISP2 group media. All MS2 spectra for the polymer show repeated losses of 162 and 180 Da due to shedding of hexose moieties in the chain. The spectrum is consistent with published MS2 data.[10]

Figure S4: Annotation of MS/MS spectra for reported compounds

Mycobacterium smegmatis MC2: **Glycopeptidolipids**

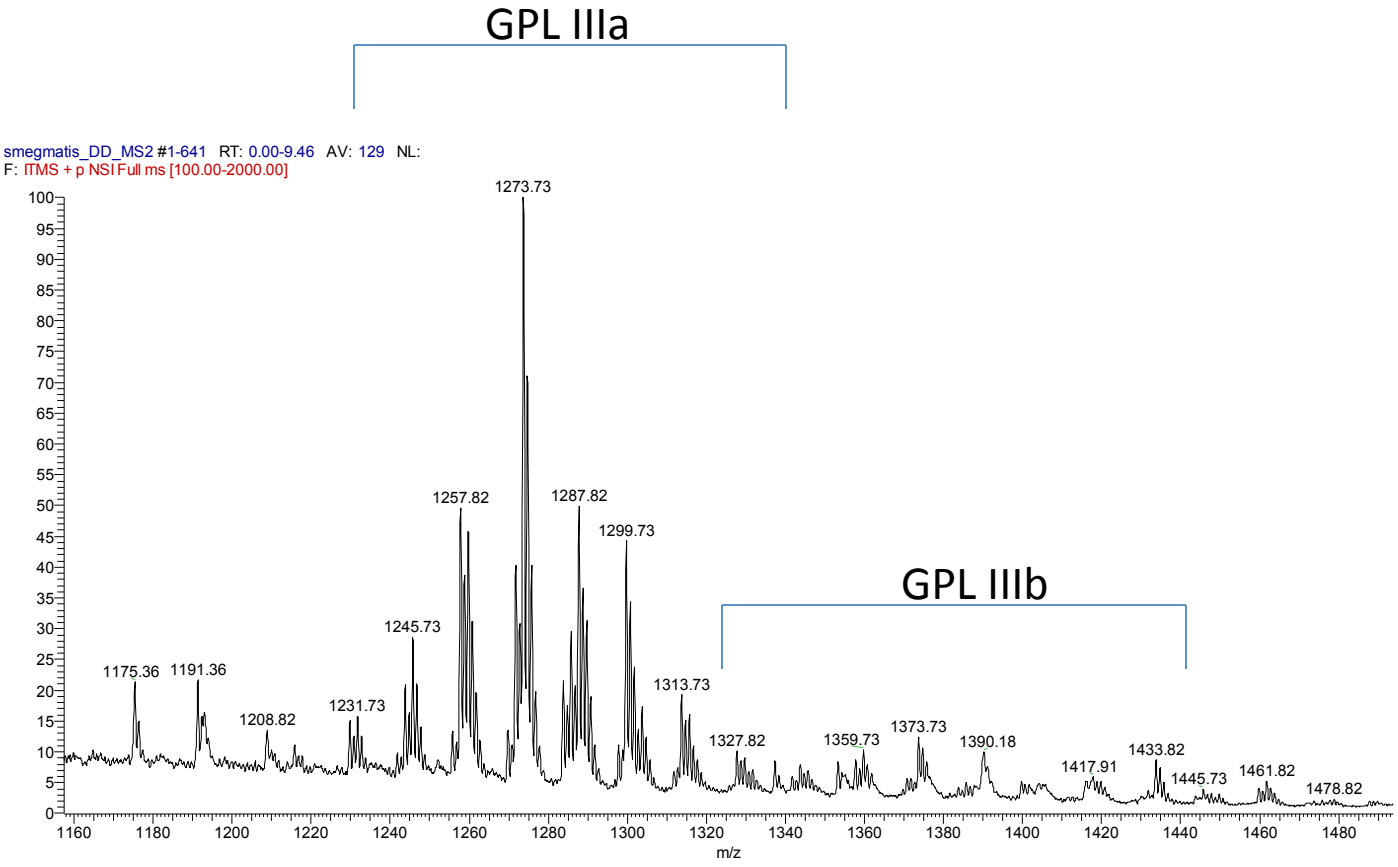

Description: Annotation of the MS1 parent mass spectra for the glycopeptidolipids (GPL's) found in *M. smegmatis*. Peaks in the cluster are separated by 12 and 14Da which is indicative of a lipid chain. GPL III a and b are identical except for b containing one additional sugar unit.[11]

Figure S4: Annotation of MS/MS spectra for reported compounds

Mycobacterium smegmatis MC2: **Glycopeptidolipids**

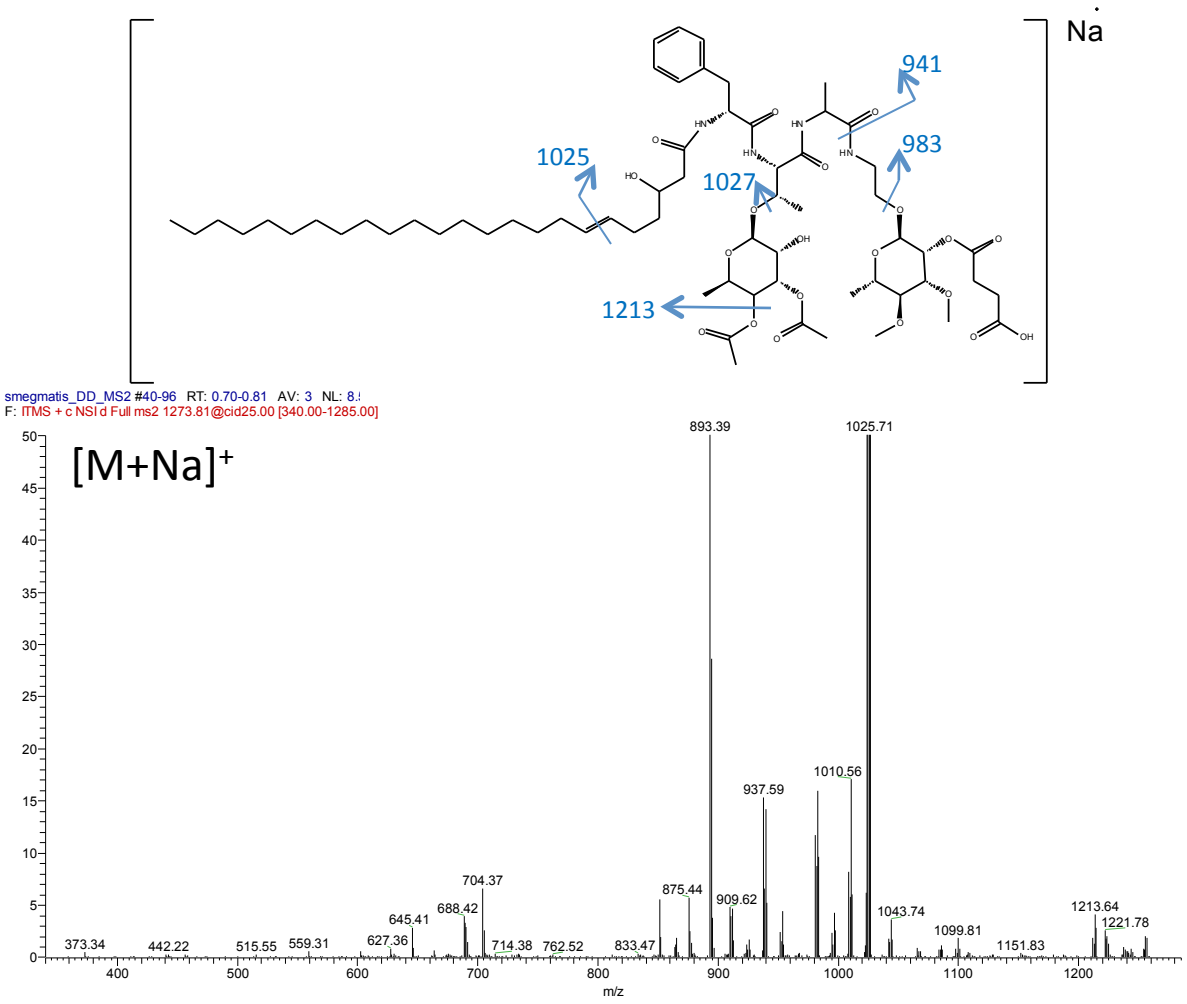

Description: Example MS2 CID spectra for a GPL IIIa compound from the nanoDESI data. Data was confirmed by manual annotation as well as correlation so FAB MS2 published data.[11,12]

Figure S4: Annotation of MS/MS spectra for reported compounds

Pseudomonas aeruginosa PAO1: **Quinolones**

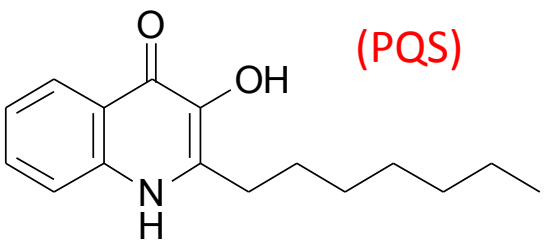

(PQS)

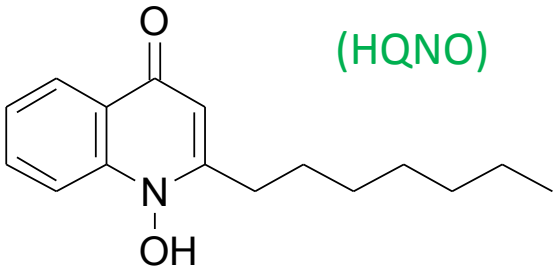

(HQNO)

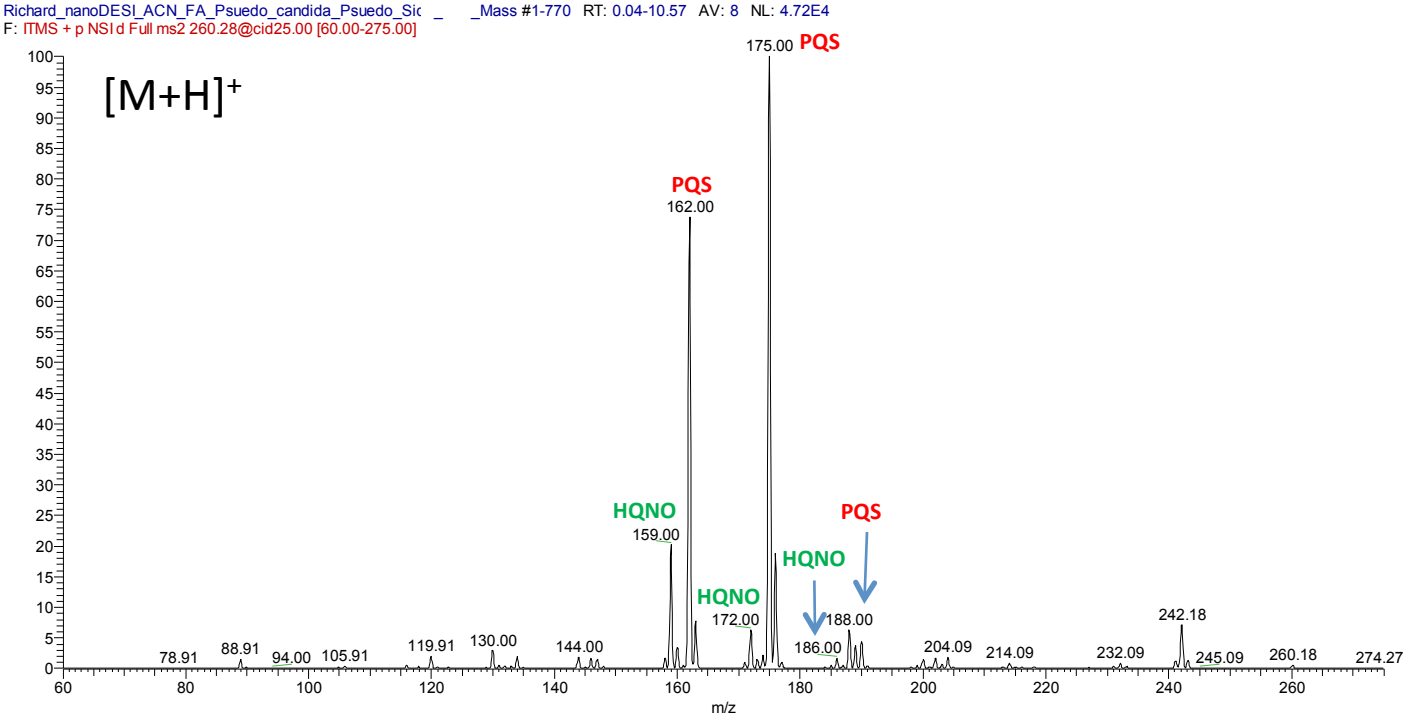

Description: Example MS2 CID spectra for the quinolone family of compounds from the nanoDESI data. The above spectrum shows a mixture of PQS and HQNO. The spectrum is consistent with published MS2 data for both compounds.[13]

Figure S4: Annotation of MS/MS spectra for reported compounds

Pseudomonas aeruginosa PAO1: **Rhamnolipids**

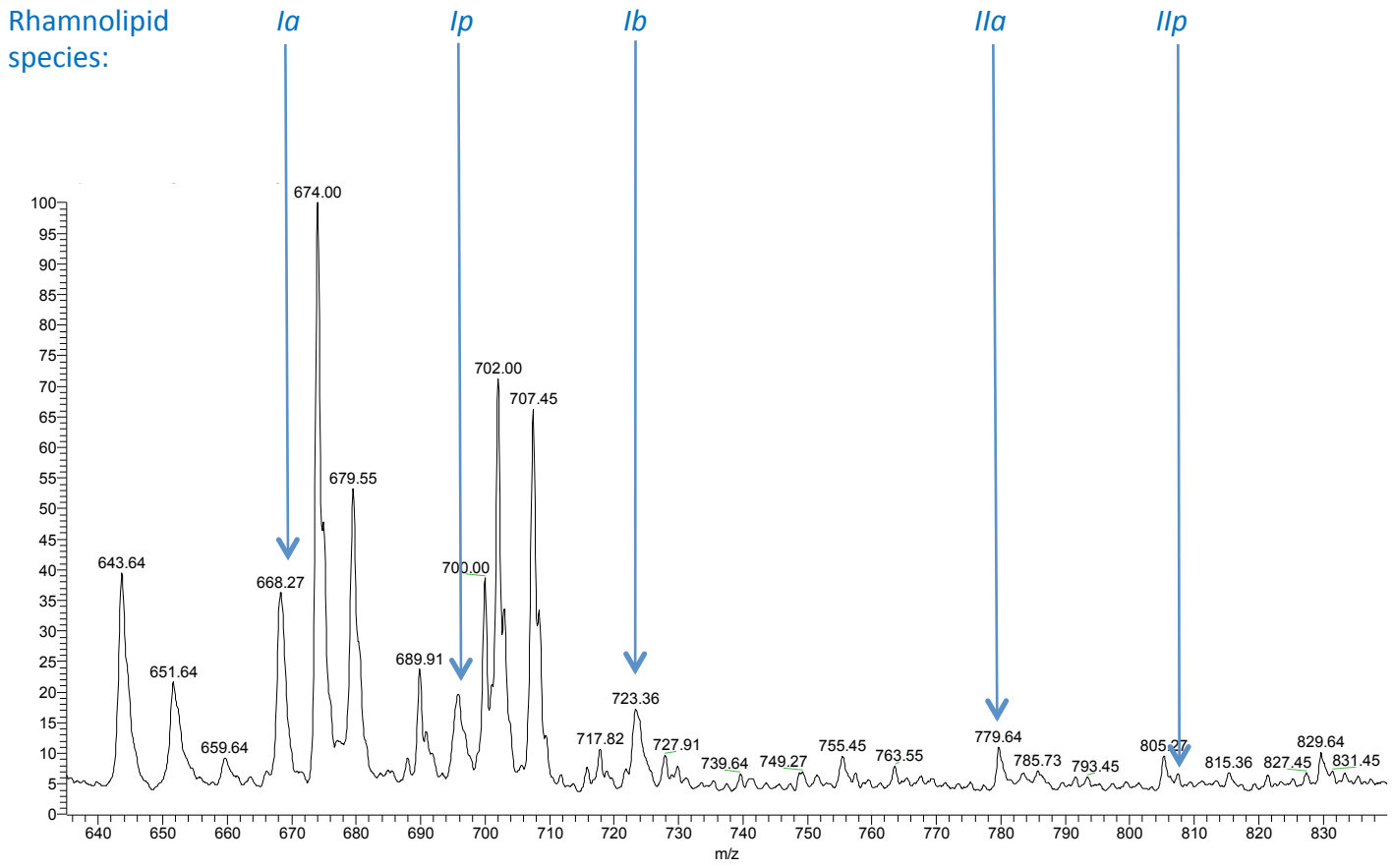

Description: Annotation of the MS1 parent mass spectra for the rhamnolipid family of compounds. All ions are $[M+2Na-H]^+$.[14,15]

Figure S4: Annotation of MS/MS spectra for reported compounds

Pseudomonas aeruginosa PAO1: **Rhamnolipids**

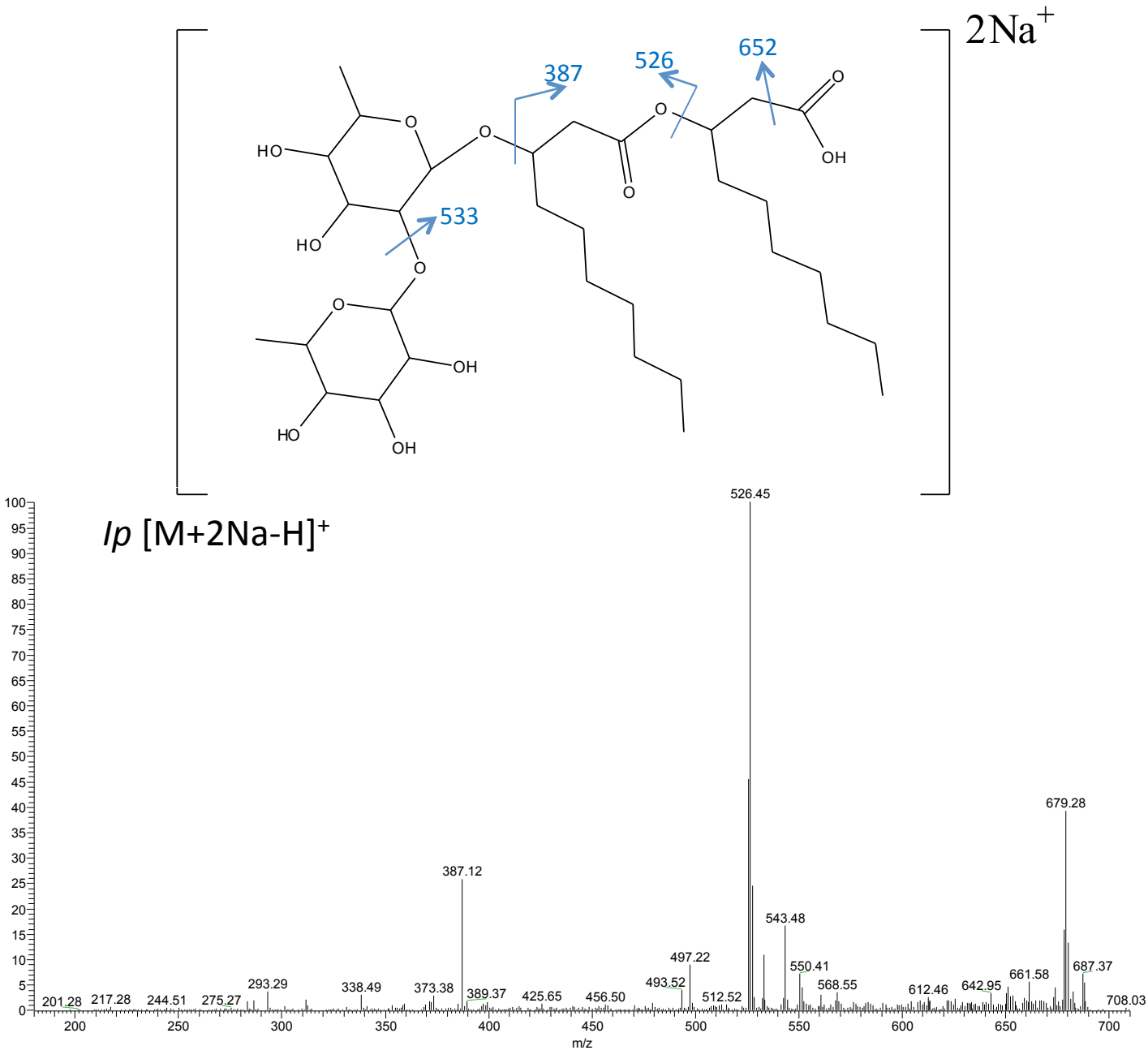

Description: Example CID MS2 for the rhamnolipid family of compounds (Rlp). The MS2 fragmentation was consistent with published MS2 data and was confirmed by manual annotation. [14,15]

Figure S4: Annotation of MS/MS spectra for reported compounds

Pseudomonas aeruginosa PAO1: **Phenazines**

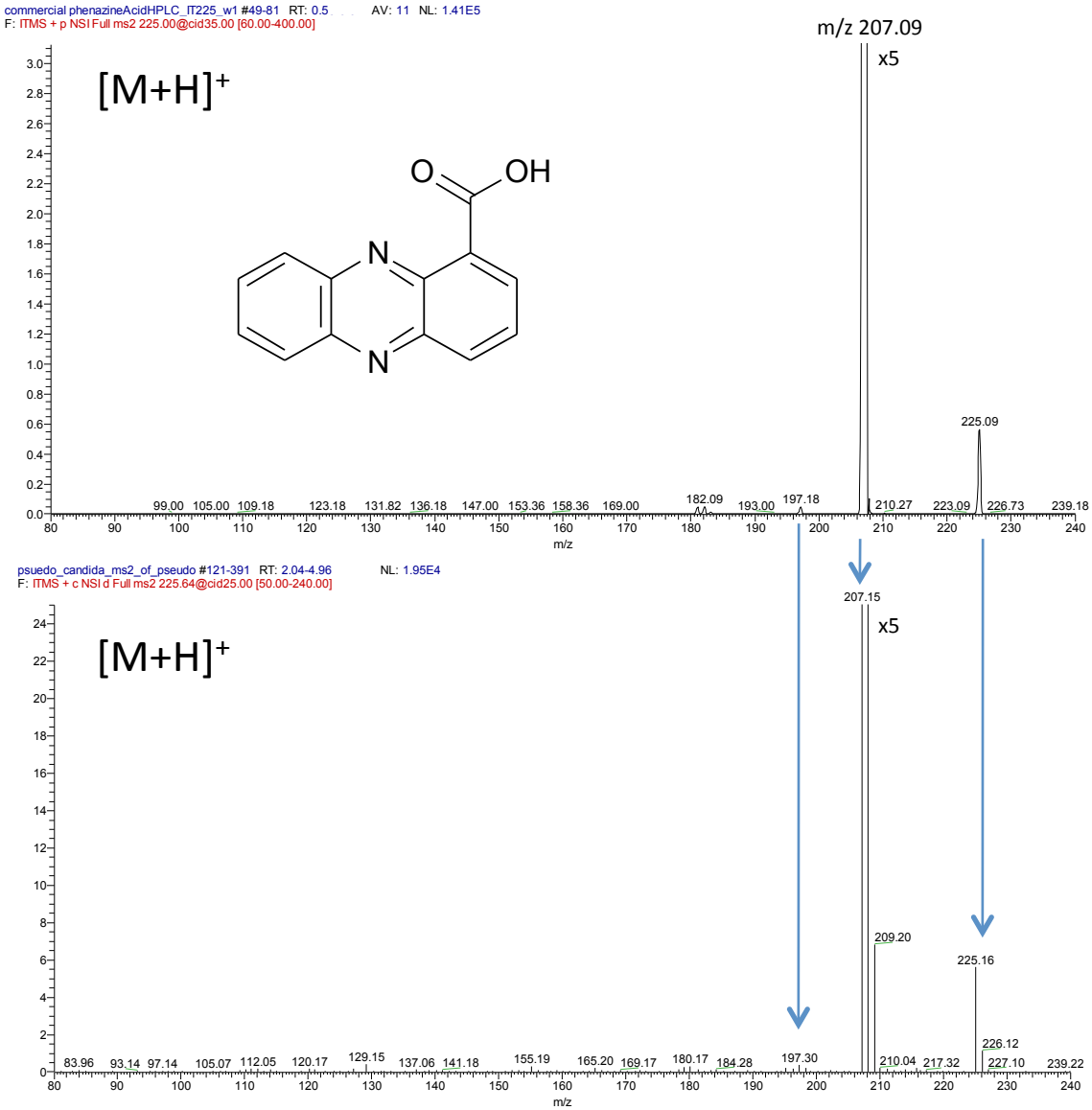

Description: Example CID MS2 for the phenazine family of compounds (phenazine-1-carboxylic acid shown). CID MS2 spectra from nanoDESI (bottom) is consistent with CID MS2 for commercial reference standard (top) as well as published data.[16]

Figure S4: Annotation of MS/MS spectra for reported compounds

Serratia marcescens ES129: **Prodigiosin**

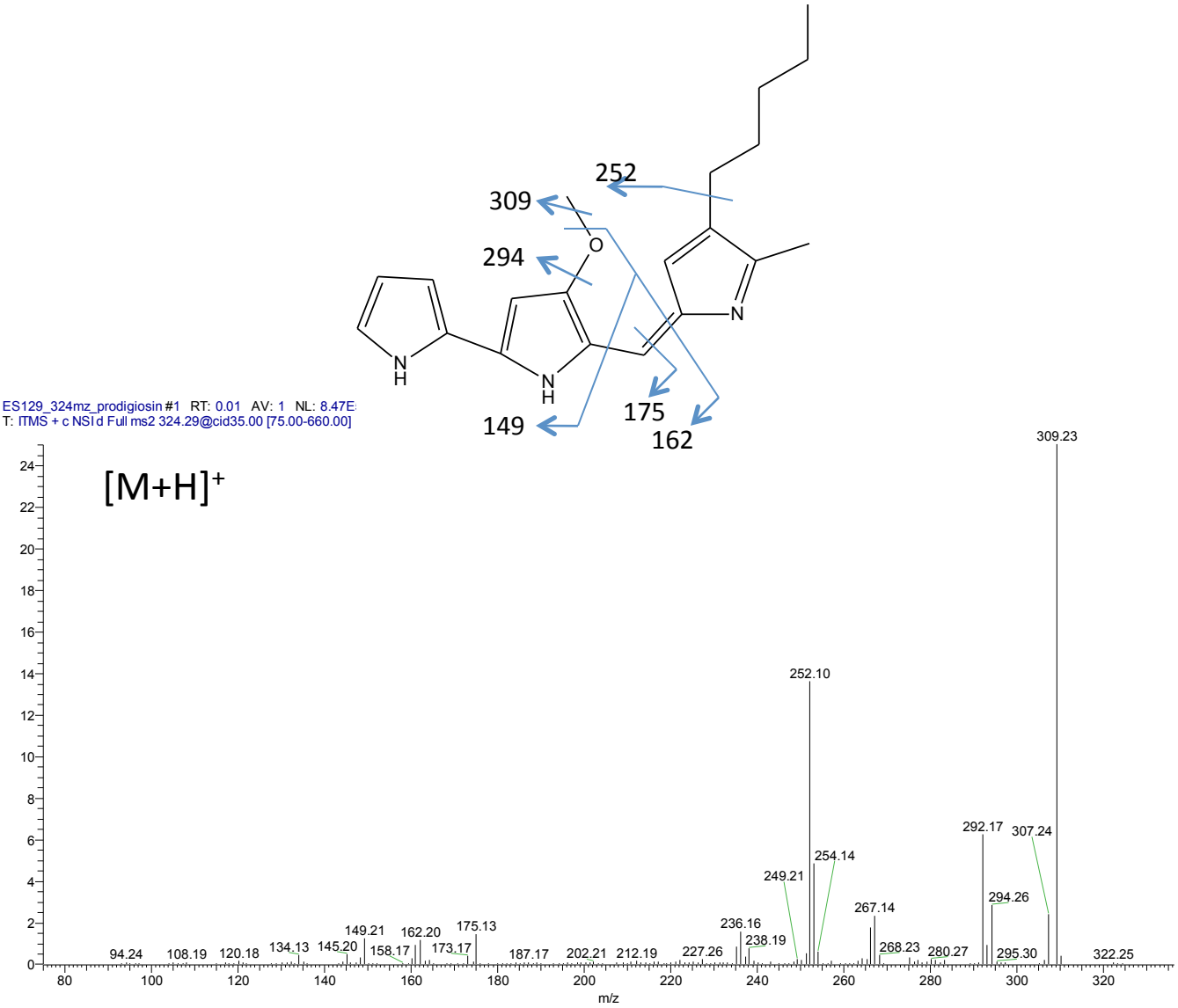

Description: Annotation of the CID MS2 for prodigiosin. Spectra is consistent with published MS2 data.[17]

Figure S4: Annotation of MS/MS spectra for reported compounds

Serratia marcescens ES129: **Serrawettin W1/Serratamolide A**

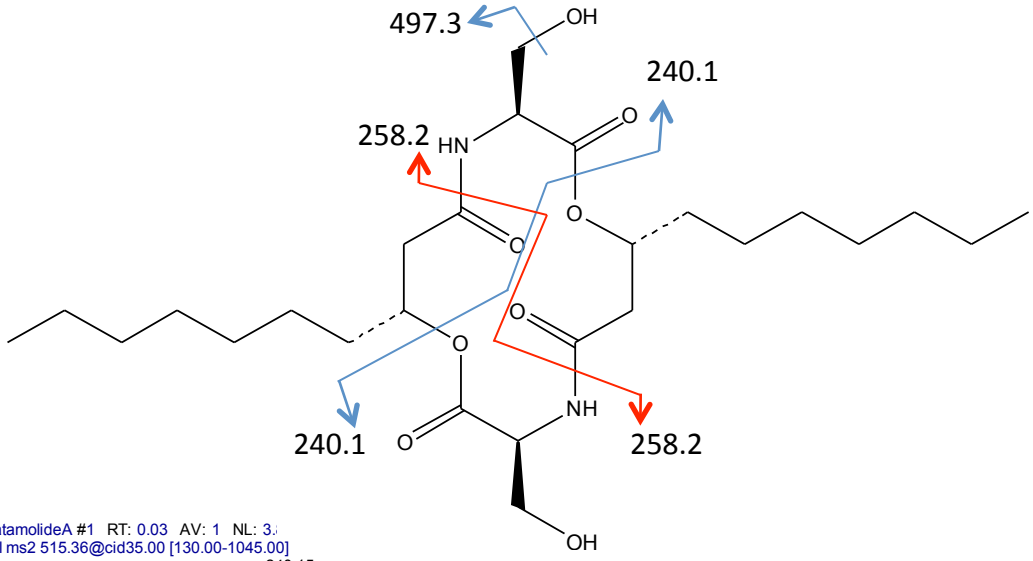

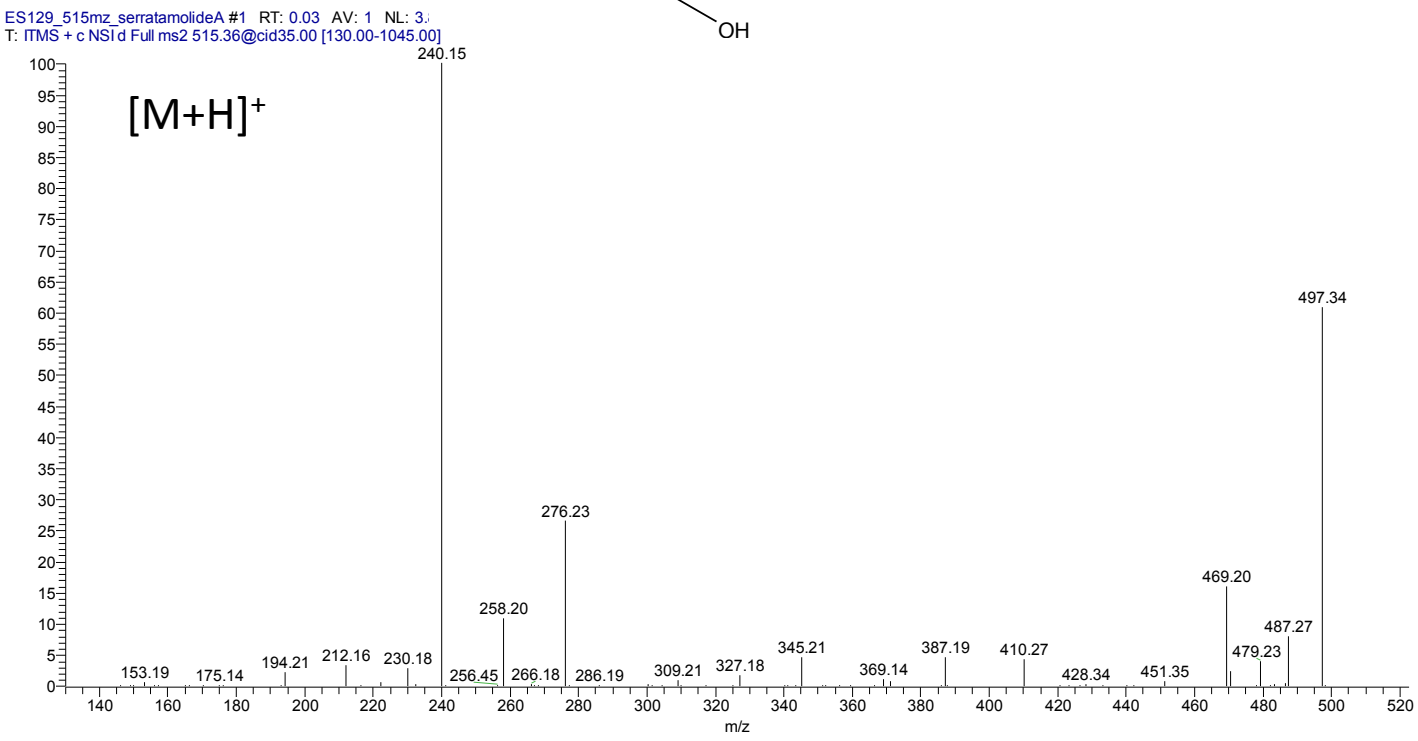

Description: Annotation of the CID MS2 for serrawettin W1/Serratamolide A . Spectra is consistent with published MS2 data.[18]

Figure S5: Annotation of MS/MS spectra for truncated linear surfactin

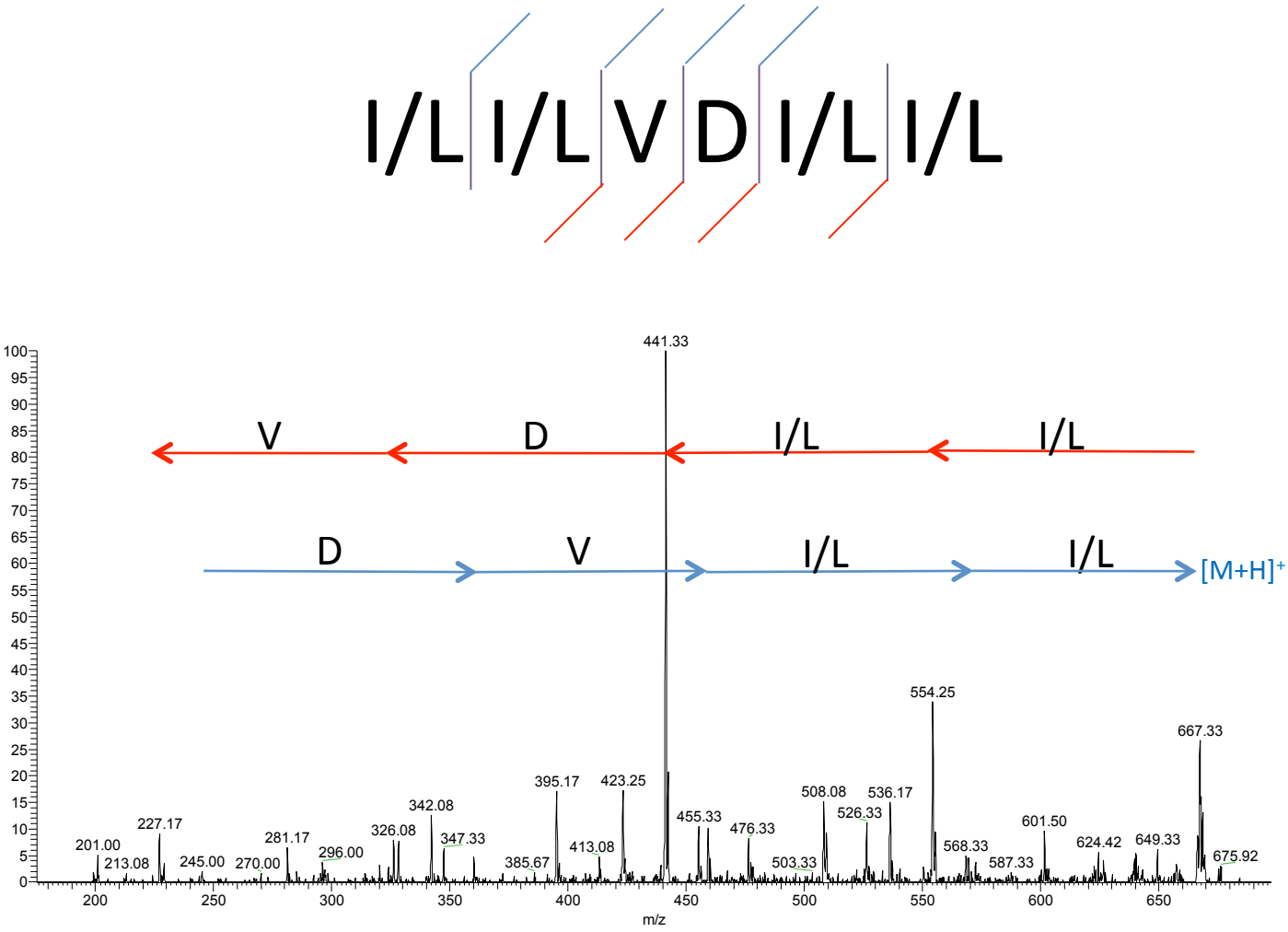

Calculated Mass: 685.4495 Da
Observed Mass: 685.4512 Da

Description: Annotated MS2 CID spectra for the truncated linear surfactin peptide.

Figure S5: Annotation of MS/MS spectra for truncated linear surfactin

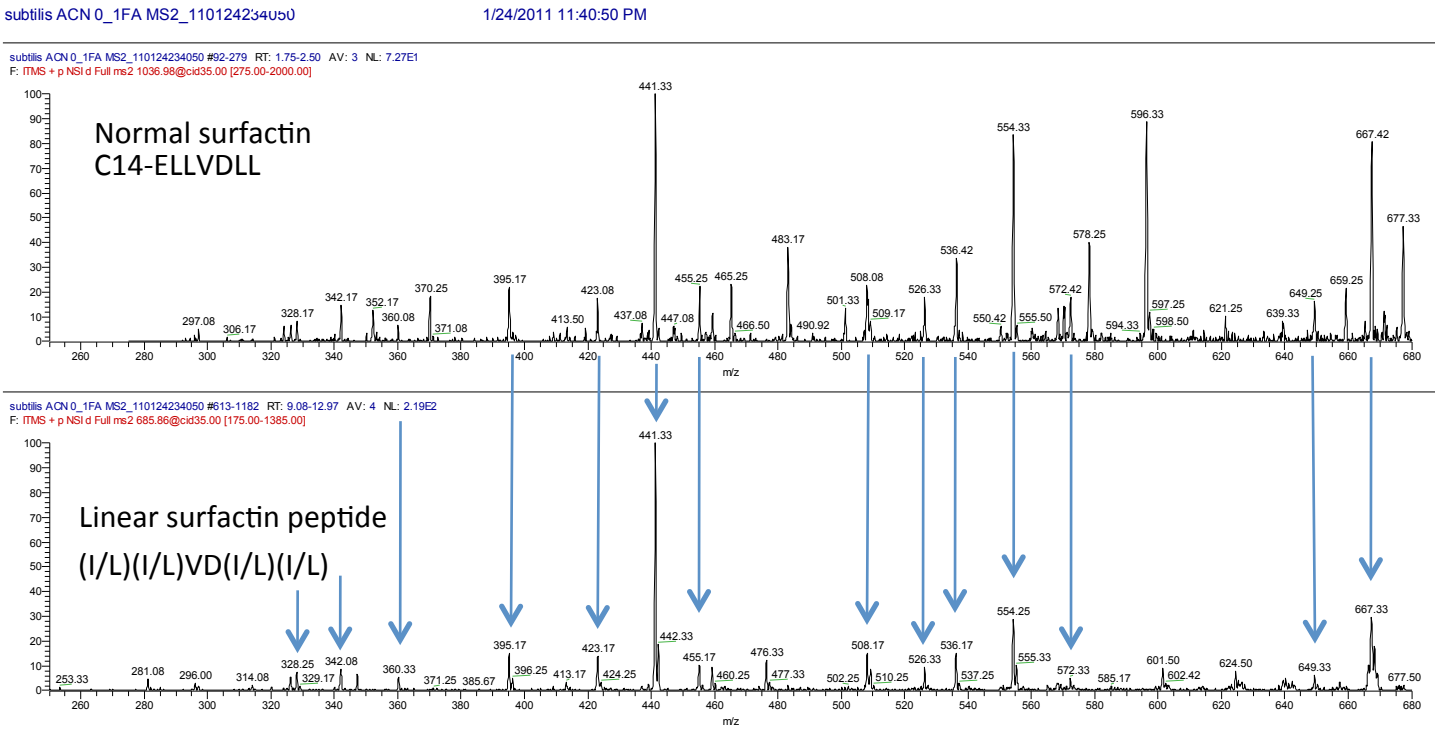

Description: Comparison of the CID fragmentation pattern of the linear surfactin peptide (bottom) with the that of the surfactin compound containing the same LLVDLL peptide sequence within the ring (top) shows identical daughter ion fragments. Note that only the lower mass fragments are displayed for the regular surfactin compound. Also, the reason for the peptide fragments for the cyclic peptide being equal to the fragments for the linear peptide is due to surfactin undergoing a ring opening upon fragmentation where the ester linkage is broken and the hydroxyl group is retained on the C-terminal side of the peptide.[1]

Figure S6: RNA transcription time course for sublancin producing enzymes and correlation with MS/MS network profile

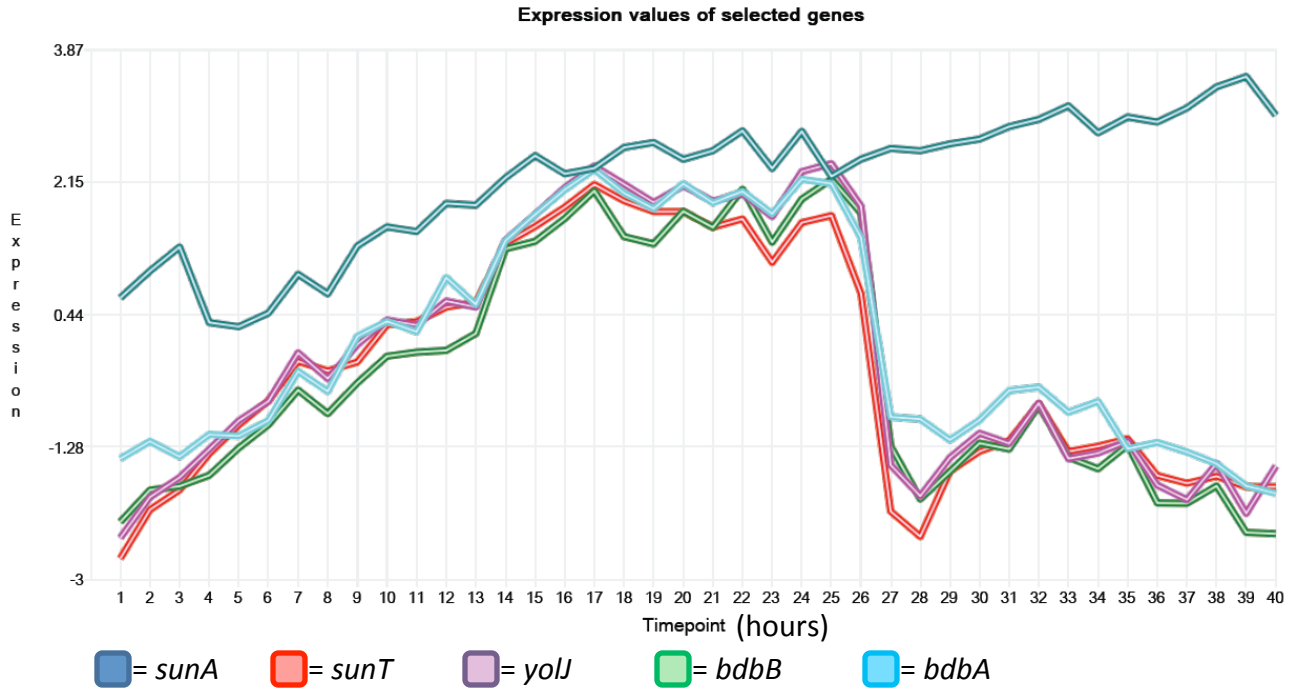

nanoDESI Time Course

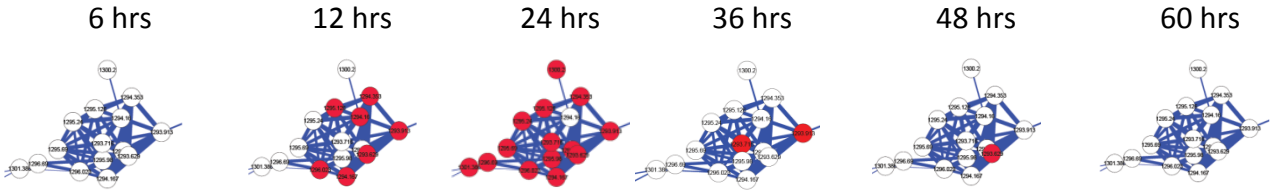

Description: Comparison of the RNA transcription data for sublancin biosynthetic machinery (top)[19] with observed sublancin masses from the nanoDESI time course (bottom). The transcript data show a steep decline in transcription for the sublancin biosynthetic machinery after 25 hours (mainly the ABC transporter *sunT*, unknown gene *yolJ* and the two thiol-disulfide reductases *bdbA* and *bdbB* with the precursor gene *sunA* remaining relatively constant), which directly correlates to a steep decrease in observed sublancin masses within the nanoDESI time course from *B. subtilis* 3610. Red nodes in the time course indicate the mass was present at that time point. RNA transcript data plotted from http://bacillus-subtilis168.appspot.com.

Figure S7: *Bacillus subtilis* 3610 time course network annotation showing time dependent production of various species of surfactin and plipastatin

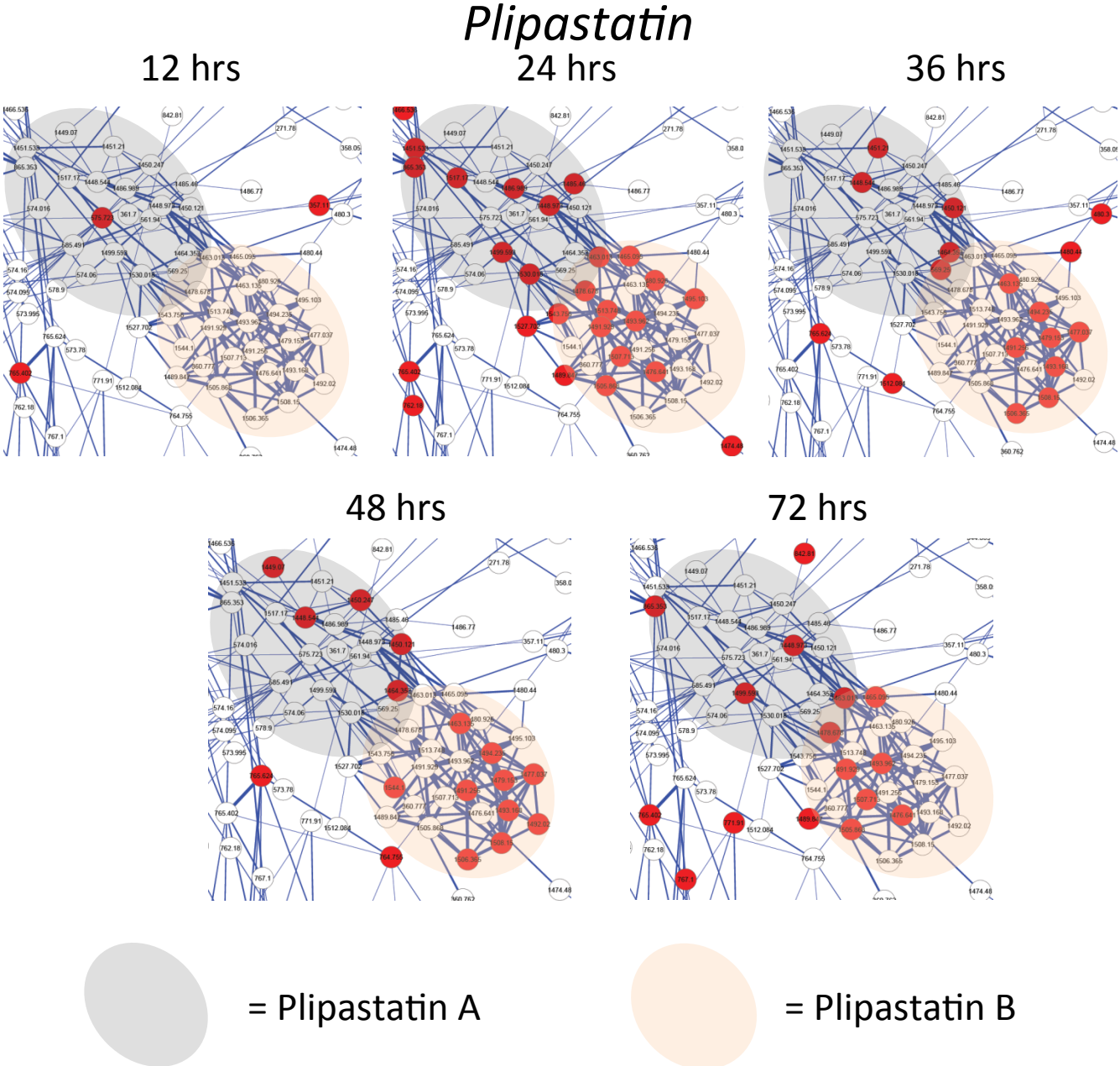

Description: When looking at the plipastatin node cluster within the molecular network for the nanoDESI time course of *B. subtilis* 3610, it was noticed that early on in the time course, plipastatin A (shorter lipid chain lengths) and plipastatin B (longer lipid chain lengths) were being made but at later time points only the longer lipid variants were observed in the mass spectra. This behavior also correlates to an overall increase in lipid production in the colony as observed by the networks after 36 hours. Red nodes indicate the mass was present.

Figure S8: *Bacillus subtilis* 3610 time course network annotation showing time dependent production of various species of surfactin and plipastatin

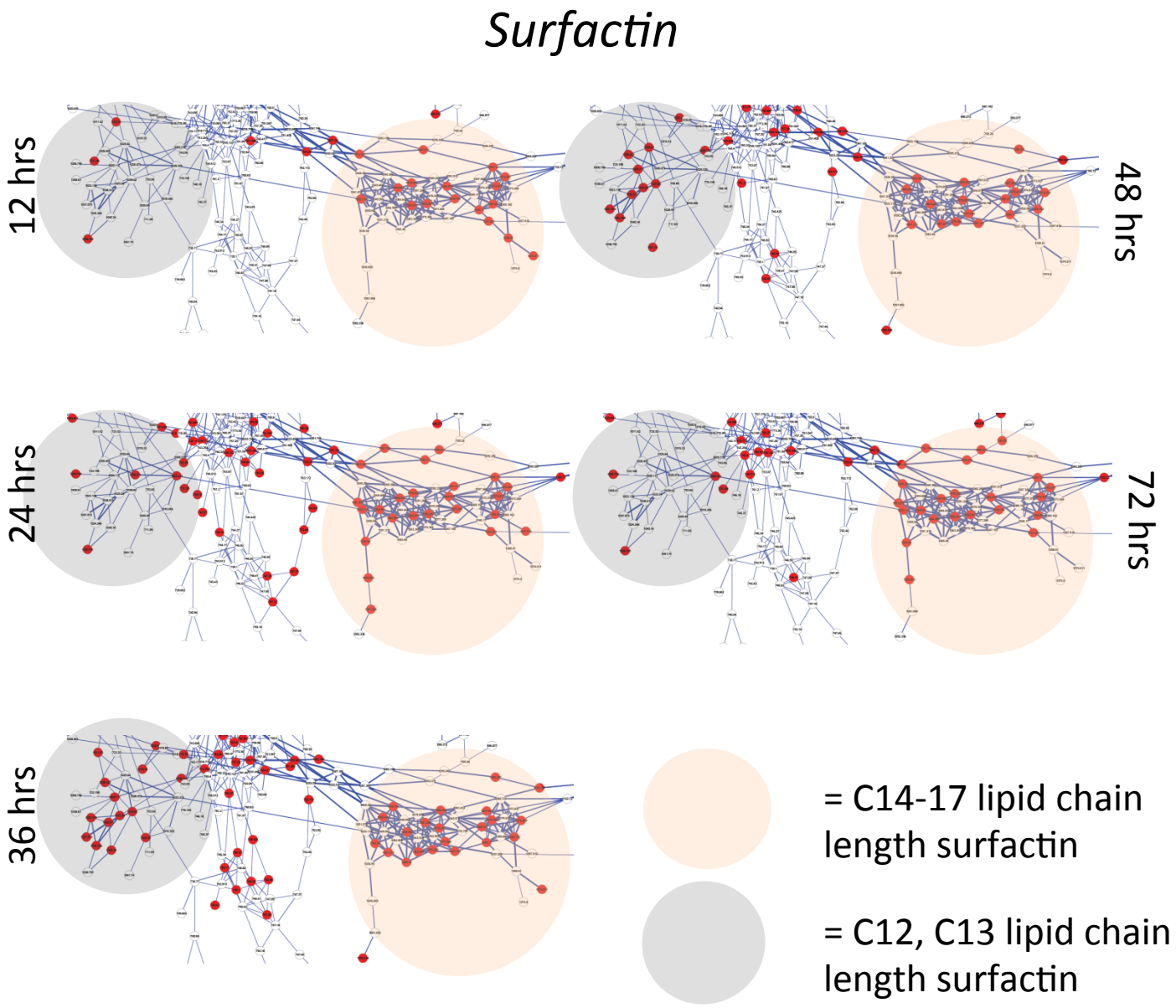

Description: When looking at the surfactin node cluster within the molecular network for the nanoDESI time course of *B. subtilis* 3610, it was noticed that while longer lipid lengths of surfactin A/B/C were being made throughout the time course, shorter lipid lengths (especially for surfactin C) were only produced within a time window of 24-48 hours after initial innoculation on the ISP2 agar plate

Figure S9: Mass spectra of prodiginine adducts/oligomers

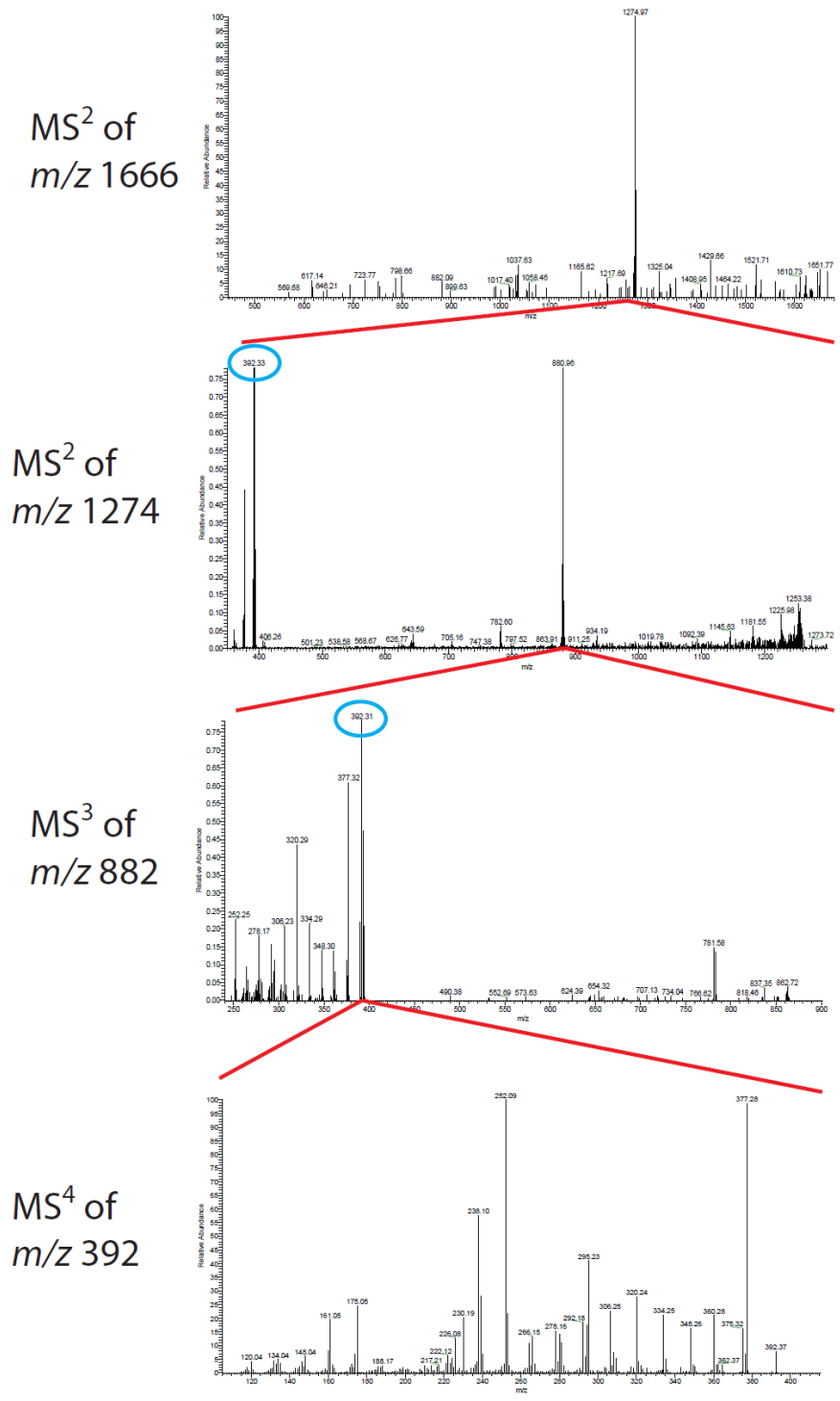

Description: Within the S. coelicolor colony that was interacting with the B. subtilis PY79 colony, an extremely high amount of cyclic prodiginine was observed in the spectra (much more than observed by MALDI and DESI previously in our lab). This was accompanied by many higher mass ions that contained prodiginine within their daughter ions indicating a possible polymer of the compound. MS2, MS3 and MS4 of one of these polymers revealed a possible oligomer of 2-4 prodiginine molecules with one phosphate.

Figure S9: Mass spectra of prodiginine adducts/oligomers

MS^4 of *m/z* 392

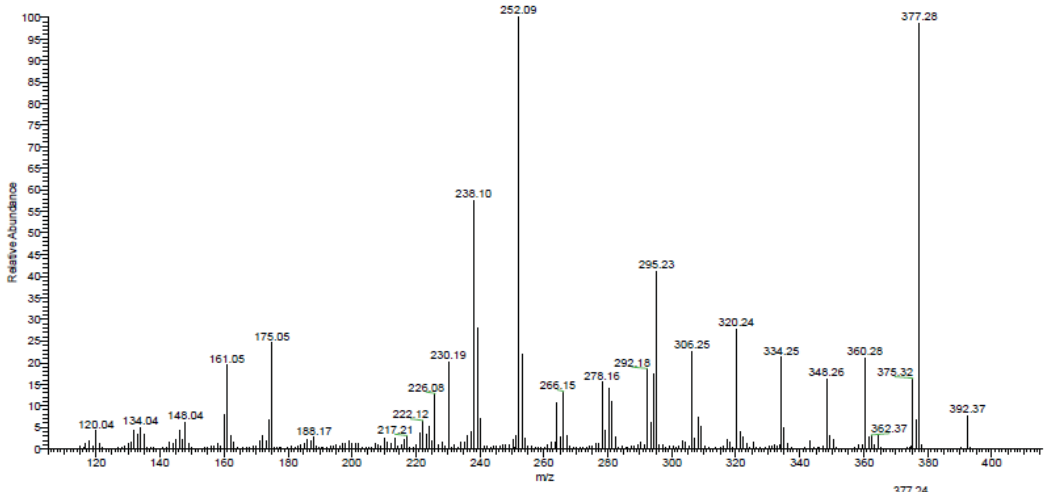

MS^2 of prodiginine

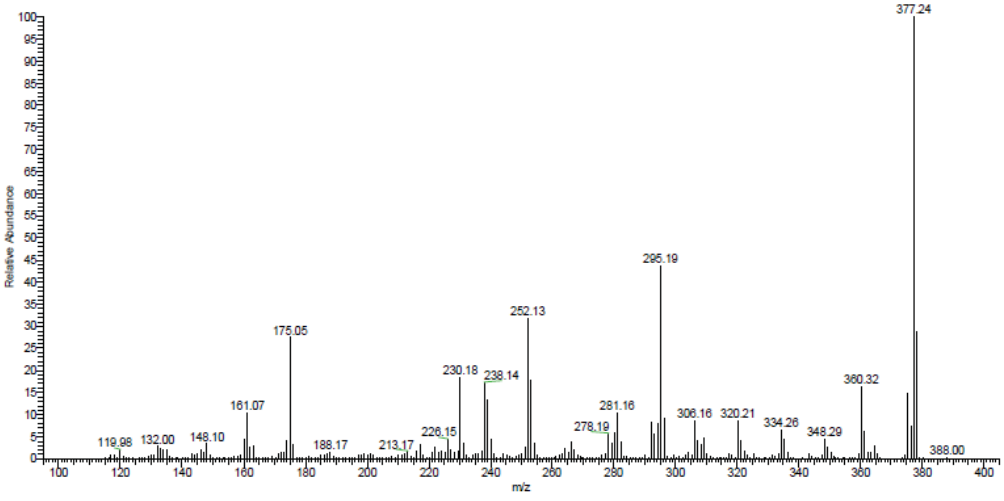

Description: To confirm that the mass of m/z 392 observed in the MS4 spectra of the oligomer was prodiginine (top), is was compared to the MS2 spectra of prodiginine to confirm its identity (bottom).

Figure S10: Example of chlorinated vs. non-chlorinated isotopic peak distributions

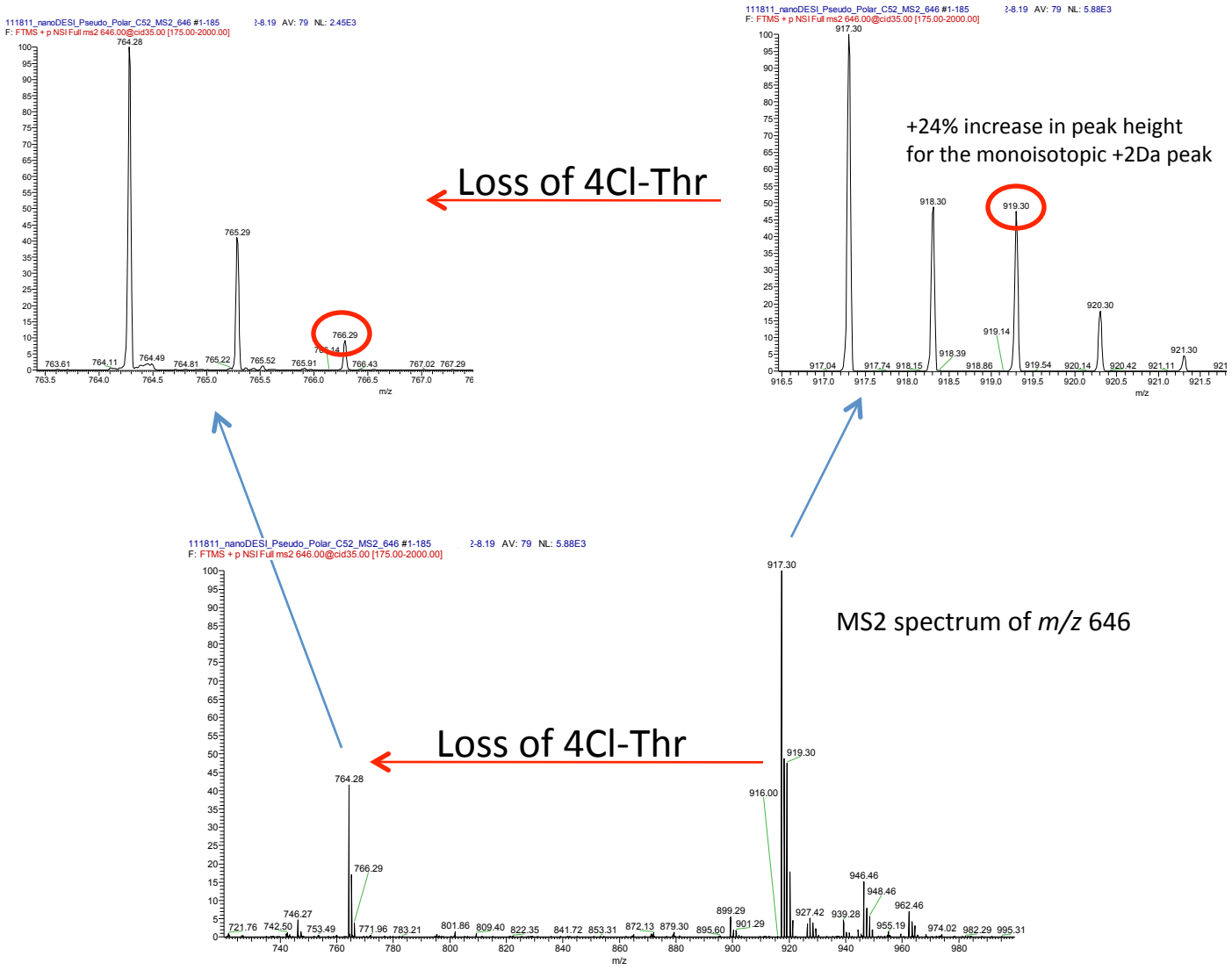

Description: Example of a typical chloronated (top right) and non-chloronated (top left) isotope distribution within the MS2 spectrum for thanamycin (MS2 of the +2 ion at *m/z* 646...bottom). Here we can clearly see that upon thanamycin losing the 4-chloro-threonine, the isotopic distribution of the mass signal changes from one indicative of halogenation (top right), where the monoisotopic peak +2 Da is 24% larger due to the presence of ^{37}Cl in addition to the typical 2x ^{13}C. The non-chloronated thanamycin fragment (top left) shows a typical carbon isotope distribution caused by the natural abundance of ^{13}C.

Video 1: This video shows the ionization and detection of microbial metabolites from living microbial colonies in real-time. This video can be found on the PNAS website.

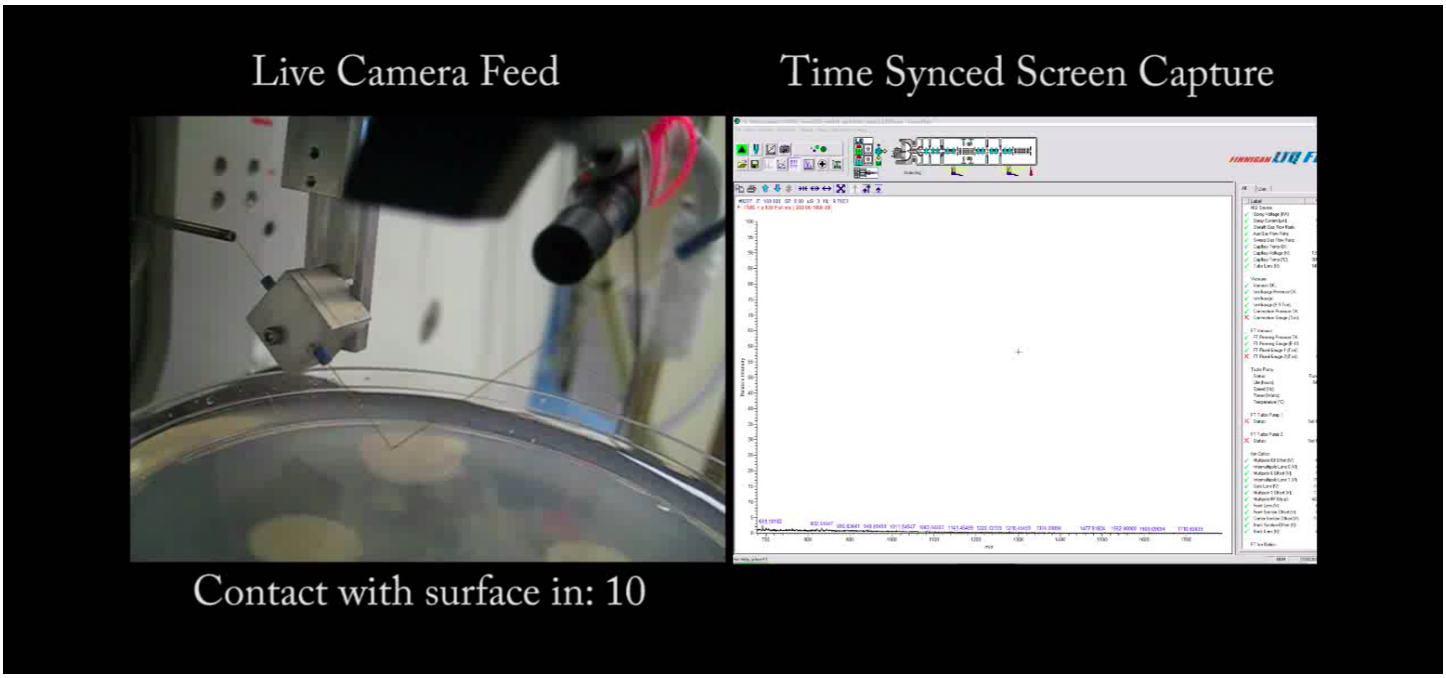

References

1. Hue *et al*. (2001) Structual investigation of cyclic peptidolipids from bacillus subtilis by high-energy tandem mass spectrometry. *Rapid Comm. Mass Spectrom* 15, 203-209.
2. Gidden *et al*. (2009) Lipid compositions in *Escherichia coli* and *Bacillus subtilis* during growth as determine by MALDI-TOF and TOF/TOF mass spectrometry. *Int. J. Mass Spectrom*. 283, 178-184.
3. Pecci *et al*. (2010) LC/ESI-MS/MS characterization of lipopeptide surfactants produced by *Bacillus licheniformis* V9T14 strain. *J Mass Spectrom*. 45, 772-778.
4. Oman *et al*. (2011) Sublancin is not a lantibiotic but an O-linked glycopeptide. *Nat. Chem. Biol*. 7, 78-80.
5. Liu *et al*. (2010) Imaging mass spectrometry of intraspecies metabolic exchange revealed the cannibalistic factors of *Bacillus subtilis*. PNAS 107, 16286-16290.
6. Kodani *et al*. (2004) The SapB morphogen is a lanitbiotic-like peptide derived from the product of the developmental gene *ramS* in *Streptomyces coelicolor*. PNAS 101, 11448-11453.
7. Gerber *et al*. (1975) Prodiginine (Prodigiosin-like) pigments from *Streptoverticillium rubrireticuli*, an organism that cause pink staining on polyvinyl chloride. *Appl. Microbiol*. 30, 807-810.
8. Hojati *et al*. (2002) Structure, biosynthetic origin and engineered biosynthesis of calcium dependent antibiotics from *Streptomyces coelicolor. Chemistry & Biology* 9, 1175-1187.
9. Lautru *et al*. (2005) Discovery of new peptide natural product by *Streptomyces coelicolor* genome mining. *Nat Chem Bio* 1, 265-269.
10. Wahl *et al*. (2010) Residual agar determination in bacterial spores by electrospray ionization mass spectrometry. *Anal. Chem.* 82, 1200-1206.
11. Villeneuve *et al*. (2003) Surface exposed glycopeptidolipids in *Mycobacterium smegmatis* specifically inhibit the phagocytosis of mycobacteria by human macrophages. *J. Biol. Chem*. 278, 51291-51300.
12. Mukherjee *et al*. (2005) Hyperglycosylation of glycopeptidolipid of *Mycobacterium smegmatis* under nutrient starvation: structual studies. *Microbiology* 151, 2385-2392.
13. Lepine *et al*. Electrospray/mass spectrometric identification and analysis of 4-hydroxy-2-alkylquinolines (HAQs) produced by *Pseudomonas Aeruginosa. J. Am. Soc. Mass Spectrom.* 15, 862-869 (2004).
14. Pajarron *et al*. (1993) Structure identification of natural rhamnolipid mixtures by fast atom bombardment tandem mass spectrometry. *Glycoconjugate* J. 10, 219-226.
15. de Koster *et al*. (1994) High-performance thin layer chromatography/fast atom bombardment (tandem) mass spectrometry of *Pseudomonas* rhamnolipids. *Biol. Mass Spectrom*. 23, 179-185.
16. Watson *et al*. (1988) Thermospray mass sprectrometry analysis of phenazines. *Biomed. Environ. Mass Spectrom.* 17, 251-255.
17. Chen *et al*. (2008) Unusual odd electron fragments from eleven electron protonated prodiginine precursors using positive ion electrospray tandem mass spectrometry. *JASMS* 19, 1856-1866.
18. Dwivedi *et al*. (2008) Antimycobacterial serratamolides and diacyl peptoglucosamine derivatives from *Serratia sp. J. Nat. Prod*. 71, 637-641.
19. Ridder *et al*. (2011) Time-resolved transcriptomics and bioinformatic analyses reveal intrinsic stress responses during batch culture of *Bacillus subtilis*. *PLoS ONE*, 6.

Supporting Information

Watrous et al. 10.1073/pnas.1203689109

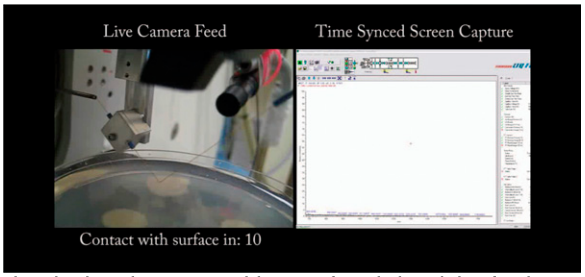

This video shows the ionization and detection of microbial metabolites from living microbial colonies in real-time.

Movie S1. Ionization and detection of microbial metabolites from living microbial colonies shown in real time.

Movie S1

Other Supporting Information Files

SI Appendix (PDF)